Microscopy behind Turbid Media

Dissertation

zur

Erlangung der naturwissenschaftlichen Doktorwürde
(Dr. sc. nat.)

vorgelegt der
Mathematisch-naturwissenschaftlichen Fakultät
der
Universität Zürich

von
Archana Malavalli Sudarshan

aus
Indien

Promotionskommission
Prof. Dr. Christof Aegerter (Leitung und Vorsitz der Dissertation)
Prof. Dr. Jürg Osterwalder
Prof. Dr. Martin Wolf

Zürich, 2018

Index

Index

Chapter 1

Introduction

When light travels though a medium it undergoes transmission, absorption and scattering. If an object is placed in a non-absorbing medium, the un-scattered light from the object travels through forming an image on the screen. However in the presence of scattering (in a weak scattering regime), the resulting image will be blurred. This way, scattering causes a hindrance to the process of image formation whereby the information of the object is simply lost. In the regime of strong scattering no image of the object can be formed at all.

We come across light scattering routinely in our day to day lives. Although Rayleigh scattering gives the blue color of the sky that we all enjoy on a sunny day, multiple light scattering of light through dense fog blinds our vision on a foggy winter night. More serious consequences of scattering are faced by astronomers when capturing images of the cosmos through their telescopes. The light coming from distant galaxies gets scattered when penetrating our atmosphere, causing the detected images to look blurred. Similarly when looking at a sample under a microscope, light emitted by a source hidden deep inside a tissue gets scattered by the complex network of scatterers. This causes a vast broadening of the Point Spread Function (PSF) and reduces the resolution of the microscope. These effects of scattering have to be compensated in order to improve the quality of imaging. There have been various advances in the imaging systems of microscopes and telescopes to correct for wavefront distortions. In imaging systems, adaptive optical techniques[1] are used to compensate for aberrations using deformable mirrors etc. In case these aberrations are unavoidable, one can use image processing techniques such as deconvolution[2], where the PSF of the system can be restored after the acquisition of images. In multiple scattering regime, one needs to determine the scattering characteristics of the medium in order to undo its effects. The Transmission Matrix(TM) encodes the relationship between various incoming and outgoing light fields[3]. But the elements of the transmission matrix can be too complex to find using adaptive optical techniques or post-processing; especially when the properties of the medium change with time. Biological samples are a good example of such medium. As shall be seen in this thesis wavefront shaping technique appears to be a promising tool to explore, especially for imaging through scattering media.

1.1 An overview of microscopy

Optical microscopy is a very important tool for biology and medicine in order to study various structural and developmental aspects of micro organisms. Many interesting biological phenomena take place in the visible part of the electromagnetic spectrum. Thereby studying these phenomena with an optical microscope makes complete sense. Using optical microscopes, biologists are able to view and record images of organisms smaller than the size of an average human hair. The auto-fluorescent nature of many biological specimens combined with the ability to also label them with other fluorescent proteins makes Fluorescence microscope an attractive tool for bio-imaging. Light coming from a specimen under the microscope passes through a set of lenses and mirrors to finally create an image on the detector. As one can imagine, the light diffraction at various interfaces along the path of light will affect the quality of images produced. Even slight misalignment in the optical path causes blurring of the detected images. The manufacturers of microscopes and microscope objectives take a number of precautions and optimize the overall design by tracing the optical path of light.

Nevertheless one can only do so much to avoid optical aberrations and produce good quality images, because in the end the nature of light itself can be a limiting factor in improving the imaging quality. There are two important characteristics of an optical microscope that affect the quality of the detected images. First and foremost is the resolution, i.e the smallest of the features that can be resolved. Second is the penetration depth, which refers to the thickness of a sample through which an image can be formed. The deep hidden features of a sample are often hard to image due to light scattering from all the layers above. Much of the signal reaching the detector is lost due to scattering and this also affects the resolution as the signal reduces at higher resolutions. The achievable resolution of a microscope is given by the Abbe diffraction limit[4], which is limited by the wavelength λ of light used and the Numerical Aperture(NA) of the imaging system. A lens focuses a parallel beam of light to a point of width given by the Airy disk. Similarly a point source visualised through a lens system is spread over a size given again by the Airy disk and called as the Point Spread Function (PSF) of the system. Its Fourier Transform which is the Optical Transfer Function (OTF) refers to the supported frequency content in the spectral domain. For an optical microscope with a condenser lens NA_c and imaging objective NA_o, the resolution limit is given by $d = \frac{1.22\lambda}{\mathrm{NA}_c + \mathrm{NA}_o}$, i.e d is the smallest distance of separation between two objects to be resolved. In an epi-fluorescence microscope, a single objective acts as both illuminating

condenser and the imaging objective, hence making NA_c =NA_o =NA and the resolution limit becomes $d = \frac{0.61\lambda}{\text{NA}}$. This distance d also happens to be approximately equal to the radius of the Airy disk $d = \frac{0.5\lambda}{\text{NA}}$.

By tweaking the various parameters of the equations written above, one attempts to achieve highest possible resolution. The choice of light source, the design of the microscope objective, the immersion medium are all optimised to suit the requirements for imaging a particular specimen. The most common microscopy technique employed in any laboratory is of the type of widefield microscope. In a widefield fluorescence microscope, a light source illuminates a 3 dimensional sample and the corresponding fluorescent signal is detected by a camera. The fluorescent signal from both in-focus and out-of-focus planes make it to the detector. The 3D optical sectioning capability of a widefield microscope is poor due to the fact that there is no mechanism to separate in-focus signal from the out-of-focus blur. In such a setting, it is typically hard to achieve resolutions of the order of diffraction limit. This is because the background fluorescence of out-of-focus planes of the sample cause an additional blur due to which the signal from in-focus plane can not be perceived as being resolved, thereby reducing the perceived resolution. With the invention of confocal microscopy technique, this out-of-focus blur can be greatly rejected by the use of a confocal aperture in the light path. The images are acquired by scanning a focused light beam through the aperture and recording the returning fluorescence signal in the way of epi-fluorescence mode (i.e using single objective for illumination and imaging). The confocal aperture blocks the scattered light from out-of-focus planes that typically arrive at larger angles, thereby only allowing the signal from in-focus plane to reach the detector. This leads to a drastic improvement in the optical sectioning capability. The effective resolution is now dependent on the size of the confocal pinhole, the smaller the size, the greater the resolution. By reducing the size of the confocal pinhole, it is possible to achieve resolution enhancement up to a factor $\sqrt{2}$ over widefield imaging. However closing of the pinhole also means lesser light reaching the detector even from the in-focus plane. So there is a trade-off between the signal-to-noise ratio and the achievable resolution. The disadvantage of this technique is the fact that the signal drastically reduces with increasing penetration depths. As the signal coming from deeper regions are scattered more, they arrive at larger angles and eventually get blocked by the pinhole. In effect the penetration depth of confocal microscope is limited by the magnitude of the signal reaching the detector from the deeper layers of the sample.

As one can see there are still unsolved challenges in fluorescence microscopy, particularly important are the resolution and penetration depth. The Abbe's diffraction limit conventionally sets the upper limit to achievable resolution. A number of new techniques have been invented to improve the resolution of a microscope. Some of them attempt to increase the quality of imaging with confocal microscopy, for example by detecting the light through confocal pihole and postprocessing the acquired images, a resolution improvement of a factor $\sqrt{2}$ over confocal microscopy has been reported [5]. Another example being iterative deconvolution of images to improve the resolution of the conventional widefield microscope [6]. Although resolution can also be increased simply by reducing the wavelength of the source used, or with electron beam sources utilising techniques such as TEM/SEM, the absorption at these wavelengths causes irreparable damage to biological specimens. Some of other techniques vary from physically narrowing the effective PSF of an illuminating light beam such as in STED [7], Saturated SIM [8] and RESOLFTs [9], to localising individual fluorescent molecules with time-resolved excitation in STORM [10], PALM [11] etc. Each technique with it's own merits and demerits provides the user with a suitable one to choose from. One particular technique that is not listed above but of most relevance to this thesis is the so called Structured Illumination Microscopy [12] (SIM). By using a periodic pattern to illuminate a sample and acquiring a series of images with shifted pattern orientations, it is shown that the OTF of the imaging system can be enhanced upto a factor two.

The problem of limited penetration depth is to some extent tackled with the use of longer wavelength light sources, i.e with the use of NIR light [13]. Two-photon and multi-photon microscopy techniques achieve penetration depth by exploiting non-linear optical properties [14]. Tomographic techniques such as OCT increases the effective penetration depth by the use of interference of non-scattered photons [15]. However the resolution offered by these techniques are often limited. That means with these techniques, there is a trade-off between the achievable resolution and depth upto which a sample can be imaged. When resolution beyond diffraction limit is desired along with higher penetration depths, most of these techniques fail. The main reason for this is the fact that the scattering of light increases with penetration depth. Therefore there is much interest in exploring avenues for imaging in the presence of scattering.

1.2 Light propagation in the multiple scattering regime

In this section we take a closer look at the process of multiple light scattering before proceeding to how we can tackle it in microscopy.

When a ray of light enters a medium it bounces off the various objects present in the medium. If the size of these objects are of the order of wavelength of light, the process is called the scattering of light; either Rayleigh scattering or Mie scattering depending on the size of the scatterers in comparison to the wavelength of light. The light ray hitting a scatterer changes its direction and moves towards another scatterer and so on. Each scattering event causes the direction of light ray to change randomly. Therefore light propagation through such a medium of scatterers can be seen as light performing a random walk. After multiple such scattering events, the light ray completely loses track of its initial direction.

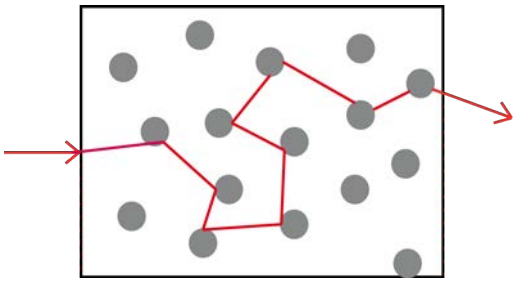

Figure 1.1: Light performing a random walk through a scattering medium

The refractive index non-uniformities in the samples causes light to scatter in random directions. A parameter called the mean-free-path shows how scattering a given sample is. Scattering mean-free-path l is the average distance that the light travels between two instances of scattering. The longer this distance is, the lesser the scattering will be. If the sample is thicker than couple of l, for a given wavelength of light it is said to be multiply scattering. The value of l or rather l^*- the trasport mean-free-path can be determined for given samples as the width of the coherent back scattering cone from the sample [16] [17]. As for a ground glass diffuser which is used as a scattering medium in most of our experiments, this metric l is ill-defined, as the scattering is caused by a single layer of material non-uniformities acting as the scattering centers. In comparison typical biological tissues tend to have a thickness of a couple of times their respective mean-free-paths. Hence they can be categorised as multiple scattering materials- the strength of which varies with the effective thickness of the sample used in relation to its mean-free-path.

Light propagation through a medium can be seen as a diffusion of light waves. Incident light takes various different paths through the scattering medium and all of these paths interfere upon exiting the medium. The interference of scattered light forms a

complex interference pattern called the speckle pattern shown in Figure 1.2.a. A thick layer of white paint (which contains TiO_2 material that is strongly scattering) is a good example of such a multiply scattering sample. The random assembly of scatterers in a paint layer make the transmitted light to form a distinct speckle pattern that is a characteristic of the many paths that the light has taken. Therefore by understanding the

a) 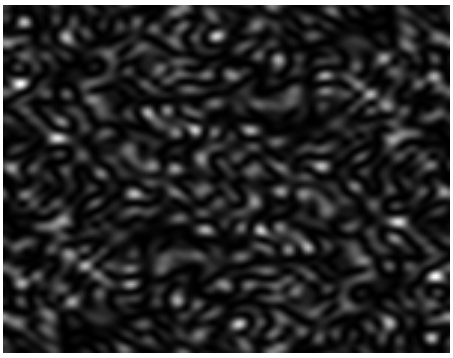 b) 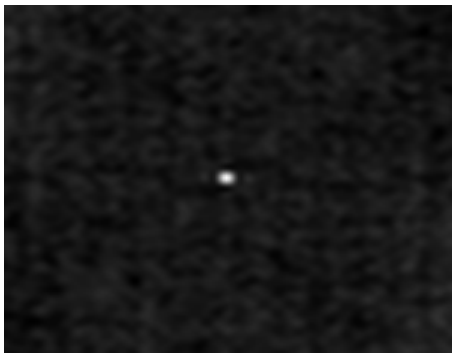

Figure 1.2: a)Speckle pattern b)Intensity Autocorrelation of a)

statistics of the speckle pattern, one can get insights into the process of scattering. Particularly of interest is to determine if there are any correlations in the transport of light through scattering medium. Such correlations can only be understood by assuming the wave nature of light, leading to interference of different waves propagating through the medium. As most of the research in this thesis involves computing the field distribution of scattered light far away from the scattering medium, we can look at the statistical nature of the speckle patterns obtained in the Fraunhofer plane. To do this, consider a region of size 'r' of the medium uniformly illuminated to observe the scattered field at a plane at a distance 'z' from the scattering medium. Scattering from a random ensemble in the medium results in a complex random field distribution at any point in the observation plane. The probability distribution of the field of the resulting speckle pattern in the observation plane is derived by Goodman [18] as

$$p(A^{(r)}, A^{(i)}) = \frac{1}{2\pi\sigma^2} \exp\left\{ -\frac{[A^{(r)}]^2 + [A^{(i)}]^2}{2\sigma^2} \right\}$$

i.e the real $A^{(r)}$ and imaginary $A^{(i)}$ part of the amplitude of the field follow a Circular Gaussian probability distribution. The intensity of the speckles $p(I)$ derived from the equation above, follows a negative exponential distribution and the phase $p(\phi)$ follows

a uniform distribution.

$$p(I) = \frac{1}{\langle I \rangle} \exp\left\{\frac{-I}{\langle I \rangle}\right\} \quad \text{and} \quad p(\phi) = \frac{1}{2\pi} \; ; -\pi \leqslant \phi \leqslant \pi$$

Also, for a random process such as this, the probability distribution of intensity fluctuation is described by the intensity autocorrelation function. The autocorrelation function of the intensity fluctuation is equal to the square of the autocorrelation of complex amplitude of the speckles in the observation plane and is given by [18]

$$\begin{aligned} C_I(x,y) &= \frac{\langle I(x+x_1, y+y_1) I^*(x,y) \rangle}{\langle I(x+x_1, y+y_1) \rangle \langle I(x,y) \rangle} - 1 = |C_A(x,y)|^2 \\ &= \frac{\langle I \rangle^2 \; 2\mathcal{J}_1\big((2\pi r/\lambda z)\sqrt{x^2+y^2}\big)}{(2\pi r/\lambda z)\sqrt{x^2+y^2}} \end{aligned} \tag{1.1}$$

where $\mathcal{J}_1(\cdot)$ is the Bessel function of first order. This gives the size of an average speckle and is an important metric for wavefront shaping. The intensity autocorrelation of a typical speckle pattern is as shown in Figure 1.2.b. As can be seen from this figure, the size of the autocorrelation function is equal to the size of an average speckle. As will be seen in the next chapter, the process of wavefront shaping results in the formation of an interferometric focus in the Fraunhofer plane that has the same size as this autocorrelation function.

1.3 Imaging in the presence of scattering

As discussed so far, scattering poses a challenge to the process of image formation. But there are ways to undo the effects of scattering by first of all understanding the process of scattering. This means, utilizing the knowledge of scattering via studying the statistics of the speckle pattern one can think of doing microscopy. The light transmission properties of a scattering medium are characterised by its Transmission Matrix(TM), which connects the various input and output modes of light. Hence by determining the TM of a scatering medium gives enough information to understand the behaviour of the medium. Additionally, by exploiting the correlations between multiply scattered light paths, one can learn how to influence the tramsitted light by changing the input in a certain way. That is, due to interference of the light taking different paths, the outgoing light can be influenced by controlling the incident light. Vellekoop *et al.* [19] used Random Matrix Theory(RMT) to show that the elements of the Transmission Matrix (TM) are correlated due to these interference effects. Therefore by controlling a large number

of modes of the input light, it is possible to couple better to the transmitting modes of the sample. These ideas of controlling the incident light via wavefront shaping to focus the transmitted light are described further in Chapter-2.

As shall be seen in the chapter to follow, wavefront shaping has proven to be a very useful tool to tackle multiple scattering and imaging in the presence of scattering. By exploiting the interference effects, light can be made to focus through strongly scattering materials. Furthermore by scanning this focus in space, images of samples can be obtained in 2D and 3D. Wavefront shaping transforms a scattering medium into a lens that can be further used for microscopy, making it a scattering microscope. The principles of imaging with such a scattering microscope will be discussed in detail in Chapter-2. However this kind of imaging with an interferometric focusing is also diffraction limited. As will be shown in the upcoming chapters, it is possible to extend the resolution of a scattering microscope via Structured Illumination Microscopy(SIM). By way of exciting a fluorescent sample with a spatially varying illumination patterns, SIM obtains resolution enhancement over conventional widefield microscopy. We show that using the indispensable tool of wavefront shaping, we are able to transform a scattering medium into a lens and obtain resolution enhancement beyond diffraction limit when imaging through multiply scattering materials.

1.4 Thesis Outline

The approach that we have taken to perform SIM in multiple scattering regime consists of two aspects. First is the fact that using wavefront shaping technique we are able to turn a scattering medium into a lens that focuses the incident light to a point behind the medium. Following the work of Vellekoop *et al.* [20] the principles of focusing light through scattering medium is described in Chapter-2. This makes use of the fact that shaping the incoming light, the scattered light from a medium can be controlled. Through this wavefront shaping mechanism, it is possible to determine a light wavefront that optimally focuses through a scattering medium. The natural extension of this technique into microscopy is also demonstrated in detail, whereby scanning the obtained focus produces images of the illuminated sections. It is possible to scan the focus not only in 2D but also in 3D which allows for 3D image stacks to be obtained by means of raster scanning the focus. Secondly we explore the possibility of application of wavefront shaping to Structured Illumination Microscopy(SIM). I will show in

Chapter-3 how to actually generate periodically patterned illumination behind scattering media. As shall be seen this requires the implementation of Phase Mask Generation algorithms that aid the process of transforming a focus behind the turbid medium into an array of periodic multiple foci. This way a scattering medium will be turned into a lens of adaptable aperture through which we can generate custom designs of multiple light foci. Once we are equipped with the techniques to obtain patterned illumination, we can perform imaging of fluorescent structures hidden behind the scattering medium. The images thus acquired are then processed using the principles of SIM. The theory of enhancing resolution using SIM principles is described in detail in Chapter-4, which is followed by the results and discussion of SIM behind scattering media. The thesis ends with a brief summary of the work in Chapter-5 followed by literary references.

Chapter 2

Focusing Light Through Turbid Medium

A turbid medium is one which scatters the light to an extent that the medium looks opaque. Some examples of such turbid medium are clouds, smoke, a glass of milk etc. All these materials scatter visible part of the spectrum strongly, causing the whitish appearance of the material. Multiple light scattering is studied widely while it affects many different fields such as astronomy, optical communication, spectroscopy, microscopy and so on. It is caused due to the non-uniform distribution of refractive index on the material which also gives rise to the name "random media". When light travels through such media, it is randomly scattered and it becomes difficult to determine the properties of the media. Multiply scattered light from a random medium interfere and form complex interference patterns called the speckle pattern. The characteristics of the scattering medium can be deduced by understanding the speckle pattern that it generates. Multiple scattering of light through random media give rise to interesting phenomena such as Anderson Localisation [21], universal conductance fluctuations [22] etc. The problem of studying light transmission through multiply scattering media has therefore attracted a lot of attention.

While being such an interesting phenomenon, multiple light scattering is however seen as a hindrance in many fields. Especially in imaging, light scattering strongly affects the process of image formation. In imaging systems, there is often a problem of single scattering from the surfaces of lenses and mirrors that causes blurring of a recorded image. These effects however can be relatively easily compensated by making use of adaptive optical approaches, or better design of the optical components. However the effects of multiple scattering can not be compensated by the same ways used for overcoming blurring by imaging systems. Reversing the adverse effects of multiple scattering in imaging has therefore been the biggest challenge in imaging.

In the experiments conducted by Vellekoop *et al.* [23], they demonstrated that due to the interference of multiply scattered light, the process of light scattering can be turned into an advantage. They used wavefront shaping technique to show that an input wavefront can be constructed that effectively maximises transmission through a medium. This means by controlling the input so as to match the transmission characteristics of the material a desired output can be obtained. Wavefront shaping makes use of a feedback mechanism to do this. For example a detector placed at the location of the focus provides the required feedback to construct the input wavefront that in turn gets focused. Using this technique it is now possible to focus light through a strongly scattering material which was otherwise not possible.

Wavefront shaping has gained increasing attention ever since, being applied in high resolution microscopy, optical trapping, improving transmission through multi-mode optical fibers and so on. The various applications of wavefront shaping are detailed in the review article[24]. Particularly relevant to further research is the ability to apply wavefront shaping to microscopy. As will be described in the following sections, wavefront shaping can be used to focus the light through a fluorescent sample and by raster scanning this focus, images of the sample can be acquired just like in image scanning microscopy. Before moving on to these applications, the experimental procedure to obtain a focus behind turbid medium is described in Section 2.1. Followed by Section 2.2, where some of the theoretical aspects are highlighted. Section 2.3 presents our results with respect to scanning the focus in 2D to obtain images of the sample. In Section 2.4 we explore yet another possible extension of focusing behind turbid medium. Finally we summarise the capabilities of the scattering lens and provide an outlook towards resolution enhancement in Section 2.5.

2.1 Experimental Details

As we have seen in Chapter-1 of this thesis, when light is incident on a multiply scattering material, a speckle pattern in formed in the far field. Each bright speckle in the speckle pattern is a result of constructive interference between the multiple light waves reaching that speckle. The aim of wavefront shaping is to go from a random speckle pattern into an interferometric focus, which is one speckle where all the light is made to constructively interfere. The logic behind interferometric focusing is the fact that the intensity of a each speckle varies as a function of phase difference between multiple paths that the light takes. This means the field at the target is a linear combination of the various scattered fields. Therefore there exist one particular phase relationship between all the light paths, for which they constructively interfere at the focus. The optimised wavefront that focuses behind a turbid medium is typically algorithmically determined. From the time of conception of this idea many different algorithmic schemes have come up with improvements in both design and execution. However the basic idea is that the different parts of the input wavefront is modulated so as to maximise the intensity of a target. This means, some sort of a feedback mechanism is required in order to construct the optimum wavefront. An iterative algorithm takes the intensity at the target as an input and tries to maximise it by cycling the phase shift of the incoming light segment

by segment.

The setup as shown in the Figure 2.1 highlights the important components required to focus light through turbid medium. It consists of a source i.e a Laser (Spectra-Physics Cyan Scientific) at $488\ nm$ wavelength and $100\ mW$ power operating in CW mode. This laser beam is broadened by a beam expansion unit by a factor of ~ 20 in order to uniformly illuminate the SLM. The reflected light from the SLM is demagnified by another lens and an *illumination objective* (Zeiss 10X 0.3NA). The sample is placed such that a minified image of the SLM forms on its *rough surface*. The other side of the sample- the *smooth surface* is brought into focus of an *imaging objective* (Olympus 20X 0.45NA or Leitz 40X 0.7NA). Each of these components is described individually in the remaining part of this section.

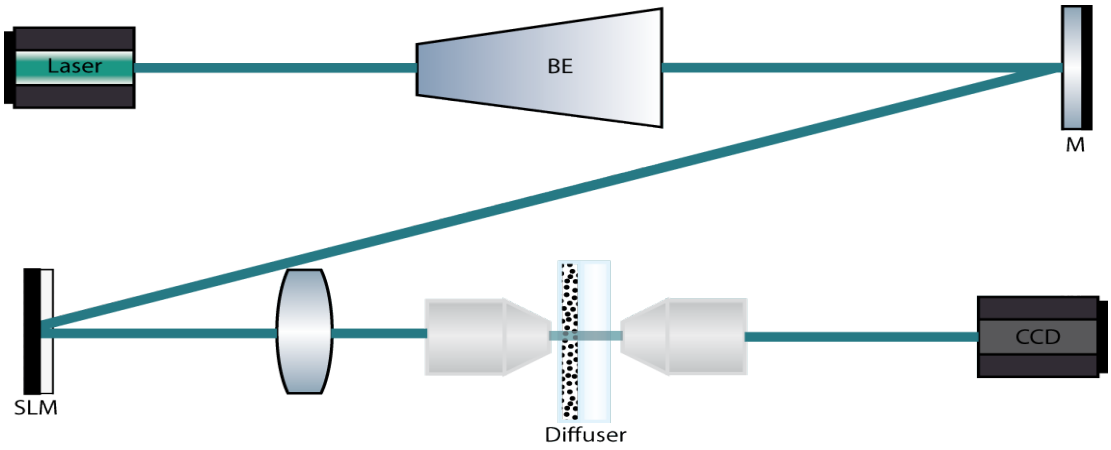

Figure 2.1: Experimental setup used to focus light through a ground glass diffuser(fluorescent beads on the smooth side is omitted); BE=Beam Expander, M=Mirror

Before moving on to the different experimental components, we first take a look at the process of wavefront modulation itself. The capability to modulate the incident field of light is made possible by wavefront modulators such as Liquid Crystal Devices (LCDs). An LCD is made up of LCs sandwiched between alignment plates, electrodes and sometimes with polarisation optics. The thickness of the LC layer is specifically chosen to optimise the total phase shift that it can impart on the incoming light. The state of outgoing light from the LCDs is changed by applying voltage on the different segments of the device. Due to the birefringent nature of the LCs, the effective refractive index experienced by light and hence its phase shift will depend on its polarisation state ($\eta_{\text{eff}} = |\eta_o - \eta_e|$), additionally modifying the state of polarisation of the outgoing light. Depending on the choice of LCs and modulation procedure it is possible to

achieve either phase and/or amplitude modulation of light; giving rise to mainly two approaches- phase only modulation and phase & amplitude modulation.

Phase modulation: Depending on the choice of LCs, there are many ways to achieve phase modulation. In the case of Twisted Nematic LCs, the incoming light is split into two polarisation states with each state experiencing a different phase shift. By letting only one polarisation state to pass through, a partial phase only modulation of light can be achieved. However, the loss in intensity due to blocking of the other polarisation state makes this choice of LCs very inefficient[25]. In our setup, Phase-only modulation is achieved with Nematic LCD. By setting the input polarisation of light linear to the director of the LC molecules $\eta_{\text{eff}} = \eta_o$, thereby accessing a full phase range of $0 - 2\ \pi$. The phase change that the light experiences is directly proportional to the grayscale value of the pixel, which in turn corresponds to the voltage applied on the pixel. A calibration procedure as detailed below is usually necessary to determine the grayscale values required to obtain a full phase shift from $0 - 2\ \pi$.

Phase and amplitude modulation: In general, amplitude modulation of light can be achieved by placing the LCD between two crossed polarisers. As the voltage ranges from 0 to maximum, the polarisation of outgoing light sees a complete transformation, thereby getting either transmitted or blocked by the second polariser. To control amplitude and phase of light independently, many optical setups have been desinged with a use of two LCDs working in parallel[26] or light passing a single LCD twice[27] and so on. van Putten *etal*[28] have designed a technique to achieve independent control over phase and amplitude modulation with any LCD. In their technique they group a set of 4pixels into a macro-pixel and adjust their respective phase differences. Further by determining their corresponding voltages the outgoing light is modulated to have a required state. Using this technique it is possible to generate any complex state of outgoing light.

The various components of the experimental setup are described below.

Wavefront modulator: The heart of our experimental setup is the wavefront modulator which is used to shape the light to obtain interferometric focus. A wavefront generator such as Spatial Light Modulator (SLM) offers an order of $\sim 10^6$ degrees of freedom to control the light wavefront. An SLM is a Liquid Crystal Display(LCD) whose electronically controllable birefringent nature makes it that the light incident on it experiences different index of refraction for different polarisation of light. We made use of a reflective SLM (Holoeye Pluto) with 1920X1080 pixels (of size $8\ \mu m$ each) that can

be controlled via DVI port by the graphics card of the computer. We operate this SLM in Phase only modulation scheme as described above. This means an incoming light that is reflected off the pixels of the SLM are phase-shifted by an amount proportional to the applied voltage on the pixel.

In our experiments, an optimisation algorithm (described below) sets the phase on each of the pixels iteratively. At each iteration, the transmitted intensity from the turbid medium is measured using a camera and the pixel phase shift is adjusted accordingly. By this way of synchronizing the SLM with the camera, we are able to perform 12 measurements per second. This is much lower than the refresh rate of the SLM which is 60Hz. But due to the slower response time of the LCs to the applied voltage the actual speed of the SLM is limited when precise phase shifts are to be made. This in fact is the limitation of the speed of the current measurement apparatus. Since we are working with stationary scattering media, we are able to perform our measurements without any problems. But there exist faster alternatives to an SLM such as Digital Micro-mirror Devices (DMDs) that operate at kHz frequencies, if one needs to focus light through dynamically scattering media such as biological tissues.

In order for an SLM to be implemented in our experiments, it has to be calibrated for the phase shifts that we intend to impart on the incoming light. The calibration procedure of the modulator is detailed in the user manual of the device. The procedure determines the voltages required to obtain a certain phase shift at a given wavelength of light. It consists of an interference technique where the light coming from half of the SLM surface is made to interfere with that coming from the other half. Any phase shift between these two light beams will result in a movement of the interference fringes on the camera. The calibration software measures the shift in the fringes as a function of applied voltage. By varying the grayscale value from 0-255 in small increments, a full profile of phase shift from $0 - 2\ \pi$ is measured. Thus generated calibration file is loaded onto the SLM and can be used for wavefront optimization.

Samples: We fashion samples that mimic the scattering properties of biological tissues and are also fluorescent. Ground glass diffusers are the best candidates as they randomly scatter the input light. The rough surface of the diffuser is grit polished with a feature size of $6\ \mu m$ (1500Grit). White paint also serves as a great diffuse scattering material. Our paint samples were produced using ZnO particles (of size roughly $200\ nm$) dispersed in ethanol. When spray painted on a glass slide, the paint mixture leaves behind thin uniform layers of ZnO. The thickness of this paint layer-

measured using an optical microscope, was found to be about $10\ \mu m$. For our imaging experiments, we make use of $0.5\mu m$ fluorescent beads (Thermo Fisher Scientific) with an excitation/emission maxima at $505nm/515nm$ respectively. The fluorescent beads are dispersed in distilled water and mixed thoroughly using an ultrasonic bath. A small droplet of $5\ \mu l$ is pipetted out and spread evenly on the smooth surface of the diffuser.

Feedback: The simplest approach to focusing light through turbid medium is to iteratively adjust the input wavefront based on signal at the detector. This is the so called "direct feedback" method, as opposed to "indirect feedback" when signal of a probe- a "guide star"- at the desired location of focus is enhanced. For example, a fluorescent bead at the location of focus can act as a probe, whose fluorescence is a measure of intensity of light reaching the probe. Latest experiments have been performed on all sorts of probes including photoacoustic [29] [30] and even non-linear absorbers [31]. The advantage of indirect feedback is the fact that no optical access is necessary to focus on a probe hidden inside a scattering medium. Whereas in direct feedback technique, the focal plane is the plane where a detector is placed, which implies the need of optical access. Most of our experiments are performed with direct feedback method, however the experiments described in Section 2.4 were performed with indirect feedback method, using signal coming from fluorescent beads.

Algorithm: There are many ways to iteratively construct an optimized wavefront that efficiently focuses to a point behind a turbid medium. The purpose of the algorithm is to communicate between the wavefront modulator and the detector and compute the necessary phase shifts required on the incoming wavefront such that intensity of the target is enhanced. The inverse diffusion algorithms developed by Vellekoop and Mosk [32] are one of the first of kind, where the phase shift on all the segments are optimised by cycling through $0-2\pi$. Then came the use of transmission matrix approach to focusing light [33], whereby the TM of the whole sample is measured. From this TM the optimum transmission coefficients that enhance the intensity at the target are later determined. By now there exist many more algorithmatic approaches including implementations of genetic algorithms [34] and random partitioning algorithm with the use of hadamard basis [35] etc. Each technique with its own set of advantages and disadvantages provides the user with suitable variations to choose from.

We have made use of the *stepwise sequential algorithm* implemented by Vellekoop *et al.* The stepwise sequential algorithm starts by grouping the SLM pixels into N number of segments, and phase on each segment is optimised one after another. The light

from the segment currently being modulated interferes with the light from rest of the segments and forms a speckle pattern on the camera. The intensity on the CCD at a region- typically of size of a single speckle- is used as the target feedback signal. The intensity of the target speckle varies sinusoidally as a function of phase difference between a segment on the SLM and the rest of the SLM. The phase of each segment is cycled through $0-2\,\pi$ and the corresponding target intensity is measured. At the end the whole measurement cycle is fit to a sine to determine the phase shift corresponding to the maximum target intensity. The optimum phase shift of the segment thus determined is saved before proceeding to the next segment. This process is repeated to determine the optimum phase values for each of the N segments, by setting the phase of each segment to 0 before proceeding to the next segment. At the end of the iteration, the phase of all the N segments are set to their optimum values, resulting in an optimized wavefront. At the focal plane this results in a pattern with the intensity of the target speckle maximized. The profile of the focus generated this way is as shown in the Figure 2.2. In order to get an initial increase in the signal to noise ratio, the whole iteration can be done with larger segments (i.e smaller number of segments N), before moving to iterations with larger N. Typically 2-3 such iterations is enough to obtain maximum enhancement.

2.2 Focusing light through scattering media

2.2.1 Theory of Scattering Lens

Light transport through a medium can be described from wave diffusion, however when the medium is multiply scattering one needs to also take into account the interference between multiply scattered light. When a light wavefront is incident on a multiply scattering medium such as a layer of white paint, different parts of this wavefront follow different paths through the medium. These multiple paths finally interfere and result in a speckle pattern on the screen. It is a characteristic pattern for a given state of illumination, i.e if either the sample or the light source is moved, the speckle pattern would look very different. Almost a decade ago, Vellekoop *et al.* [23] proposed that one can determine an optimised wavefront of light for which the transmission is maximised in one mode (or several chosen modes).

Using continuous field formalism one can determine how an optimum wavefront can result in a desired focus at the target [23]. It enables to determine the shape and

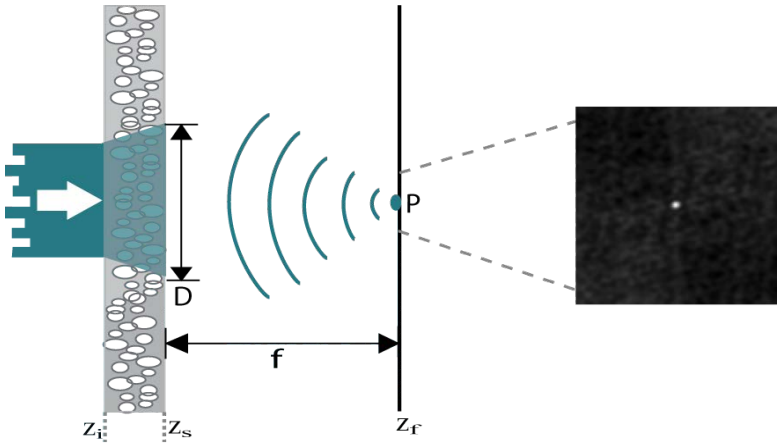

Figure 2.2: Optimised wavefront is incident on a scattering medium at $z = z_i$. The scattered field due to optimisation forms a converging wavefront that propagates from scattering plane at $z = z_s$ to focal plane $z = z_f$ and gets focused.

intensity distribution of the interferometric focus. The process is as follows: a small region of width 'd' is illuminated on the scattering medium by light field $\mathcal{E}_0$ as shown in Figure 2.2. The incident light is divided up into N different segments and the amplitude and/or phase of each segment is modulated by a wavefront modulator placed before the scattering medium. In order to focus the light to a point 'p' on the focal plane z_f the amplitude and/or phase of the incident field is optimised such that light from all the N segments constructively interfere at the point 'p'. The modulated filed can be written as

$$\tilde{\mathcal{E}}_{z_i}(r) = \mathcal{E}_0 t_{z_i p}$$

where $t_{z_i p}$ is the transmission coefficient of light coming from N different segments at z_i to point p at z_f. This means the field is modulated such that transmission to the point 'p' is optimised.

The modulated light transmits through the medium and produces a scattered field at the plane z_s behind the scattering medium. This field fluctuates proportional to the intensity fluctuation in scattering plane, i.e

$$\tilde{\mathcal{E}}_{z_s}(r) \propto I_{z_s}(r)$$

This scattered field produces a far field diffraction pattern on the focal plane z_f. That means the field at z_f is a Fourier Transform of the field at z_s.

$$\tilde{\mathcal{E}}_{z_f} = \iint_S \tilde{\mathcal{E}}_{z_s}\, d^2r = \iint_S c\, I_{z_s}(r) \exp\Big[-\frac{\mathrm{i}k}{f}\,(x_s x_f + y_s y_f) \Big]\, d^2r \tag{2.1}$$

Integration is over the entire scattering plane of the sample 'S'. Here 'k' is the wave vector of light and 'f' is the focal length of the 'scattering lens'.

A part of the scattered field forms a spherical wavefront which converges to a focus at 'p' while the rest of the field forms the background speckles. The profile of the focus is found to match that of speckle correlation function that is described in the previous chapter. This means, the focus has a size equal to an average speckle. Note that the width of the diffuse scattered intensity distribution is roughly $D = d + L$; where 'L' is the thickness of the scattering medium. This has a remarkable consequence that the aperture of the convergent field can be controlled by varying 'd' and/or 'L', which in turn varies the intensity distribution at z_s. This means, the size of the speckles and in turn that of the focus can be influenced by altering the aperture of the scattered field. By optimising these parameters Vellekoop *et al.* [23] showed for the first time that a focus smaller than that possible by a glass lens can be obtained. All thanks to wavefront shaping which transforms a scattering medium into a *scattering lens*.

Furthermore, the intensity of the focus is scaled by the number of segments N controlled by the modulator at z_i plane. The more the number of segments controlled, the more of the scattered field contributes to the intensity of the target.

$$I_p \propto N I_{z_s}(r)$$

It is safe to assume that it is impossible to focus all the incoming energy into the focus. So it is important to determine what the upper limit could be. As estimated in [36], the maximum achievable enhancement in intensity of the focus depends on the number of modulated segments of incoming wavefront. Furthermore depending on the modulation scheme used, the overall achievable enhancement can be different. The enhancement (η) is a ratio of intensity at the target after optimisation to the ensemble averaged intensity before optimisation and is given by

$$\eta = \frac{I_p}{\langle I_p \rangle} \tag{2.2}$$

This enhancement η is proportional to the number of degrees of freedom of input light that is controlled, i.e the number of segments the SLM is divided into. But then, as the number of segments increase, the size each segment decreases. As the segments get smaller, their respective contribution to the intensity enhancement at the target also reduces. This leads to an upper limit to the maximum achievable enhancement of about $\eta_{\text{max}} = 1000$ [37]. The maximum degree of control of incident light is achieved

when both amplitude and phase are modulated on all the segments. However for phase only modulation scheme $\eta_{\max}$ reduces to $\frac{\pi}{4}N$.

Wavefront shaping causes an increase in intensity at a chosen target, but at the same time it increases the intensity of background speckles as well, even though the algorithm did not optimise on the intensity of the background. Vellekoop *et al.* [19] describe this consequence using Random Matrix Theory as a proof of coupling of light to the various transmitting modes of the scattering medium in addition to coupling to the chosen target mode. In addition to this, the increase in overall transmitted intensity is attributed to the fact that the otherwise reflective modes of the scattering medium are now transmitting, as a consequence of optimisation.

2.2.2 Memory effect/Scanning the focus

In 1988, Feng *et al.* [38] showed that coherent light propagating through a multiply scattering medium exhibits a memory of its origin up to some extent. This was followed by the experimental results of Freund *et al.* [39] determining the extent of such a *memory effect*. Due to correlations between the multiple paths that light takes through a scattering medium, there exist a small range of distance up to which the light has a memory of it's origin i.e a small shift in the input wavefront is retained in the transmitted wavefront. This small shift can be, for example, tilting of the input wavefront, due to which the transmitted wavefront is also tilted. The result of such a tilt is the corresponding lateral shift of the whole transmission pattern in the observation plane. In scattering samples where transmitted light forms a speckle pattern, the speckle autocorrelation function peak has a non-zero width.

Since the focus is nothing but a brightened speckle; a tilt in the incoming wavefront $\Delta\theta$ shifts the focus laterally by Δf, like the rest of the speckle pattern.

$$\Delta\theta \approx \frac{\Delta f}{z}$$

here 'z' is the distance between scattering medium to the focal plane. The *isoplanatism* of the optimum wavefront is maintained within this range $\Delta\theta$ of applied tilt, beyond which the wavefront no longer retains the focus.

The tilt is equivalent to adding a linear gradient to the input wavefront. The maximum possible gradient without destroying the transmitted wavefront is obtained for an angle $\Delta\theta \approx \frac{\lambda}{2\pi L}$;where L is the thickness of the sample.

$$\Delta f \approx \frac{z}{n}\,\Delta\theta = \frac{z\lambda}{2\pi nL} \tag{2.3}$$

where 'n' is the refractive index of the medium. Similarly if a parabolic gradient is applied to the input wavefront, the focus shifts in the direction of light propagation. This too is possible due to memory effect. As long as the curvature of the parabola is small enough relative to the thickness of the sample, the corresponding shift in focus is given by

$$\Delta z \approx \frac{\lambda}{2\pi L}\frac{z^2}{nr}$$

where 'r' is the radius of curvature of the applied parabolic gradient.

2.3 Imaging with "scattering lens"

With the apparatus and the algorithm detailed above, we transform a scattering medium into a lens that focuses the scattered light to a point. One can draw parallels between such a scattering lens to conventional glass lens by comparing some of their properties. The following subsection provides such a comparison. It is followed by application of the scattering lens to microscopy. Thanks to optical memory effect, a focus created by wavefront shaping can be raster scanned just like scanning a focus of conventional lens. This allows for capability of the scattering lens to be used for imaging.

2.3.1 Resolution of scattering lens

Wavefront shaping allows for converting any scattering medium into a lens that focuses the scattered light to a point. The advantage of a scattering lens compared to a conventional lens is the fact that its focal length is tunable and so is the Numerical Aperture(NA).

As detailed in the Figure 2.4, NA of a scattering lens can be tuned in many different ways. NA of a lens is defined as the maximum half angle of the cone of light that can still make it through the lens.

$$\begin{aligned} NA &= n\sin(\theta) && \text{;where } \theta \text{ is the half angle of the cone} \\ &= n(\tfrac{D}{2f}) && n \text{ is the refractive index of the sample medium.} \end{aligned}$$

We can see that the half angle can be approximated to $D/2f$. This gives us two parameters to manipulate in order to tune NA. For a scattering lens, ‘D’ corresponds to the diameter of the diffused speckle pattern generated by the scattering medium. The thicker the scattering medium is, the larger the diffuse transmitted spot would be. Therefore a thick layer of paint produces a tighter focus than a ground glass diffuser. In the case of a ground glass diffuser, the diffuse spot is as wide as the illuminated beam. Secondly, NA can also be improved by reducing the focal length of the turbid lens to some extent. Figure 2.4 shows different ways of improving the NA of a scattering lens. A diffraction limited focus is achievable by using just a layer of scattering material [23].

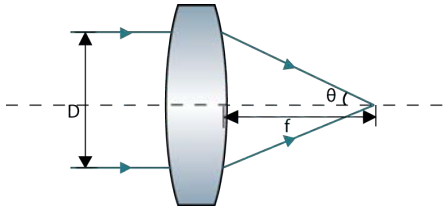

Figure 2.3: Numerical Aperture (NA) of a glass lens

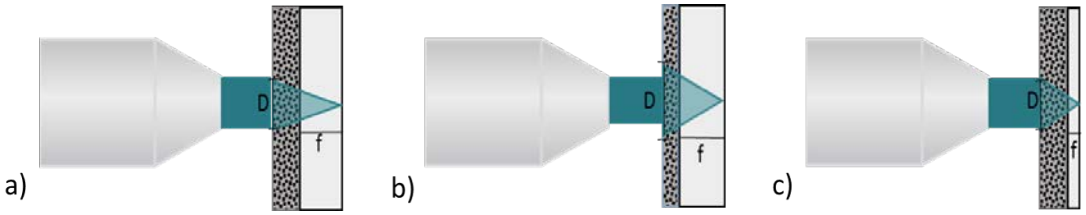

Figure 2.4: Improving NA of scattering lens: a)for a ground glass diffuser D before and after the scattering layer is the same. b) For a highly scattering sample such as white paint, D increases with the thickness of the paint layer due to diffusion; thus increasing the NA. c) NA can also be increased to some extent by bringing the focal plane closer to the scattering plane.

van Putten *et al.* [40] demonstrated yet another way of obtaining high NA lens out of scattering material, which they call the HIRES lens. They make use of a very high refractive index ($n = 3.41$) material such as Gallium Phosphide (GaP) as the substrate. By grit polishing one of the surfaces of this substrate a scattering medium is created. Using wavefront shaping technique this scattering surface is transformed into a high NA-HIRES lens. They have reported focusing light using this lens to sub-diffraction dimensions.

2.3.2 Scanning Results

Using the optimization procedure outlined in Section 2.1, a focus is obtained behind a scattering medium. Fluorescent particles present in the focal plane can now be ex-

a)

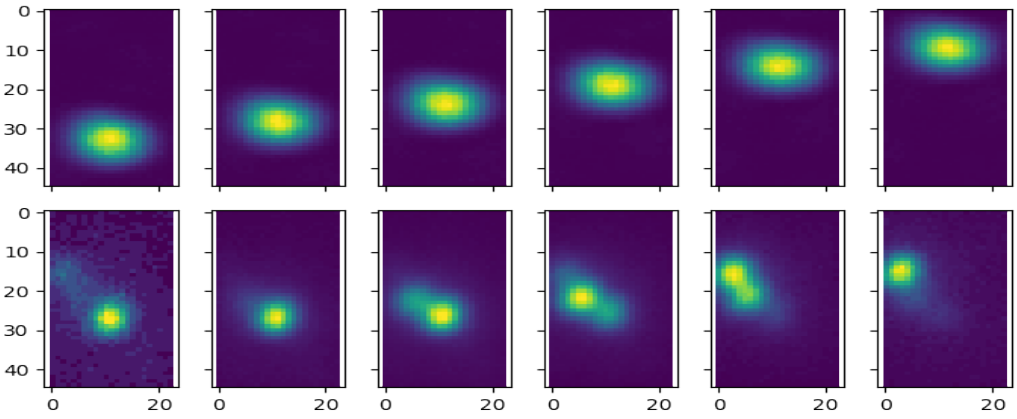

b)

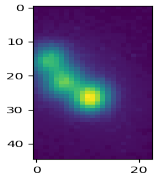

Figure 2.5: Memory Effect: a) Scanning the focus in lateral direction and resulting fluorescent response from the underlying beads. b) Beads constituting the scene that is being scanned in a)

cited with the focus and their response recorded. The turbid focus provides a contrast mechanism whereby the intensity at the focus is enhanced compared to it's background. As the sample response would be higher at the focus than due to the background, an image of the sample can be obtained with a good contrast. Such an imaging application is possible due to the ability to move the focus around in the focal plane, which is in turn possible due to optical memory effect (refer Section 2.2.2).

Once the optimum wavefront is constructed to obtain a focus at the target, a linear gradient is added to the optimum wavefront that then moves the focus around. The movement of the focus can be controlled by the precise phase shifts applied to the incoming light. The required linear phase gradient is generated either by using 2D scannable Galvo mirrors in the optical path, or it can also be generated by adding a linear gradient phase profile on the SLM. As for the movement of the focus along optical axis, parabolic phase shift is applied on the SLM. The response of a fluorescent sample lying in the focal plane, to the moving focus is then synchronously recorded to compose an image of the scene.

The results of 2D scanning of the focus and corresponding images of fluorescent beads are shown in Figure 2.5. Movement of the focus along the optic axis has been previously reported by Ghielmetti and Aegerter [41], the results of which are reproduced here with permission in Figure 2.6.

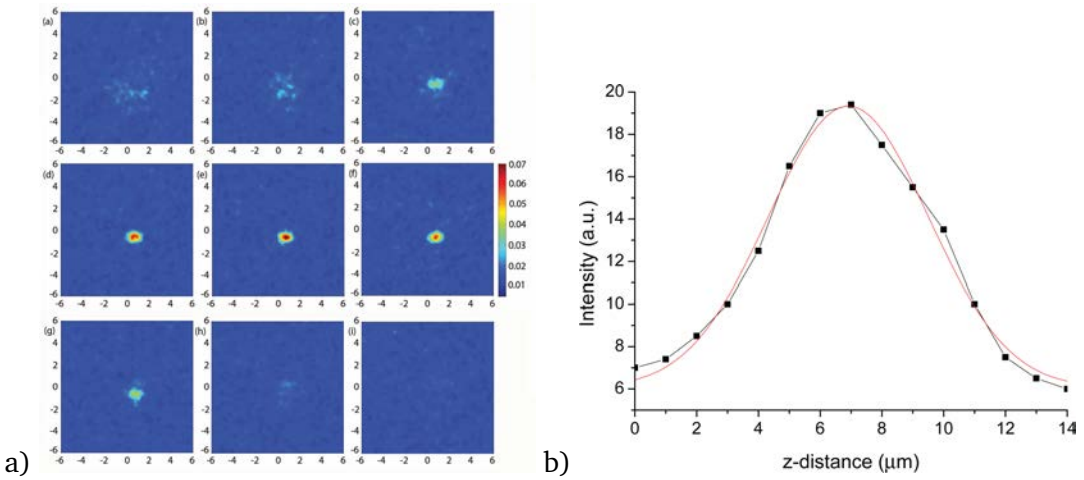

Figure 2.6: a)3D sections of a fluorescent bead captured by moving the focus along optical axis. b)Intensity at the position of focus at different depths. Reproduced with permissions from Ghielmetti and Aegerter[41]

Applying linear and parabolic phase gradients allows for a focus movement in a small volume of space which constitutes a the field-of-view(FOV) of the turbid microscope. This FOV depends on the range of memory effect available due to the scattering medium used. As stated before this range is limited by the thickness of the scattering medium used. For thick layers of white paint, this range quickly reduces with the thickness of the paint layer, and so does the FOV. Using eq. (2.3), for $L = 10\ \mu m$ of white paint, memory effect range $\Delta\ f \approx 6\ \mu m$. Whereas, for ground glass diffusers, since the thickness L is ill defined, the range of memory effect can be theoretically unlimited. Therefore a large FOV can be expected for diffusers.

2.4 Iterative Refocusing

In this section I will briefly describe our experiments with continuous scanning and refocusing behind a scattering medium. This section is a brief summary of the experiments we conducted with our post-graduate student Mr. Subas Scheibler and further details can be found in his thesis titled " Focusing and scanning light through turbid media"[42].

As shown in this chapter, imaging behind a turbid medium is made possible due to interferometric focusing of scattered light. The focus can be translated point by point in the focal plane due to memory effect. However as described before, the range of

memory effect reduces with the thickness of the turbid medium. Also if the arrangement of scatterers in the sample varies with time, as in the case of live biological tissues, the corresponding speckle pattern will also decorrelate, making the focus disappear. The optimum wavefront that focuses the light is valid only within the memory effect range and for time scales less than the speckle decorrelation time. Therefore when a scattering sample offers limited range of memory effect, or if the sample is a dynamically varying one, it can pose challenges to imaging with the turbid focus.

We set out to address the problem of limited memory effect range, with an outlook to cover also the short speckle decorrelation problem. For these experiments we use scattering medium of limited memory effect range, such as white paint samples with thicker layers. The range of memory effect was determined using eq. (2.3) and also experimentally verified from the procedure described in Section 2.3.2. The next step is to experimentally demonstrate that the interferometric focus can be regained outside of the memory effect simply by re-optimising the focus.

In order to demonstrate the working of this idea we conducted the following experiments. As samples, we worked with both diffusers and spray painted glass slides with varying thicknesses. The feedback for optimisation is derived from the fluorescent beads coated behind the scattering medium i.e indirect feedback mechanism. Before we start optimizing the incoming wavefront, K-means clustering algorithm is run on the camera image to get a rough estimate of the existing fluorescent probes in the entire field of view, as shown in the Figure 2.7. The live camera image is taken as an input to the clustering algorithm along with an initial guess of the number of clusters- K that potentially contain fluorescent beads. Then the algorithm assigns the K cluster centres randomly to the brightest of the camera pixels. Next, the pixels of the image are assigned to their closest cluster centres depending on their intensities. The clustering algorithm iteratively minimises the distance between each pixel and its corresponding closest center. At the same time it also updates the cluster center to be the mean of all the pixels in that cluster. At the end of this clustering procedure, a number of clusters that can potentially contain fluorescent beads are marked. This is further used as an input to the optimisation algorithm to actually enhance the intensity on the brightest cluster.

When the optimisation routine is run, the light starts to focus on the brightest of these fluorescent clusters. As the intensity of the focus is maxium when the intensity of probe is maximum, we get an indirect measure of increase in intensity of the turbid

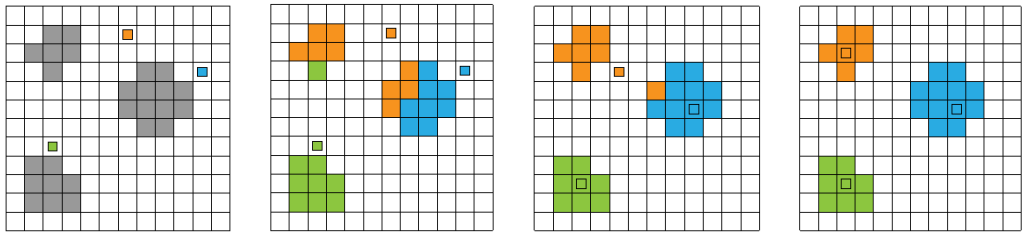

Figure 2.7: K-means clustering: iteratively determining the clusters containing fluorescent beads

focus. Therefore enhancing fluorescence intensity is equivalent to enhancing transmitted light[43]. At the end of the optimisation routine, we are left with the intensity of one of the probes maximised than the others, meaning that the focus is formed. The obtained focus is then scanned laterally by adding a linear gradient on the SLM, while continuously monitoring its intensity. The intensity drops as soon as the focus is moved away from the fluorescent probe. The focus is further translated in space around this probe in a raster scanning manner. If within this scan area there exist another probe, the camera records an increase in signal. Whereas the intensity in the focus itself may have dropped because of the translation. Therefore the overall intensity at this new position of the focus is not its maximum but requires refocusing. At this point, the optimisation procedure starts all over again to refocus the light onto the new probe. The newly obtained focus is scanned again and this procedure is iterated to cover all the K clusters in the entire field of view of the camera.

The results of this experiment are depicted in the Figure 2.8. Each frame in the figure shows a direct image of the fluorescent beads in the entire field of view of the camera. The inset shows the fluorescent intensity being maximised on one of the probes. The eventual scanning and refocusing results in the subfigures b) and c).

The fact that interferometric focusing can be achieved using fluorescence feedback implies that an optical access to the sample plane behind a scattering medium is not always required. Using fluorescence feedback, one can look not only behind scattering samples, but also inside them. With our experiments we further show that limited memory effect range no longer poses threat to imaging. These experiments show that it is indeed possible to expand the field of view of a turbid microscope by employing iterative refocusing. This can be a valuable tool to imaging in highly scattering materials with very small memory effect range. At this stage we have also limited ourselves to working with stationary scattering samples, but it can also be implemented on dy-

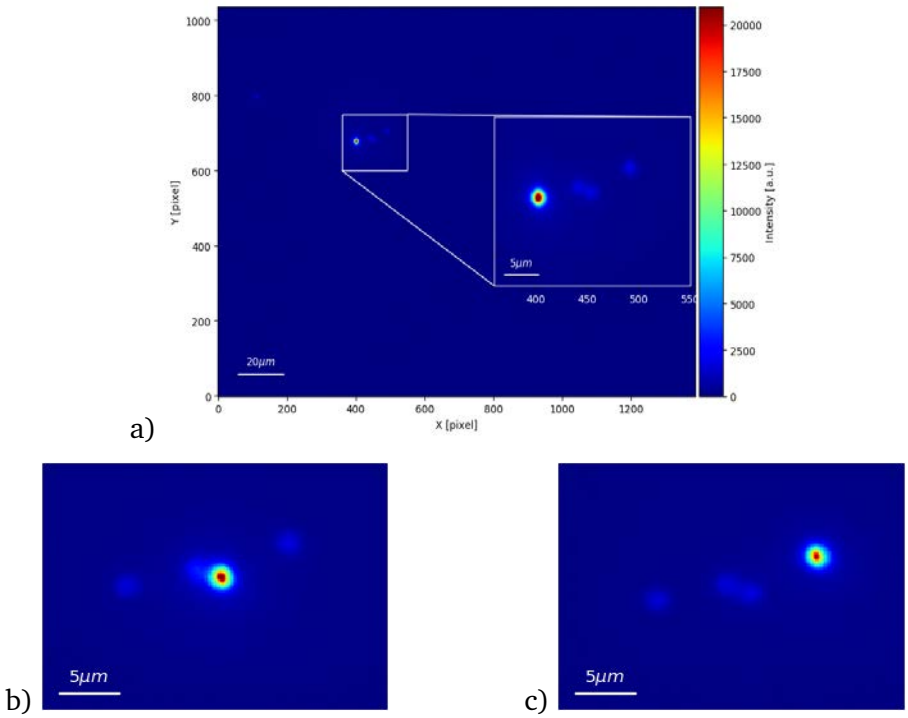

Figure 2.8: Iterative Refocusing: a)Initial focus is created on one of the beads. b)by scanning the focus, a second bead is encountered and light is refocused on it c)the process is repeated to focus on yet another bead

namically moving samples. The important factor to consider when working with such moving samples is the fact that the time it takes to obtain a focus should be smaller than the speckle decorrelation time. Although it is important to note that there are many factors that may affect the speed of interferometric focusing. For example, the speed of the wavefront modulator, the electronics that transfer large amounts of data as a part of optimisation routine. Most of all the signal from the fluorescent probe itself can pose a challenge, as typically due to weak signals from the probes, the camera exposure time will have to be increased which further affects the speed of optimisation.

2.5 Outlook

Wavefront shaping continues to work as an indispensable tool for understanding light propagation in diffusion regime. I have highlighted a specific application of wavefront shaping to microscopy. Using wavefront shaping a scattering medium is transformed into a lens that focuses the light to a point behind the medium. This so called turbid

focus provides a contrast mechanism through which optical signal is enhanced at the focus relative to its background. Such a contrast mechanism particularly calls for an application to imaging. Thanks to optical memory effect, a focus obtained in this manner is raster scannable like that of a conventional lens. The focal movement in 2D and 3D facilitates to obtain 3D volumetric images of samples of interest. The results pertaining to images of fluorescent samples thus obtained have been reported in this chapter. Due to the diffraction limited nature of the obtainable turbid focus, the images acquired by scanning this focus will also be diffraction limited, unless a HIRES lens made of higher refractive index is used, with which sub-diffraction imaging has been reported elsewhere. Nevertheless as shall be seen in upcoming chapters there are other ways to approach resolution of optical imaging beyond diffraction limit.

Chapter 3

Phase Mask Generation

Laser beam splitting and beam shaping are useful tools to manipulate a laser beam. Operating with lasers require it to have a certain beam shape i.e irradiance distribution depending on the application. The beam shape can influence its application greatly, a suitable beam profile improves the way to excite matter, or its effective propagation through wave guides and so on. The most common mode of operation across different lasers is the TEM_{00} mode with its Gaussian irradiance profile. Beam shaping refers to reshaping this Gaussian profile to some other profile such as a donut profile or a top-hat intensity profile or into one of the Laguerre-Gaussian modes [44]. For this reason beam shaping is sometimes also referred to as the mode conversion. Beam shaping can also refer to compression of laser pulses in space and time, that is useful in obtaining high energy short duration laser pulses.

Beam splitting on the other hand deals with splitting up of one laser beam into many smaller beamlets. These beamlets- typically organised on an ordered or random lattice can parallelize laser operation. Holographic optical tweezers [45],Optical trapping and manipulating micro structures [46] require multiple laser beams to operate in parallel. Some of the other applications include laser etching, micro-machining, image processing and so on. Laser beam splitting is achieved by introducing an aperture such as a diffraction grating in the beam path that breaks up the input beam into multiple orders in the far field.

Traditionally binary transparencies were designed to split the laser into multiple orders. But it is rather a challenging exercise to design suitable transparencies that can generate beamlets with custom structures that have different intensities or complex phase relationships among different orders. With the advent of Spatial Light Modulators(SLM), variety of complex light fields can be easily generated even in real time. These devices offer pixel by pixel control of amplitude and phase of light. Using devices such as Digital Micromirror Devices (DMDs) offers additional benefit of unprecedented speeds. By adjusting the voltage on individual pixels, desired aperture functions can be dynamically generated at kHz rates. One can also customize these aperture designs beforehand and apply them onto the SLMs. Aperture designs of this sort are given names across literature as- Diffractive Optical Elements(DOEs), Computer Generated Holograms(CGHs), array generators and so on. I refer to them as “Phase Masks” as I obtain them by modulating only phase of incoming light.

Some contents of this chapter have been published as: “Structured illumination behind turbid media”, A. Malavalli, M. Ackermann, and C. M. Aegerter, Optics Express Vol. 24, Issue 20, pp. 23018-23026 (2016)

Wavefront shaping to focus light through a scattering medium as described in the previous chapter can also be seen as an exercise of beam shaping. The goal of the current chapter though is to describe the methods used to generate beamlets out of a focus behind a turbid medium. It is worthwhile to compare some of the design strategies used to pre-compute these phase masks. In the following sections I will describe the theory and techniques to successfully transform a focus behind a turbid medium into an array of beamlets (also referred to as focal spots) using pre-computed phase masks.

3.1 Theory-Fourier Transforms and Convolution

Wavefront shaping provides a way of controlling the scattered light from a random medium to focus to a point. This kind of control over the scattered field can be further exploited to turn the random medium into a customisable aperture that produces user defined light fields. It is only a matter of determining the relationship between the scattered field and the target field- which can be recognised as that of a Fourier Transform relationship.

If $\tilde{\mathcal{E}}_i = \mathcal{E}_0 \exp(\mathrm{i}\phi)$ is the electric field of the light wavefront with phase ϕ modulated by the SLM to obtain a focus, it produces a scattered field $\tilde{\mathcal{E}}_s = c\, I_s(r)$ behind the turbid medium. Here, 'c' scales the fraction of the input intensity that is scattered.

The far field diffraction pattern of this scattered field resembles a focus obtainable by a normal lens, coining the term 'scattering lens'. The field at the focus is given by,

$$\tilde{\mathcal{E}}_f = \iint_S \tilde{\mathcal{E}}_s \, d^2r = \iint_S c\, I_s(r) \exp\Big[-\frac{\mathrm{i}k}{f}\,(x_s u + y_s v) \Big]\, d^2r \tag{3.1}$$

integrated over the scattering plane of the sample 'S'. Here (x_s, y_s) are the coordinates in the scattering plane and (u, v) in the focal plane respectively. Also, 'k' is the wave vector and 'f' is the focal length of the 'scattering lens'. The shape of this interferometric focus is same as the speckle correlation function eq. (1.1) [23].

To split the focus into multiple beamlets, we can make use of the convolution theorem. It states that, if

$\mathcal{F}\{\mathcal{E}_f(x,y)\} = E(k_x,k_y)$ and $\mathcal{F}\{f(x,y)\} = F(k_x,k_y)$, then

$$\begin{aligned}\mathcal{F}\{\mathcal{E}_f \circledast f\} &= \mathcal{F}\Big\{\iint_{-\infty}^{+\infty} \mathcal{E}_f(x,y)\, f(X-x, Y-y)\, dx\, dy\Big\} \\ &= \mathcal{F}\{\mathcal{E}_f(x,y)\}\ \mathcal{F}\{f(x,y)\} \\ &= E(k_x,k_y)\ F(k_x,k_y)\end{aligned} \tag{3.2}$$

i.e if $\mathcal{E}_f(x,y)$ represents the field distribution of the interferometric focus and $f(x,y)$ represents Dirac delta functions with their peaks located where the focal spots are desired,

$$f(x,y) = \sum_{m,n} \exp[\mathrm{i}\,\phi_{m,n}]\delta(x-x_m)\delta(y-y_n) \tag{3.3}$$

the convolution between the two leads to a multiple focal pattern in the image plane. Furthermore, the phase that needs to be added on the SLM plane in order to obtain the desired delta peaks as in eq. (3.3) can be extracted by propagating backwards to the SLM plane and by noticing that,

$$E(k_x,k_y) = c\, I_s(r) \exp\Big[-\frac{\mathrm{i}k}{f}\,(x_s u + y_s v)\Big] \tag{3.4}$$

Applying Fresnel diffraction formula [47] to eq. (3.3)

$$\begin{aligned}F(k_x,k_y) = \frac{\exp[\frac{\mathrm{i}k}{2f}\left(u^2+v^2\right)]}{\mathrm{i}\lambda f} \iint_{-\infty}^{+\infty} f(x,y) \exp\Big[+\frac{\mathrm{i}k}{2f}\left(x^2+y^2\right)\Big] \\ \exp\Big[-\frac{\mathrm{i}k}{f}\,(xu+yv)\Big]dx\,dy\end{aligned} \tag{3.5}$$

which takes us to the scattering plane $z = z_s$ plane in the Figure 2.2. Now, treating the scattering medium as a thin lens, $F(k_x,k_y)$ acquires a quadratic phase of the form $\exp[-\frac{\mathrm{i}k}{2f}\left(x^2+y^2\right)]$ which cancels with the corresponding term in eq. (3.5). Substituting eq. (3.3) in eq. (3.5), gives:

$$\begin{aligned}F'(k_x,k_y) = \frac{\exp[\frac{\mathrm{i}k}{2f}\left(u^2+v^2\right)]}{\mathrm{i}\lambda f} \iint_{-\infty}^{+\infty} \Big[\sum_{m,n} \exp[\mathrm{i}\,\phi_{m,n}]\delta(x-x_m)\delta(y-y_n)\Big] \\ \exp\Big[-\frac{\mathrm{i}k}{f}\,(xu+yv)\Big]dx\,dy\end{aligned} \tag{3.6}$$

where $F'(k_x,k_y)$ is the field obtained at the SLM plane that is capable of producing delta peaks in the image plane. Since phase-only modulation scheme is used in the experiments, only the phase of $F'(k_x,k_y)$ is extracted to be added onto the SLM.

We make use of this immense control over scattered field combined with the Fourier Transforming property of a lens to design a custom phase mask. To use it in our experiments, we first optimize the incoming light wavefront to focus behind a turbid medium. Then, the generated phase mask is simply added onto the SLM, which results in desired pattern of foci on the CCD.

3.2 Beam shaping behind turbid medium

The very first beam shaping optic ever to be designed was the so called Fresnel lens used on lighthouses to focus incoherent light. Fresnel lens is typically made up of concentric ring elements of varying thickness. Compared to conventional glass lenses, Fresnel lens requires a lesser material to manufacture. Therefore it is more favoured in places where huge diameter of lenses are required but with lower weight. However the quality of light focus is poor due to the non-continuous phase profiles imparted by the lens.

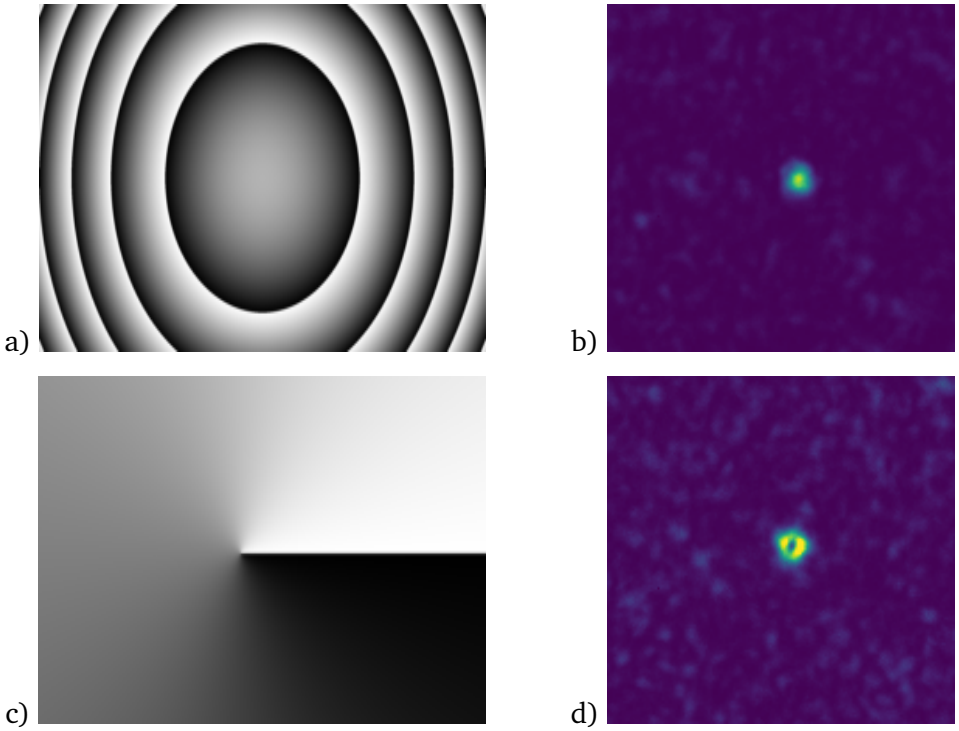

Figure 3.1: Beam shaping the focus of a scattering lens: a) & b) Fresnel Lens mask and corresponding focus. c) & d) Radial Phase mask and resulting shape of the focus.

Unlike conventional glass lens that uses refraction of light to focus light, Fresnel zone lens uses diffraction. An amplitude zone lens is made up of concentric rings of al-

ternating transparent and opaque regions. The transparent zones are placed at varying distances from the center such that the light coming from these zones constructively interfere at a particular distance along the direction of light propagation. This distance is then the focal length of the zone lens. Contrarily, a phase zone lens is made up of repeating elements of modulo 2π phase profiles. It serves the same purpose as an amplitude zone lens but only more efficiently. Traditionally, Lithographic etching techniques were used to design such zone lenses. However with the advent of SLMs, they can be generated more easily and in real time.

As discussed in the Section 3.4, similar patterns can also be used to move the focus behind turbid medium. Figure 3.1a shows a Fresnel lens pattern loaded onto the SLM move the focus along the optical axis. By adjusting the number of rings and width of the outer most ring, the focal length of the lens pattern can be varied. In the Figure 2.6, the authors have used these patterns to scan the focus in 3D.

A radial phase profile such as in Figure 3.1c would apply a radial gradient in phase shift of π such that the light coming from the radially opposite segments destructively interfere in the center, thus creating a vortex Figure 3.1d. This beam profile has been popularised recently through its application in Superresolution-STED microscopy[7], where a secondary de-excitation beam with donut profile suppresses the fluorescence in a ring like region around the focus of a primary excitation beam, thus enhancing the resolution.

3.3 Algorithms for phase mask generation for beam splitting

A diffraction grating splits the laser beam up into multiple orders in the far field, with varying intensities. Different applications require the gratings to diffract light into specific orders more intensely than others. The optical power distributed among different orders depends on the grating design. Specialised design strategies are adapted by the manufacturers to suppress the unwanted orders thereby increasing the efficiency of the gratings. Blazed gratings are one such design strategy that puts maximum power in a chosen diffraction order with negligible losses. However more complicated strategies may be necessary for splitting the beam into multiple orders in 2D or even 3D. With the advent of SLMs designing of gratings has taken a different direction. Any complicated design of the grating can be realised by electronic means cheaply and efficiently. This has given rise to a new field of designing Diffractive Optical Elements (DOEs) that mask

the SLMs to behave like diffraction gratings. By electronically controlling the individual pixels of the SLM, tiny aberrations can be tweaked and the loaded DOE can be stably held for long periods of time, or one can load many different DOEs sequentially so as to dynamically generate different diffraction patterns. In this section I will describe some of the analytical and programmatic approaches to designing DOEs to generate specific diffraction patterns.

Before SLMs came into existence, binary amplitude transparencies were used as the beam splitting elements. Binary means that they have regions that either allow or block the light to pass through, making them easier to manufacture. Dammann and Klotz [48] pioneered phase grating designs containing binary (or finite) phase levels as well as continuous phase distributions. Due to its simplicity and ease of manufacturing, the binary Dammann gratings are widely used, so much so that HOLOEYE-Photonics provides a software interface to realize many different Dammann gratings using their SLMs. These binary Dammann gratings are useful in producing diffraction patterns consisting simple configurations of beamlets.

As we intend to generate a diffraction pattern behind a turbid medium, we would be splitting up a focus behind the turbid medium into an array of foci, rather than splitting a direct laser beam. As described in the theory section, once we determine the optimum wavefront that perfectly focuses through a scattering medium, we have the means to split this focus up into multiple foci. In this process we are basically designing the function $f(x, y)$ in eq. (3.3). In order to generate a lattice of delta peaks of the form in eq. (3.3), we use a programmatic approach using FFT functions of Python. For the purpose of generating phase masks, we can ignore the fact that a turbid medium is used, as the effect is the same as if using a thin lens. Then the designed aperture is Fourier Transformed by our "lens" onto the camera. As I will show in this section, this Fourier Transform relationship between the SLM plane and the CCD plane makes it easier to calculate the required phase mask.

Inspired by Dammann gratings, I set out to design binary phase masks that can generate a regular lattice of 3X3, 4X4 upto 6X6 focal spots. Starting in the focal plane where the delta peaks are desired; with a simple design of 2 delta peaks along horizontal axis on either side of origin at distance 'd'. Eq. (3.3) takes the form,

$$f(x) = \delta[x - (+d/2)] + \delta[x - (-d/2)]$$

whose Fourier Trasform is,

$$F(k) = \mathcal{F}\{f(x)\} = \mathrm{e}^{(+\mathrm{i}kd/2)} + \mathrm{e}^{(-\mathrm{i}kd/2)} = 2\cos(kd/2)$$

which simply corresponds to a cosine function on the SLM plane. This cosine function of spatial frequency $(kd/2)$ in binary state resembles a pattern of black and white stripes. Using linearity property of Fourier Transforms [47] this idea can be extended to a sum of many cosines.

$$\begin{aligned} F(k) = \mathcal{F}\{f(x)\} &= \mathrm{e}^{(+\mathrm{i}kd/2)} + \mathrm{e}^{(-\mathrm{i}kd/2)} + \mathrm{e}^{(+\mathrm{i}3kd/2)} + \mathrm{e}^{(-\mathrm{i}3kd/2)} \\ &= 2\cos(kd/2) + 2\cos(3kd/2) \end{aligned} \tag{3.7}$$

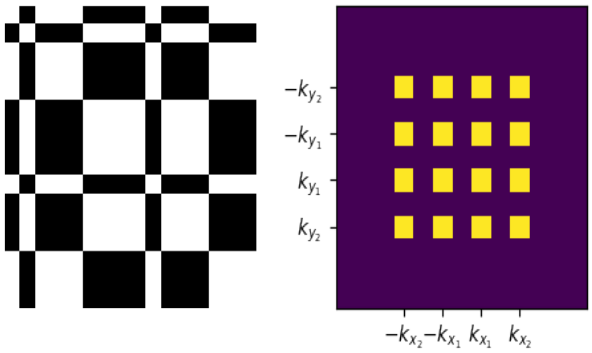

Figure 3.2: Phase mask to generate an array of 4X4 delta peaks and its Fourier Transform

A binary mask made out of Eq. (3.7) will produce 4 delta peaks at positions $\pm 1k$ and $\pm 3k$ respectively along with other unwanted background peaks. By adjusting the phase difference between these two cosines we can shape the relative intensities of the delta peaks along with suppressing the unwanted peaks. Thus by altering 3 parameters - the spatial frequency, phase and amplitudes of the individual cosines it is possible to obtain delta peaks on a regular 1D grid. Rotating the pattern by 90° rotates the delta peaks onto the vertical axis. A 2D array of peaks can be generated by then combining a horizontal and a vertical array producing gratings. A sample phase grating that can generate 4X4 peaks is shown in the Figure 3.2.

In other terms, a grating that generates several delta peaks or the diffraction orders can be seen as a linear combination of its Fourier components. The amplitude of each order is proportional to its corresponding Fourier component making up the grating. Then the problem is rephrased as to determine these Fourier components that maximise the amplitude of desired orders. Dickey *et al.* [49] provided an analytical framework for such a beam spitting problem. They formulated it as a constrained optimization problem where an input grating of the form $\mathrm{e}^{\mathrm{i}\phi(x)}$ splits the incoming beam into a set

of symmetric modes a_k ;$(k = 0, \pm1, \pm2, .. \pm m)$, subjected to a constraint that all those modes have same amplitude. The resulting modes represent the delta peaks placed on a desired lattice in the Fourier space. The efficiency of such a grating is given by the ratio of energy in these 'm' modes to the total energy in all possible modes. They show that the optimum phase function can be found as

$$e^{i\phi(x)} = \frac{s(x,\alpha,\mu)}{|s(x,\alpha,\mu)|} \quad \text{;where} \quad s(x,\alpha,\mu) = \sum_{k\in K} \mu_k e^{i\alpha_k} e^{ikx} \tag{3.8}$$

which then shapes the amplitude of the k modes

$$a_k = \frac{1}{2\pi}\int_{-\pi}^{\pi} e^{i\phi(x)} e^{-ikx} dx$$

This constrained optimization problem is solved for the parameters μ_k and α_k for a set of modes $k \in K$. The set K for example constitutes the modes $\{\pm2, \pm4, \pm6\}$, i.e 6 beamlets, making its corresponding grating $\phi(x)$ a 1:6 beam splitter. The solutions μ_k and α_k to eq. (3.8) for a number of 1:k beam splitters has been determined by Dickey *et al.* [49]. The estimates for μ_k and α_k are first determined by solving a least squares optimisation, these estimates are then used as inital guesses to solve the actual problem given by eq. (3.8). The least squares step tries to reduce the difference between the desired function $e^{i\phi(x)}$ and an optimal function that maximises the efficiency of the grating [50] [51]. These estimates obtained in this step help to shape the optimal phase function $\phi(x)$ using methods such as gradient descent.

Beam splitting problem can also be solved using phase retrieval algorithms. Gerschberg and Saxton developed an algorithm to determine the phase information from an intensity measurement [52]. Since its inception, this so called GSalgorithm has been applied in various fields such as signal processing, image analysis and so on. Most of the iterative phase retrieval algorithms in the literature are a modified version of GSalgorithm [53]. Other type of algorithm include phase retrieval by Gradient Discent such as a two step iterative phase retrieval technique demonstrated by M. Farn [54]. Although originally developed for retrieving phase information of an intensity pattern on the diffraction/image plane, GSalgorithm can be applied just as well for the generation of phase masks [55]. GSalgorithm has been applied to design phase masks that generate not only 2D but also 3D arrays of focal spots [56]. As the configuration of target focal spots in the image plane is known *a priori* (because it is user defined), the corresponding phase pattern on the object plane can be determined by iterative forward and inverse

Fourier Transformation. At each iteration, constraints are applied so that the result in the image plane approaches closer and closer to the target.

A cartoon describing the algorithm is shown in Figure 3.3. The target pattern is formed by an intensity distribution of the focal spots in the image plane. The algorithm starts from the object plane, where the complex field is formed by a Gaussian laser intensity and a random phase pattern. It is padded with zeros to increase the sampling in the image plane; such that when Fourier transformed, the resulting spots can be observed in more detail. Upon forward propagation with FFT, one obtains a random intensity and phase distributions. The phase information of this result is kept as is, whereas the amplitude is replaced with that of the target. This constitutes the Fourier domain constraint and the new field obtained is back propagated to the input plane by Inverse Fourier Transformation. In the object plane another constraint is applied so that the amplitude of the resulting field is replaced with that of the laser while keeping the phase information as is. The field obtained is Fourier Transformed again. This process is repeated over many iterations; eventually the obtained amplitude converges to the arrangement of focal spots in the target. However the relative intensities of the peaks may not be uniform. We found it useful to impose additional constraint in the Fourier plane to reduce the variance in intensities among the focal spots.

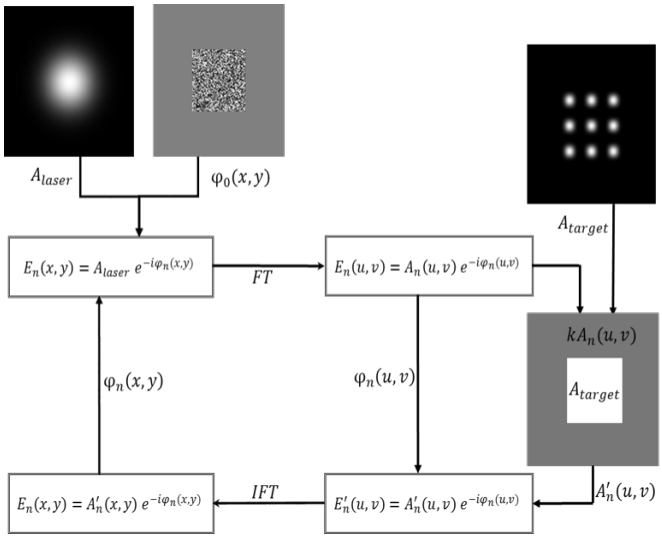

Figure 3.3: GS Algorithm

Using the algorithm described so far, we obtained phase masks that enhance the intensities of the desired focal spots. However in addition to the desired spots some unwanted background spots were also enhanced. In an article by Ogura *et al.* [57] followed by another one by Wu *et al.* [58], they showed that by dispersing some of the energy from the spot array region to its surroundings it is possible to obtain sub-diffraction spot arrays. We found that this approach of dividing the target region and applying different constraints in each- is

actually also useful to get rid of the unwanted background spots. This trick aims at dispersing the energy from the spot region to the surrounding region, thus it helps to suppress the unwanted background spots along with making the spots narrower. In order to achieve this, the Fourier plane is divided into two regions, one where the spots are to be placed and the other is the region surrounding the spots. A modified set of Fourier domain constraints are imposed to the amplitude of the field, while phase information is kept. In the region of the spots, the amplitude $A_n(u,v)$ is changed to the that of the target as before i.e A_{target}. In the surrounding region, the amplitude is scaled by a constant 'k' i.e $kA_n(u,v)$. The value of the constant 'k' between 0 and 1 was chosen empirically by trial and error. This modified amplitude $A'_n(u,v)$ and the phase $\phi_n(u,v)$ constitutes the new field which is back propagated to the object plane by Inverse Fourier Transformation. After a fixed number of iterations, an amplitude distribution closest to the target was obtained, this time without any unwanted background spots. The corresponding phase masks were saved in the formats acceptable by the SLM, so that they can be used in the experiments.

This kind of iterative approach to phase mask generation has the advantage over shaping the diffracted modes using eq. (3.8), and that is the fact that the focal spots generated using iterative approach can have any custom configuration. Whereas with constrained optimisation approach in eq. (3.8), only those modes allowed by the phase grating are enhanced, which are typically on an ordered or semi-ordered(asymmetric) grid. In the constrained optimisation approach, the coefficients of the Fourier components have to be determined only once, thereafter the process of phase mask generation is straight forward, whereas with GSalgorithm, phase masks will have to be iteratively determined each time a different configuration of spots is desired. The experimental performance of the approaches described so far are compared in the next section.

3.4 Results and Discussion

After generating phase masks using the techniques described so far, they were tested in the experiments. These phase masks are typically saved as bitmap files containing 8bit grayscale values(0-255). When loaded onto the SLM, its hardware refers to the look-up table (LUT) to set the voltages corresponding to these grayscale values.

The experimental setup to obtain multiple focal spots behind turbid medium is as shown in Chapter-2. Light from the SLM incidents on a scattering medium such as a

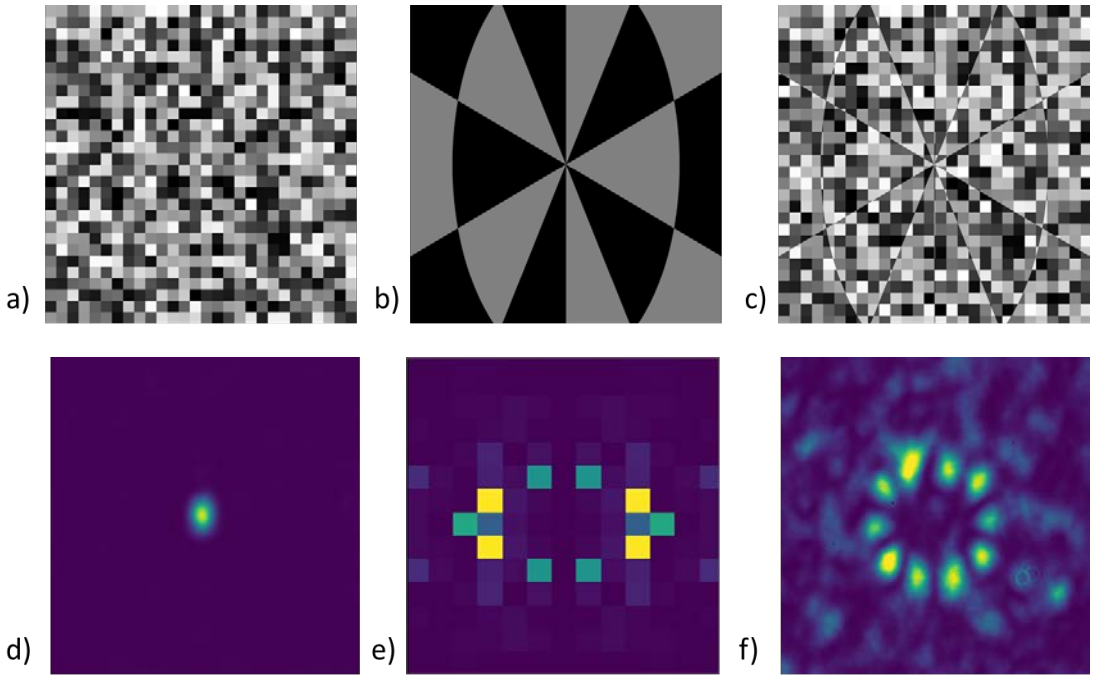

Figure 3.4: Figure above shows the phase at the SLM plane producing multiple foci. To the optimum wavefront a) leading to a focus behind the turbid medium, when a phase mask such as b) is added, the resulting phase would look like c). Figure below shows the convolution operation on the CCD plane. When the turbid focus d) is convolved with a lattice of delta peaks e), it results in the same lattice of multiple foci f). Also, the bottom subfigures d), e), f) are respectively the Fourier Transforms of the top subfigures a), b), c).

diffuser. The transmitted light leaving the diffuser forms a speckle pattern on the CCD. The intensity at a small region of the size of a single speckle is monitored on the CCD. An optimization routine described in Chapter-2 determines the optimum wavefront required to focus light on the speckle being monitored. The optimum wavefront focuses to a point on the back side of the diffuser. In order to transform this focus into an array of multiple focal spots, the generated phase mask is loaded onto the SLM[59]. This step is better understood from the Figure 3.4 and thanks to the convolution theorem described by eq. (3.2). Due to the rectangular display of the SLM, the obtained focus attained an oval shape instead of a circular one. This also meant that the multiple spots would be placed on a rectangular lattice. As and when required, a more aesthetically pleasing square lattice was obtained by simply blocking away the edges of the SLM with a pinhole. The region corresponding to the blocked region of SLM are shown in black color for some of the phase masks in the following figures.

This way a diffuser is made to not only focus the incoming light but also to act as

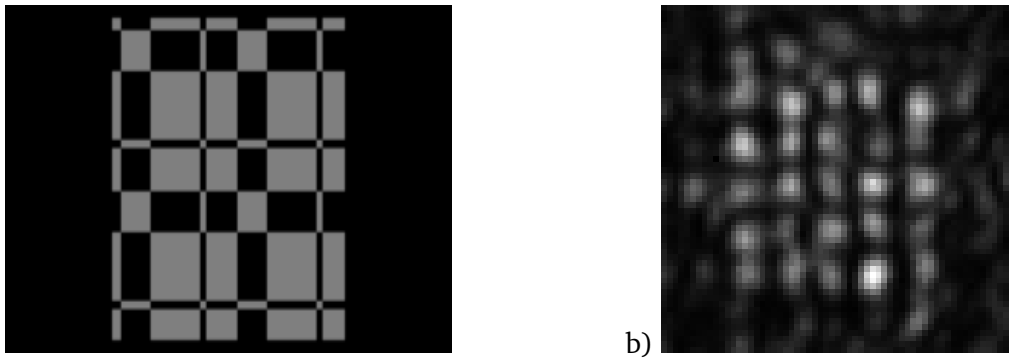

Figure 3.5: Result of 5by5 spot generation using eq. (3.7), background speckles are not due to the lower efficiency of the technique but rather the number of spots tending towards the upper limit.

a flexible aperture that generates array of foci of any user defined configuration. Figure 3.5 shows the result obtained with phase mask generated using eq. (3.7). As can be seen in this figure, the focus is transformed into an array of 5X5 foci placed on a periodic square lattice. We observe that there is an upper limit to the maximum number of obtainable foci. As the intensity at each focal spot is derived from the overall intensity enhancement achieved during optimisation process, there is a trade-off between number of focal spots and intensity of each focal spot. The intensity of the initial focus gets redistributed among the multiple foci created by the phase mask. Therefore with the increasing number of foci, their respective intensities reduce to an extent that if the number of foci is roughly > 30, then due to their lower intensities, they can not be distinguishable from the background speckles.

The constrained optimisation approach in eq. (3.8) is compared with the GSalgorithm approach in Figure3.6 for the case of 1D array of 9 focal spots. In terms of efficiency of distribution of energy among a set of chosen modes, both these approaches perform equally well. The generated focal spots have an intensity uniformity close to 1. The important difference between these approaches subtly shows up in the shape of the resulting spots. In the GSalgorithm approach, as the applied constraints only account for the placement of the spots on a grid of a given distance of separation it performs well on that aspect. But in the direction perpendicular to the grid, there is no constraint applied to limit the size of the foci. This results in boradening of the foci along this direction. i.e the size of the foci perpendicular to the grid is greater than the size of the foci along the grid direction. When GSalgorithm approach is used to split the focus into a 2D grid, there is equal control in both the directions. In this case we saw that the

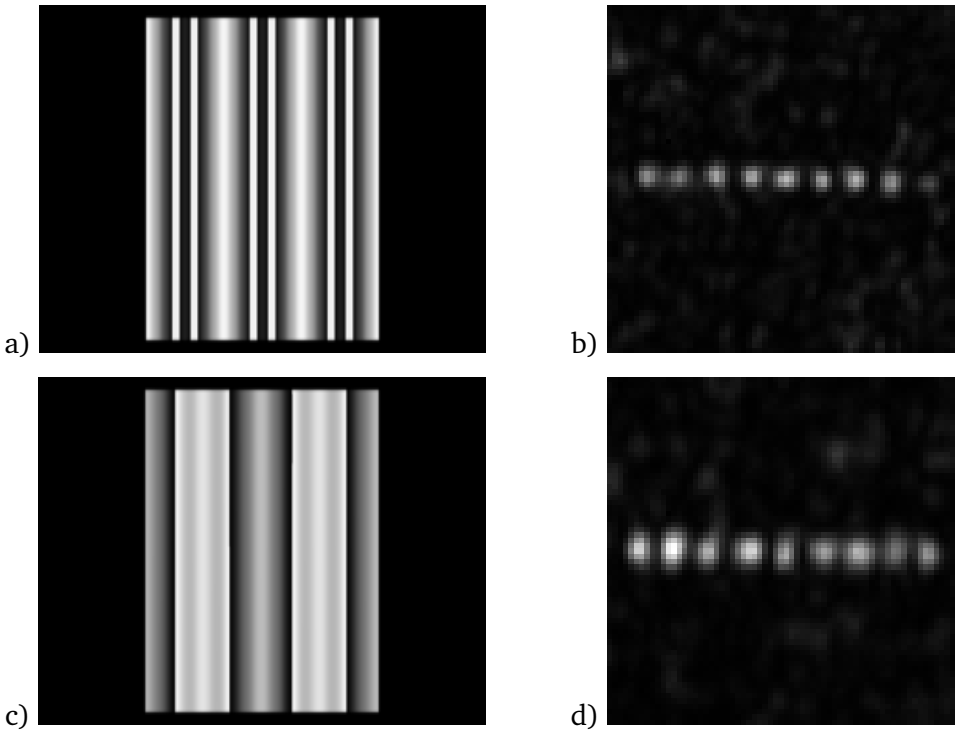

Figure 3.6: Comparison performance of constrained optimisation and GSalgorithm. a) & c) show the phase mask and resulting focal spots obtained with constrained optimisation technique. c) & d) show the same for GSalgorithm. The focal spots are slightly oval in the latter case.

individual spots were more circular than in the 1D grid case. This fact is also heightened in the article[58], where they show that the spots on the extrema of the lattice were broader than the ones in the center. This is however not the case with solutions obtained for the eq. (3.8), which shows circular focal spots placed on a regular grid.

The multiple foci generation described so far works consistently and efficiently. However there are some experimental factors that often influence the quality of focal spot generation. Some of the observed glitches include: i)missing spot problem- some focal spots that are supposed to appear at given locations sometimes do not appear. This happens only in the limit of maximum number of foci. ii)The intensity profile of each foci are different from each other. iii)The spacing between the foci may not always be constant. These factors turned out to be the consequence of either diffuser uniformity, or presence of dust particles or scratches in the plane where focal spots are generated. One of the other factors that also cause these glitches was the fact that the illumination of the diffuser not being uniform. If the illuminating beam is tilted, the contribution of

the scattering medium to the optimized focus will vary, and thus affect the result of the loaded phase mask as well. It is also clear that the achieved enhancement of intensity of the focus in turn affects the intensities of the subsequent multiple foci.

The technique of generating focal spots using phase masks can also be extended to further move around the generated foci in space. By applying an additional phase gradient on the SLM, it is possible to move the multiple foci in the focal plane. For example, a linear gradient across lateral direction shifts the foci by precise amounts. A rotation in co-ordinate system in the phase mask rotates the foci around origin. By choosing the base spatial frequency of the grating in the generated phase mask, all the higher frequencies get scaled resulting in increased spacing between the spots. These operations are demonstrated in the Figure 3.7.

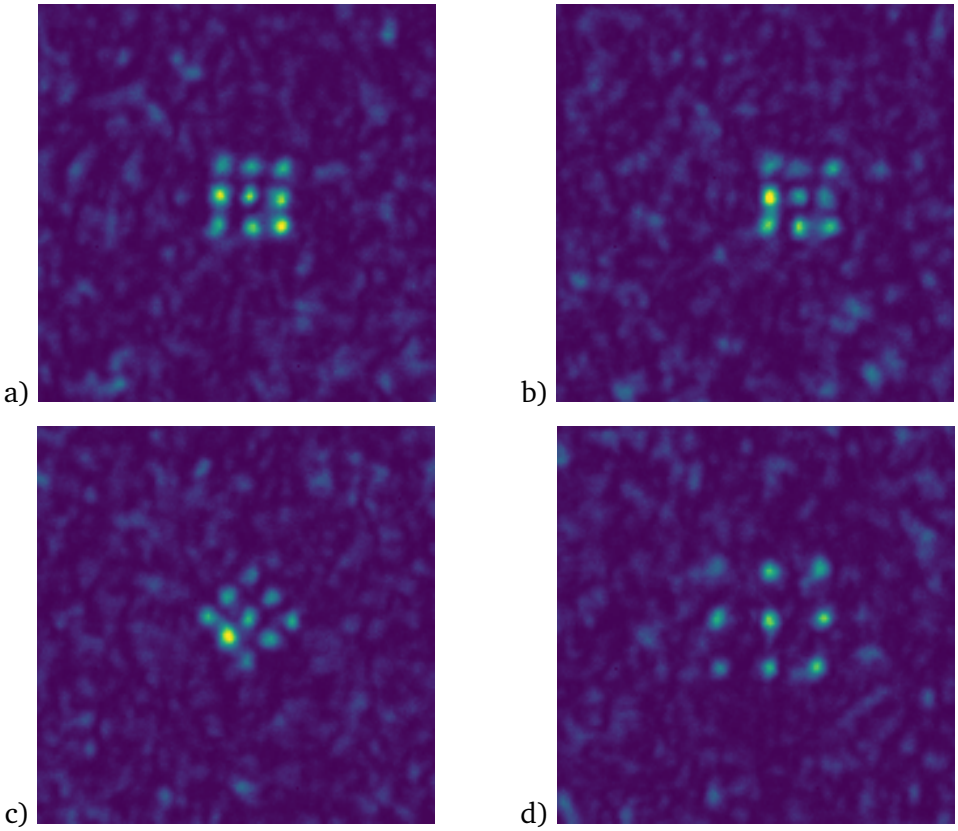

Figure 3.7: a)original foci b) a) when translated c) a) when rotated d) a) when scaled.

The multiple foci generation behind a scattering medium using phase mask technique is straight forward and robust. The fact that phase masks can be generated offline and loaded in the experiments when needed, makes the technique time efficient.

The focal spots can be moved around flexibly in space and their positions can be determined precisely by measuring the distances in the image in pixels. This sort of control and precise movement of the focal spots makes it a valuable tool to further explore its applications. As shall be seen in next chapter, the precise measurement of movement of focal spots has bigger consequences in the implementation of Structured Illumination Microscopy.

3.5 Direct Optimization on a lattice of focal spots

As an extension to the direct feedback optimisation method described in the previous chapter, we explored the possibility of generating multiple foci rather than single one. In the direct feedback optimisation scheme, a group of pixels on the camera corresponding to a small region behind the turbid sample is defined as a target. The algorithm takes the intensity at this target as an input and iteratively enhances this intensity by modulating the input wavefront. When an array of foci is desired, one can in principle define multiple target regions on the camera and simultaneously enhance the intensity in all of them [20].

Our qualitative observation of multiple configurations of foci suggest the following. The intensity of the generated foci decreases with the increasing number of foci. This is as expected, because the intensity at an otherwise single focus is now distributed among multiple foci. So the more the number of foci, the lesser their respective intensities are. Further, the uniformity in intensities among the focal spots is not uniform, as the optimisation algorithm tries to increase the intensities of the foci only, and does not take into account the variance among their intensities. This leads to variation in intensities of the spots depending on the configuration of the spots desired and initial conditions.

When comparing the spots generated with phase masks and those obtained by direct optimization (in Figure 3.8), it is clear that phase mask technique is more robust. Although technically direct optimization can be performed by imposing additional constraints (as also applied for in GSalgorithm for example), the optimization routine would be time consuming and computationally challenging. Besides, phase mask technique is more straight forward, as the necessary patterns can be generated *a priori* and loaded on the SLM in real time experiments. A bigger advantage of this technique is that the pre-computed phase mask can be used when the focus is obtained by indirect optimization routines as well (for example with fluorescence feedback etc, refer

Chapter-2). This is however not possible to do with direct optimisation, as a regular array of feedback probes will have to be arranged for.

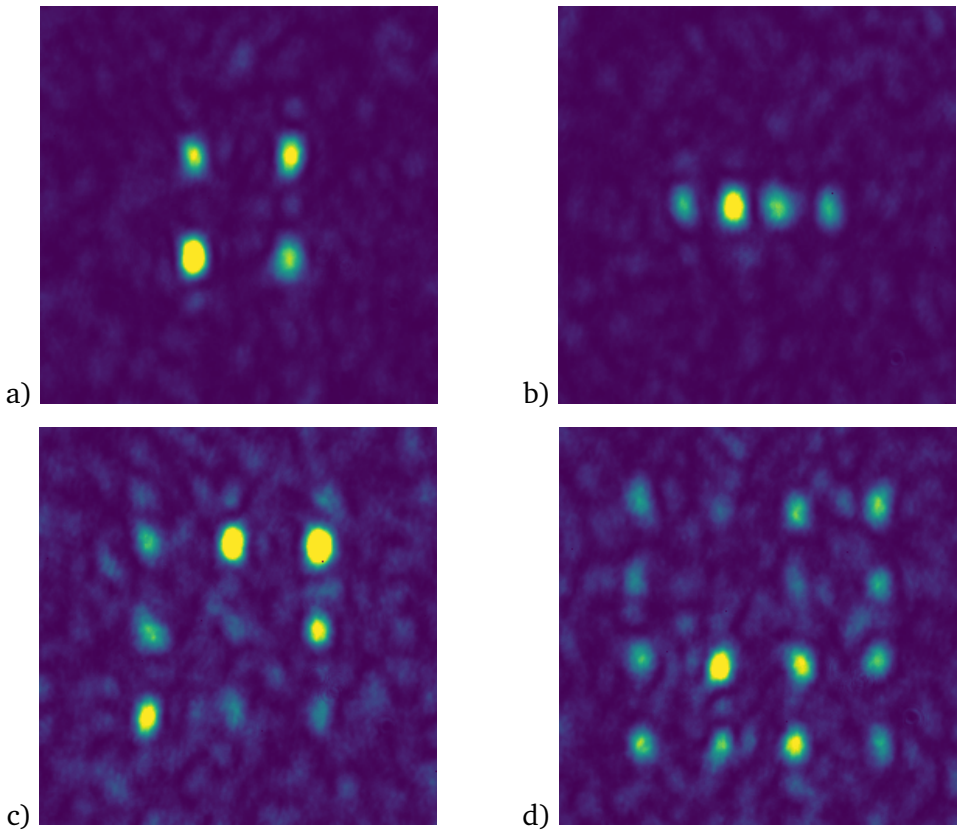

Figure 3.8: Direct optimization onto various configurations of focal spots

3.6 Outlook

In this chapter, I have demonstrated a technique to transform an interferometric focus behind turbid medium into an array of focal spots. This is made possible due to the Fourier transforming property of the scattering lens and the relationship between the scattering plane and the focal plane. It is exploited to design a phase mask that can be loaded onto the input plane of a scattering medium to influence the result on the camera plane. I have described different strategies to design such phase masks and compared their corresponding results. The main application of splitting the focus into multiple foci as shown in this chapter is to parallelize its operation. For example, instead of a single focus exciting a sample underneath, now multiple foci can do the job simultaneously.

The future scope of multiple foci behind scattering media relevant to this thesis is its application in imaging. i.e the foci simultaneously excite a sample at multiple locations in the focal plane. The response of the sample from these locations is recorded as an image. By exploiting the flexibility in movement of the foci, multiple positions of the sample can be simultaneously excited and scanned across just like how it was done with a single focus in Chapter-2. This will in turn reduce the image acquisition time, thereby increasing the efficiency. However more interesting application can be thought of for the periodic focal spots. As will be seen in the next chapter, a super-resolution fluorescence microscopy technique such as Structured Illumination Microscopy(SIM) requires a periodic illumination system just like the focal spots that we are able to generate. This means the lattice of focal spots can be treated as a periodic illumination system in a widefield imaging setup. Using SIM it is possible to enhance resolution of an optical microscope beyond diffraction limit. Therefore we further explore this possibility of enhancing the resolution of our *turbid microscope* by the application of SIM behind turbid media.

Chapter 4

Structured Illumination Microscopy with “scattering lens”

Flourescence Microscopy is an ubiquitous tool for bioimaging. The resolution of a microscope has been for long considered limited by the diffraction of light, also called Abbe's diffraction limit. But in the past couple of decades many new techniques have emerged that overcome this limit and allow super-resolution imaging. They include near-field scanning optical microscopy (NSOM) [60], stimulated emission depletion microscopy (STED) [9], stochastic optical reconstruction microscopy (STORM) [10] etc. These techniques make use of special mechanisms to narrow the PSF of the microscope, thereby enhancing the resolution. This is either due to the specially tailored light source, or by exploiting non-linear nature of fluorescent dyes. Structured Illumination Microscopy (SIM) [61] on the other hand, instead of exploiting the nature of fluorophores achieves resolution enhancement due to patterned illumination. In recent years, another patterned illumination technique called Multi-spot Image Scanning Microscopy(MISM) has demonstrated an improvement in resolution of a confocal microscope by a factor two [62]. Also other deconvolution approaches have been demonstrated to enhance the resolution by factor $\sqrt{2}$ over widefield imaging [63]. The reported resolutions of state of the art systems of localisation techniques or STED are about a few tens of nanometers. The patterned illumination techniques on the other hand achieve upto about a $100nm$ resolution which is much below the diffraction limit for visible light ($200 - 300nm$).

There is another important characteristic of a microscope- the penetration depth, which describes the maximum depth/thickness of a sample up to which the images can be obtained. All the above mentioned techniques are designed to address imaging of optically thin samples. The penetration depth achievable with these techniques however is limited, typically to a few tens or hundreds of microns. Penetration depth is greatly affected due to scattering of light. There exist spectroscopic and tomographic approaches to obtaining sample information from the scattered light instead of the ballistic light; such as Diffuse wave spectroscopy, Infrared Optical Tomography and diffuse optical tomography [13]. Optical Coherence Tomography(OCT) [15] is capable of obtaining remarkable optical sectioning, relying on the unscattreed or ballistic light through optically transparent tissues. By virtue of this OCT is widely used in Opthalmic Imaging [15]. However the resolution achievable with OCT is limited to few microns. On the other hand methods such as Two-photon or Multi-photon microscopy attempt to increase the penetration depth of a confocal microscope by employing non-linear behaviour of the samples [14]. But due to the application of high intensity light sources

or choice of dyes or both, these techniques fail to be versatile. So one clearly sees a trade-off between achievable resolution and penetration depth.

With the advent of wavefront shaping or interferometric focusing of light [23], the problem of microscopy can be seen in a very different perspective. Using wavefront shaping, light can be made to focus through thick multiply scattering materials, as already described in Chapter-2. Moreover the ability to control the scattered light makes it that light scattering is no more a hindrance to imaging. Therefore by utilising interferometric focusing and the translation invariance of the obtained focus due to memory effect (refer Chapter-2), a scattering medium is transformed into a lens that can be used for imaging samples hidden behind the medium. As shown in Chapter-2, diffraction limited images can be produced by scanning the interferometric focus in 2D and 3D. This is called the Scattered Light Fluorescence Microscope [64] [43] [41], which is able to produce images with resolution similar to widefield fluorescence microscopes but at unprecedented depths of multiple scattering regime.

Imaging through multiply scattering materials has gained increasing attention in the recent times [65] [66]. A review of latest developments in this field is nicely covered in an article by Mosk *et al.* [67] Using the autocorrelation function of the speckle pattern through a scattering medium, Bertolotti *et al.* [68] showed that the sample information can be deconvolved from the acquired images. They make use of the fact that the autocorrelation of measured intensity in the acquired image is a product of sample autocorrelation and speckle autocorrelation. Since the speckle autocorrelation is known precisely, the sample information can be iteratively deconvolved with a resolution given by the average speckle size [68]. Using similar principles a single shot imaging in the diffuse scattering regime was also demonstrated by O.Katz *et al.* [69]. Yet another attempt has been made by J.Schneider and Aegerter [70] where they employ guide-star deconvolution method to obtain diffraction limited sample information with the knowledge of the system PSF in the presence of scattering.

It is remarkable that diffraction limited images of the samples hidden behind scattering media can be obtained using these techniques. However one attempts to go beyond the diffraction limit to explore the possibilities of super resolution microscopy behind scattering media. As described before in Chapter-2 the NA of a scattering lens is limited by the diameter of the diffuse scattered spot behind the lens. van Putten *et al.* [40] have invented an extraordinary lens (HIRES lens) made of GaP semiconducting material. By folding the multiple scattering paths of the light scattering through the HIRES lens,

they are able to increase the NA to up to ~ 3.41. This in turn leads to enhancement in resolution to about 77nm. Using such a HIRES lens and iterative deconvolution using speckle autocorrelation function, it has been demonstrated that it is possible to enhance resolution of widefield microscope[71].

Even though using HIRES lens allows for enhancement in resolution of the illuminating system, the acquired fluorescence response will still be limited by the Optical Transfer Function(OTF) of the imaging system. There is still scope for improvement in terms of reliably extracting high resolution information from fluorescent specimens hidden behind scattering media. In the view of super resolution microscopy in the presence of scattering, Structured Illumination Microscopy(SIM) proves as a worthwhile technique to explore. SIM works by exciting a sample with periodic patterns to extract high resolution information. By doing so SIM achieves a resolution doubling beyond the diffraction limit of the imaging system[12]. In this chapter I will describe our experiments to obtain sub-diffraction resolution images behind scattering media. As will be seen, firstly this involves making use of wavefront shaping technique to obtain an interferometric focus behind a scattering medium. Secondly generating multiple focal spots behind a scattering medium from the interferometric focus. Finally it will be shown that SIM techniques can be applied behind a scattering medium to enhance the resolution of such a *scattering microscope*. An array of light foci serves as the periodic pattern that in-turn illuminates the underlying fluorescent structures. Images of these structures thus acquired are processed using SIM algorithm to enhance the resolution of the microscope.

In the upcoming sections, the working principles of SIM are described. This is followed by the description of implementation of SIM behind a scattering medium and the corresponding results and discussion.

4.1 Working of SIM

Structured Illumination Microscopy (SIM) is a super-resolution microscopy technique developed individually by Gustafsson *et al.* [12] and Heintzmann *et al.* [72]. As the name suggests, this technique involves illuminating a sample with periodically varying intensity patterns i.e "Structured Illumination". It is a super-resolution technique that allows to increase the resolution of a microscope beyond the diffraction limit. The resolution enhancement aspect of SIM technique has evolved from attempts to increase optical sec-

tioning capability of widefield microscope using non-uniform illumination [73] and from attempts to expand the system OTF using two opposing objectives [74] [75]. Although initially it was introduced to be applied in fluorescent microscopy, SIM can also work with non-fluorescent samples. However in our experiments we make use of SIM only with fluorescent samples.

The technique is better understood by looking at image acquisition in frequency space rather than the image space, as the spectral content of an image neatly separates out into different frequencies. As an example, Figure 4.1 looks very different depending on the its spectral content. An imaging system acts as a low pass filter, allowing only lower spatial frequencies to pass through and thus forming a rather blurry image of the scene. In the limit of diffraction, the maximum allowed spatial frequency is given by the OTF of the imaging system. If the sample information in a "scene" is assumed to be made up of a number of sinusoids of various frequencies, the OTF limits the maximum of those frequencies that will be allowed to pass through the imaging system. However when such a scene is superposed with another sinusoid, it leads to formation of yet another sinusoidal fringe pattern. This fringe-like pattern is called the Moiré pattern, as shown in Figure 4.2.

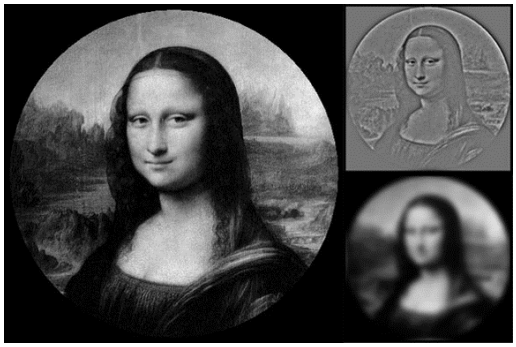

Figure 4.1: Understanding spatial frequencies: right-top shows the image containing high spatial frequencies and right-bottom shows the low frequency blurring.

The working of SIM can be understood to some extent in the same sense as the Moiré effect. By making use of spatially periodic illumination patterns, the sample information is coupled to the periodicity of the illumination pattern due to Moiré effect. Thereby it down-modulates the otherwise inaccessible high frequency information within the reach of OTF. With a precise knowledge of the illuminating pattern, this high resolution information of the sample can be algorithmeticallty extracted leading to an overall enhancement of resolution of the microscope. The resolution enhancement is realised in the narrowing of the Point Spread Function (PSF) of the microscope or broadening of the corresponding frequency spectrum(OTF). SIM has been shown to yield a full resolution improvement of a factor 2 beyond diffraction limit as compared to conventional

widefield microscopy. It is also considered to be the most light efficient technique among the super-resolution modalities, as moderate excitation intensities are often sufficient to get good signal. The ability for optical sectioning with SIM is realised due to the fact that the sample response is highly modulated by the illumination pattern in the focal plane compared to off-focal planes. 3D volumetric imaging with SIM is made possible by 3D-SIM [77]. It is also a versatile technique as SIM can be applied at any wavelengths, therefore making it easier to choose different fluorescent dyes freely. SIM also doesn't impose strict constraints such as use of pulsed lasers or complex optical alignments that are otherwise demanded by super-resolution techniques such as STED/STORM etc. A disadvantage of SIM could be the fact that resolution enhancement is limited to only a factor two. However there are approaches such as Saturated-SIM [8] etc. to improve the resolution even further. Although exploring this approach is out of scope of the current thesis.

Figure 4.3 shows the basic working of SIM technique. A sinusoidally varying illumination pattern with the frequency of illumination chosen to be at the edge of detection objective. Such an illumination pattern is represented by 3 delta peaks in the Fourier space. This pattern is shifted in space, each time acquiring a fluorescence response from the sample. This movement in object space corresponds to obtaining the object spec-

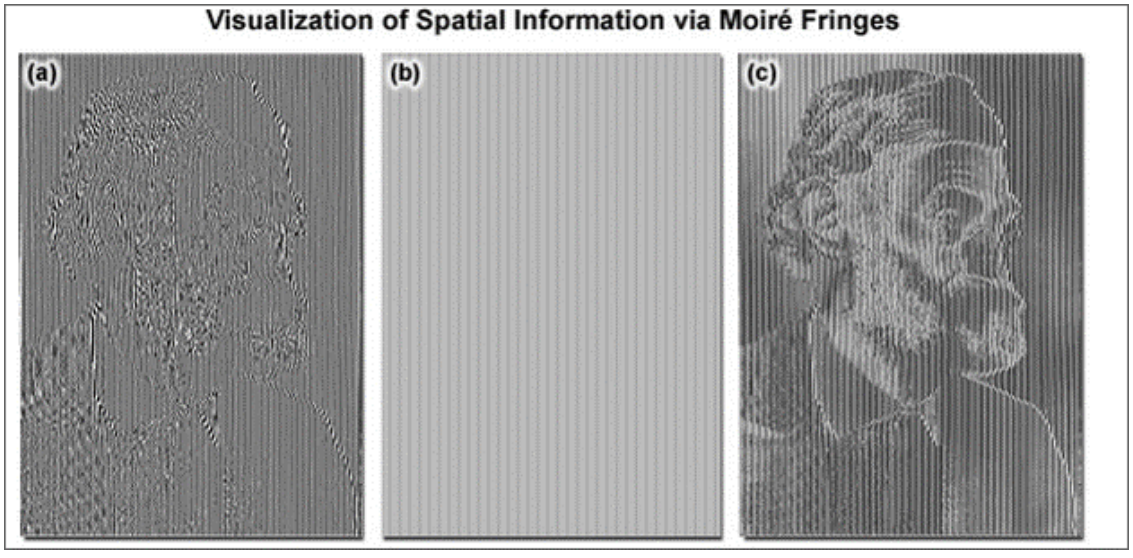

Figure 4.2: Moiré effect: When an image a) with high frequency sinusoids is mixed with another sinusoid b), the otherwise unobservable information (portrait of Ernst Abbe) appears as lower frequency Moiré fringes. Picture taken from Zeiss website [76]

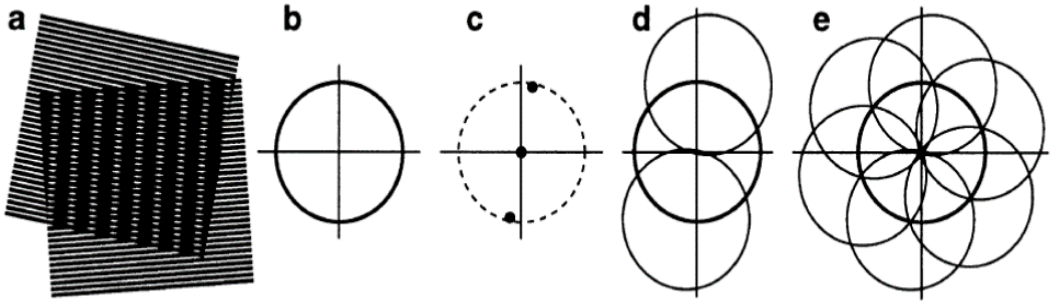

Figure 4.3: a)Illumination sinusoid super-imposes with sample (which is also a sinusoid) to generate Moiré fringes. b)OTF of the imaging system represented by the circle. c)Fourier Transform of the illumination sinusoid shows 3 peaks in the spectrum. The two-off center peaks are at the spatial frequency of illumination. d)By shifting the illumination pattern in space and acquiring images at each position, sample information coupled with the 3 peaks can be extracted. e)Step d) is repeated for other orientations of illumination and the extracted high frequency information is shifted back in freqeuncy space to reveal the expansion of the OTF by a factor two. After step e) the frequency domain information is Inverse Fourier Transformed to get the super-resolution image in real-space. [12]

trum from 3 regions centered around the 3 delta peaks. In order to uniformly illuminate the object the pattern is rotated and phase shifted while acquiring corresponding fluorescence responses. It is sufficient to acquire a total of 9 images to uniformly cover the entire object space as well as Fourier space as shown in Figure 4.3. By a linear combination of acquired images with known pattern orientations, it is possible to extract the higher frequency information, thus leading to an enhancement in the resolution of the microscope. Since the maximum possible illumination spatial frequency is limited by the detection OTF, theoretically this leads to a maximum possible resolution enhancement to a factor two [12].

The high frequency high modulation constrast sinusoidal illumination pattern required for SIM is generated either by coherently interfering two plane waves, or by incoherently imaging the surface of a transmission grating onto the sample plane. Both these modalities generate a fringe-like pattern whose intensity varies sinusoidally along one dimension and the frequency of modulation is chosen to be at the resolution limit of the imaging apparatus. Not only 1D fringe pattern, but also 2D sinusoids can also be generated in this manner. As in the case of Saturated SIM [78], 4 beam interference can be used to obtain 2D grid like pattern of illumination spots instead of fringes. The patterned illumination can also be easily generated using SLMs or DMDs [79], thus avoiding the sensitivity associated with alignment of the grating. Whether with 1D or 2D sinu-

soid, the theory of resolution enhancement is the same, except for the terminologies adapted for the case of 2D multi-spot illumination. Our multi foci pattern obtained in Figure3.5 resembles such a 2D grid and can be written as,

$$I(x,y) = I_0[1 + m\cos(k_x x + \phi_x)][1 + m\cos(k_y y + \phi_y)] \circledast H_1(x,y) \tag{4.1}$$

where $k_x = k_y = k_0$ is the spatial frequency and $\phi_x = \phi_y = \phi_0$ is the phase of the illumination pattern. 'm' is the modulation contrast of the pattern and is measured as the normalized difference in maximum and minimum intensity (where $0 \leqslant m \leqslant 1$). $H_1(x,y)$ is the PSF of the illumination objective- in our case the scattering lens. If the sample structure is represented by $S(x,y)$, the illumination with equation 4.1 results a fluorescent emission with a distribution

$$D(x,y) = [S(x,y)I(x,y)] \circledast H_2(x,y) + N(x,y) \tag{4.2}$$

where $H_2(x,y)$ is the PSF of the imaging objective and $N(x,y)$ is the noise.

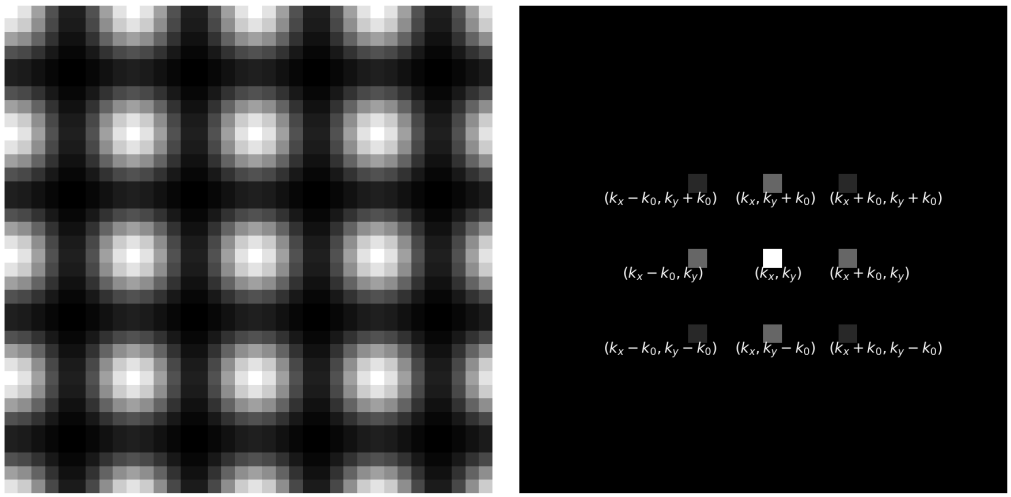

Figure 4.4: Simulated 2D sinusoidal illumination pattern for SIM and its corresponding frequency spectrum. The spectrum shows 9 delta peaks labelled with their corresponding spatial frequencies.

The above convolution operation "$\circledast$" is easily dealt with upon Fourier Transformation, when it becomes a simple multiplication.

$$\widetilde{D}(k_x,k_y) = [\widetilde{S}(k_x,k_y) \circledast \widetilde{I}(k_x,k_y)]\widetilde{H}_1(k_x,k_y)\widetilde{H}_2(k_x,k_y) + \widetilde{N}(k_x,k_y) \tag{4.3}$$

Notice now the sample spectrum is convolved with the spectrum of the illumination pattern. For a 2D sinusoidal illumination of the form shown in Figure 4.4, the spectrum

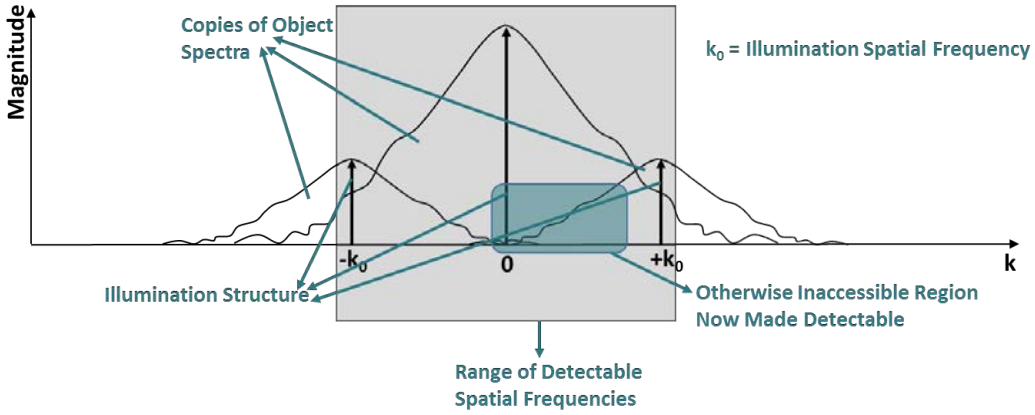

Figure 4.5: Due to coupling of the object spectrum with that of the illumination pattern, the otherwise inaccessible high frequency content is brought within the reach of optical support. The blue region represents this high frequency content that needs to be now reliably extracted and shifted to its actual location.

consists of 3X3 set of delta peaks- one at the origin and the rest located at the edge of the OTF ($\widetilde{H}_2(k_x, k_y)$) shifted in frequency by the same amount as the illumination spatial frequency (k_0). That is, an image acquired with such a periodic pattern is a superposition of 9 Fourier components.

Each SIM acquisition of a sample contains diffraction limited information. The unshifted component at the origin contains information that is also accessible by widefield illumination. However the ones shifted off-centre contain in them the otherwise inaccessible higher frequency information, as shown in Figure 4.5 for 1D illumination case. A reconstruction procedure aims at retrieving this higher frequency information in order to expand the conventional OTF and thereby increasing the resolution.

In order to extract sample information from the off-center components, each component has to be separated out. Extracting a total of 9 Fourier components requires at least 9 images of the sample to be acquired at different orientations of the illumination pattern. This is done by noting that laterally shifting the illumination pattern in space is transformed as the phase shift of the Fourier peaks. It leads to 9 different phase shift values of the delta peaks in each acquired image. With the knowledge of these precise phase shifts it is possible to separate out sample spectrum from 9 different positions in the Fourier space. The acquired images are written here as a linear combination of respective Fourier components

$$\widetilde{D}_n(k_x, k_y) = \sum_m M_{nm} \widetilde{S}_m(k_x, k_y) \widetilde{H}_1(k_x, k_y) \widetilde{H}_2(k_x, k_y) + \widetilde{N}(k_x, k_y) \tag{4.4}$$

$$\text{with} \qquad M_{nm} = \exp\Big[2\pi\mathrm{i}\Big(\frac{m_x n_x}{3} + \frac{m_y n_y}{3}\Big)\Big]$$

where $n_x = n_y = \{0, 1, 2\}$ index the number of acquired images. Also $m_x = m_y = \{-1, 0, 1\}$ are the indices of the 3X3 set of Fourier peaks in each of the (n_x, n_y) images. The noisy estimates of the sample information are obtained by inverting the mixing matrix M_{nm} and solving equation(4.4) for $\widetilde{S}_m(k_x, k_y)$. For a precise inversion of the equation, it is important that the matrix M_{nm} be non-singular.

Thus extracted off-center components are then rid of noise using Wiener filtering. These noise-free components are shifted back to origin by shifting the phase of each of the component. After re-shifting all the components to origin, they are recombined to obtain a super-resolved frequency spectrum. The recombined spectrum is Inverse Fourier Transformed to obtain a resolution-enhanced image in real-space.

This concludes the brief summary of the working of SIM. However it is important to realise that the theory of resolution enhancement can also be extended to SIM with a *scattering lens*. As the chapter title suggests, we intend to implement SIM with a *scattering lens*. That means that a scattering medium such as a ground glass diffuser is transformed into a lens that generates required patterned illumination, which is further utilized to excite fluorescent structures and process the images for resolution improvement.

4.2 Experimental Preliminaries

The procedure starts by choosing the various components of the experimental setup. It is important to choose the right experimental conditions to properly quantify the obtained results.

Scattering medium: First we start by optimising the scattering sample from a choice of a $1mm$ thick ground glass diffuser or a spray painted glass slide painted with ZnO ($10 - 15\mu m$ thick). Both these samples randomize the incoming light and form a speckle pattern in the far field. The aim then is to choose the right sample that can act as a perfect *scattering lens* upon wavefront shaping. The illumination lens system is optimised so as to obtain average speckle size of the order of diffraction limit of the imaging system. It is also important to consider the fact that range of memory effect will limit the field-of-view of our scattering lens. As already described in Chapter-2 of this thesis, the range of memory effect is limited by the thickness of the scattering medium.

A ground glass diffuser has an extended range of memory effect whereas for a spray painted glass slide, it depends on the thickness of the paint layer.

In order to determine the range of memory effect of the scattering media, we setup the following experiment. Using wavefront shaping, the scattered light from the paint layer is made to focus to a behind the glass slide. An optimisation routine as described in Chapter-2 was used to iteratively optmize an input light wavefront. By monitoring the intensity at a target speckle, input light is modulated iteratively. At the end of the procedure, we get an interferometric focus behind the glass slide. Now, by appling a linear gradient on the optimized wavefront, it is possible to move the focus around in space, as already stated. So we apply such a linear gradient while monitoring how the intensity of the focus changes with respect to the applied gradient. The gradient at which the intensity of the translating focus drops to $(1/5)^{\text{th}}$ of its maximum value gives us the range of memory effect. This is measured in terms of translated distance of the focal spot. We observed that even for a thin $10\mu m$ paint layer on glass slide, the range of memory effect was limited to about $10\mu m$. This means that the area over which the focus can be translated i.e the field-of-view corresponds to about $10^2\mu m^2$. However for a ground glass diffuser, the range of memory effect -even though theoretically unlimited- was found to be much more than this. Hence we chose to work with ground glass diffusers.

A $1mm$ thick ground glass diffuser with a grit polished surface (1500 grit) forms the scattering medium. The other side of this diffuser is smooth and can act as the focal plane. The smooth surface is coated with fluorescent beads to provide the fluorescence response required for SIM reconstructions. These beads adhere to the glass surface pretty well, allowing for mounting of the diffuser on a sample holder. A cover slip of thickness $0.17mm$ is glued on top of the beads, for easy handling of the sample. An optimisation routine as described in Chapter-2 focuses the scattered light from the grit polished surface onto the focal plane that is coated with fluorescent beads. For this, direct optimisation routine is used, i.e by using the transmitted light as the feedback signal. The focal plane is addressed to as the sample plane from now on, as the "sample" for these experiments is the fluorescent beads.

Diffraction limit of Illumination and Imaging systems: The illumination objective, imaging objective and the fluorescent beads are all specially chosen for the experiments with SIM. When the optimisation routine is run, the combination of illumination objective (10X NA=0.3) and diffuser form our *scattering lens*. The situation in the

sample plane is monitored using an imaging objective (40X NA=0.7) and CCD camera. When fluorescence images have to be acquired, a bandpass filter is added onto the camera that blocks the direct laser light and allows only the fluorescent light to be detected.

It is important to note that the Numerical Aperture(NA) of the illuminating system is the NA of the *scattering lens*. The approximation of NA of scattering lens is determined from the equation $NA = \sin[\tan^{-1}(\frac{D}{2f})]$. Here '$D$' is the diameter of diffuse scattered spot behind the diffuser, which is almost same as the spot illuminating the diffuser (i.e the laser beam diameter before and after the diffuser are the same). This is because the diffuser being just a randomiser of the light field, does not cause the transmitted beam to expand. Hence 'D' can be fixed by the 10X 0.3 NA objective mentioned before. As a parallel beam of light of diameter $8mm$ from the SLM is being focused using this objective, the light beam on the grit polished surface is demagnified to a size of $\approx 500\mu m$. As the focal plane of the scattering lens is chosen to be the smooth side of the diffuser, the focal length is equal to the thickness of the diffuser i.e $f = 1mm$. This allows us to get a rough estimate of the NA of the scattering lens to be between $0.2-0.3$.

The NA of imaging objective is just the one provided by the company $= 0.7$. This leads to a combined NA of the system to be $NA = 0.2 + 0.7 = 0.9$. The diffraction limit of this custom microscope is then determined by Abbe's diffraction limit[4] as $\frac{1.22\lambda_{em}}{NA} = 700nm$. This gives the width of the PSF of the microscope. This theoretical value is then compared to the experimentally obtained PSF of the system. In order to experimentally determine the PSF, the system response for a point source should be measured. For this reason, images of single fluorescent beads were recorded by illuminating them in a widefield mode. The bead size was chosen to be small enough to be considered as "point sources". The $0.5\mu m$ beads emitting at $515nm$ serve as our point sources. From these recorded images, the intensity profile of the fluorescence emission -which is typically a Gaussian distribution- was determined. The image with a good contrast of intensity and a uniform Gaussian profile was selected to represent the PSF of the imaging system with a FWHM of about $1\mu m$. After compensating for the size of the beads, the PSF value turns out to be $= 860nm$, slightly more than the theoretical value. The Fourier Transform of this PSF image will yield the OTF of the system. The edge of this OTF spectrum represents the maximum cutoff spatial frequency of $k_{\text{cutoff}} = (860nm)^{-1}$. In the case of simulations, the PSF is set by a Gaussian function with the FWHM matching that of the experimental PSF. The experimentally determined

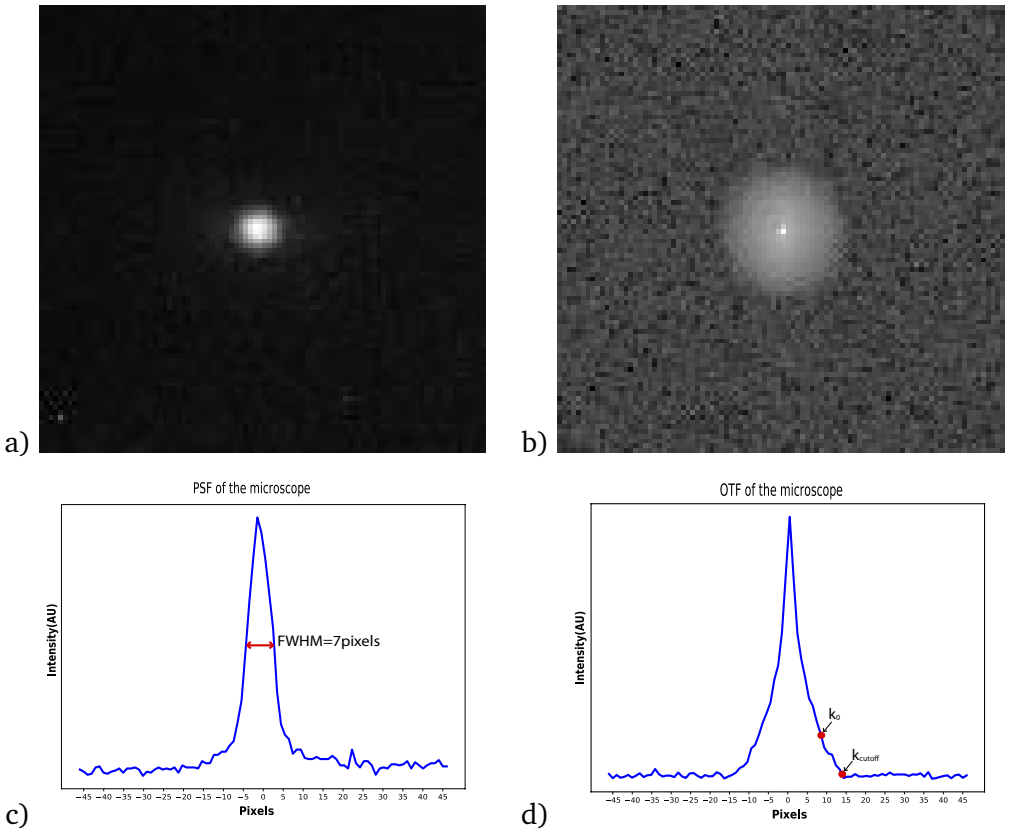

Figure 4.6: PSF and OTF

PSF and its corresponding OTF are plotted in the Figure 4.6.

Generating structured illumination: When optimisation algorithm is run, it produces a focus behind the diffuser with a size limited by diffraction. A phase mask is applied to transform the focus into an array of foci. As described in Chapter-3 of this thesis, there is an upper limit on the number of foci that can be generated. However it is also important to make sure the generated foci are of good quality, in order to apply SIM techniques. This means, the focal spots need to have uniform intensities and a well defined spot spacing. As the contrast of focal spot intensity compared to the background reduces with increasing number of foci, there is a trade-off. The number of foci along each direction is an important factor because it decides the size of the region of the sample that can be simultaneously illuminated. The smaller the number of foci, the smaller is this region. We found that a good contrast periodic pattern was obtained when 9 focal spots were generated along a line, i.e 1D array of 9 foci. Even though in principle upto 30 focal spots can be generated, their respective intensities would be

much lower. This is not favourable for illuminating fluorescent structures. Although the lower excitation intensities can be compensated by longer exposure times, it severely affects the total time of acquisition of each SIM image. Therefore there is a trade-off between effective field of view (FOV) of the microscope, i.e the area of illuminated region and the acquisition time of the image, which also depends on the response of fluorescence structures. Increasing the input intensity also helps to an extent, although this also increases the intensity of background speckles (refer Chapter-3), hence it is not desired.

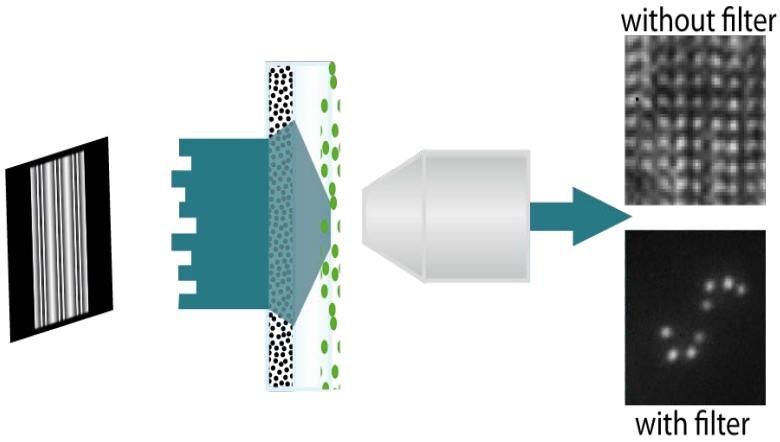

Figure 4.7: Figure shows a part of the experimental setup. A *scattering lens* produces multiple focal spots upon adding a phase mask. The mask is raster scanned to obtain a lattice of 9by9 spots. The camera sees the focal spots when no filter is added and the fluorescent beads when a filter is added.

An ideal periodic illumination is the one with uniform intensities and diffraction limited spacing. Prioritizing the intensity uniformity of the focal spots and a good modulation contrast, we resorted to using 9 focal spots as the most suitable one. However a comparative study with 5 focal spots was also performed. The corresponding phase mask required to generate the 9 focal spots was obtained by the method of constrained optimisation as described in Chapter-3. In order to make a 1D array of 9 focal spots into a 2D grid, the 9 spots were raster scanned to 9 vertical positions. The CCD camera records the entire motion in one single frame, thus making up one acquisition of SIM made up of 9X9 focal spots. The vertical displacement is kept same as the horizontal spacing, so as to make the horizontal and vertical spatial frequencies $k_x = k_y = k_0$ alike. The Figure 4.7 shows a sample 2D focal spot array recorded in this manner. This helps to judge the quality of illumination which will be further used for SIM of fluorescent

structures. The image of the illumination pattern is cropped such that the edges of the outermost spots are cropped out, making the image size $= 94$pixels. With a sampling frequency of 1pixel $\approx (150nm)^{-1}$, the illumination spatial frequency corresponds to $k_0 = 8$pixels $\approx (1.8\mu m)^{-1}$. The illumination spatial frequency is marked by a red dot in the Figure 4.6. To determine the modulation contrast m of the illumination pattern, the pattern intensity is plotted in space. The factor m is then determined as the ratio $\frac{I_{\max}-I_{\min}}{I_{\max}+I_{\min}}$. For our illumination patterns, we found m to have values varying between $0.2 - 0.4$.

SIM acquisition: As described above SIM imaging comprises of acquiring a total of 9 images with the pattern translated to 9 different positions. So the procedure outlined above is repeated to acquire an image at each location of the focal spot array, making up in total a set of 9 SIM images. Each time, the illumination pattern is shifted by an amount $= \pm 2\pi/3$ of the spatial period of the pattern, along 4 different directions. By doing so, the entire field of view is uniformly illuminated without leaving any unexposed regions. When the bandpass filter is added, this procedure allows for imaging the underlying fluorescent beads as shown in Figure 4.7. Thus recorded set of $D_n(x, y)$ SIM images are processed using the SIM reconstruction algorithm. In order to improve the SNR, multiple acquisitions of each of the 9 images $D_n(x, y)$, are performed. The average of the acquired set of $D_n(x, y)$ images are then processed using SIM algorithm. We found the period of the illumination pattern is $= 1.8\mu m$, this corresponds to a illumination spatial frequency of $(1.8\mu m)^{-1}$. As shown in Figure 4.6 the illumination spatial frequency is at $\sim 48\%$ of the cutoff frequency of the OTF $= 1.8\mu m$. Due to such a periodically varying illumination, each of the $D_n(x, y)$ acquisitions will now each consist of $(1.8\mu m)^{-1}$ additional spatial frequencies that were otherwise not detectable. Thus with a reconstruction using SIM algorithm, we can extract these conventionally inaccessible spatial frequencies, thereby expanding the system OTF. This implies we expect a resolution enhancement of about $\sim 48\%$ more than the conventional widefield imaging, which is given by the illumination spatial frequency.

4.3 Image post-processing using SIM algorithm

The reconstruction algorithm we use, is based on OpenSIM developed by A.Lal *et al.* [80] for 1D sinusoidal illumination. It is an open source software package written in MATLAB and was re-written to suit our SIM illumination which is an array of 2D focal spots.

The necessary modifications are done in the software so as to handle both simulated SIM acquisitions and the experimental counterparts. In simulations, a sample image is "illuminated" with sinusoidal pattern given by eq. 4.1 and simulated Gaussian noise. The parameters such as spatial frequency (k_x, k_y), phase (ϕ_x, ϕ_y), noise level $(N(x, y))$, modulation contrast (m) of the pattern are all set to match the experimental values. A sample simulated illumination and its spectrum is shown in the Figure 4.4. In the case of experiments the images are acquired using patterned illumination behind a scattering medium, and the procedure is described in the upcoming sections. Simulated as well as experimentally acquired images are processed using the OpenSIM software to obtain higher resolution reconstruction of the sample.

A reliable extraction of high resolution information depends on the quality of illumination pattern as well as the knowledge of various parameters associated with it. This includes the knowledge of the system PSF (and its corresponding OTF), illumination spatial frequency, phase shift and modulation contrast. Of these many parameters, the system PSF is experimentally determined using the procedure outlined in Section 4.2. The modulation contrast (m) is set by multiple foci generated using the phase mask. In our experiments 'm' varied between $0.2 - 0.4$. In the case of simulations these are given by the user, however in the experimental acquisitions the parameter values particularly that of the phase shifts may deviate from the intended ones. The experimental fluctuations in the optical path or drifting of the sample may occur which affect the precise reproducibility of the illumination pattern. Such a drift in the illumination pattern means that the pattern phase shifts deviate from the intended phase shifts. In the experiments, the illumination pattern generated is more or less accurately placed on a grid within a variation of about 1-2pixels, which can be enough to cause distortions in the reconstructed images. Hence there is a need to determine the phase shifts post acquisition of the SIM images. In commercial SIM systems, in order to precisely determine the illumination structure, typically one makes use of an *a posteriori* phase shift estimation step. Therefore we also make use of similar *a posteriori* estimation of the illumination pattern shifts from the experimentally acquired images. In the following section I describe the techniques we used to precisely determine the illumination phase shifts.

4.3.1 Phase shift estimation

A precise separation of Fourier components associated with the sample via SIM is only possible when the illumination parameters are precisely known. Particularly this implies that the illumination frequency vector and the phase shifts applied in each of the SIM images be known. The illumination frequency vector though, hardly fluctuates around the intended value, whereas the phase is rather more sensitive to experimental conditions. In our experiments, we saw that it was mostly enough to work with *a priori* assumed spatial frequencies. If and when required, we determined the spatial frequency post acquisition by minimizing the autocorrelation function of each acquired SIM image [80].

An intuitive approach to *a posteriori* phase shift estimation is to determine the complex angle of the delta peaks arising in the Fourier Transform(FT) of the acquired image. That is, first FT of an acquired image is computed using FFT function in Python and the delta peaks associated with the illumination pattern as shown in the Figure 4.4 are located. The complex angle of these delta peaks is nothing but the phase shift of the underlying illumination pattern. This method of phase shift determination is the called **Phase-of-Peak method** in the literature [81]. But as also stated in literature, this method is not suitable for finer illumination patterns and in the presence of noise. This is because it is hard to locate the delta peaks associated with the illumination pattern in the computed FT, in the presence of noise. It is especially more unreliable if the ambient noise oscillates at the same spatial frequencies as that of the illumination pattern.

The OpenSIM software [80] comes with another way of estimating the phases using the **Real-Space cross-correlation** (CCo) method. It determines the phase shifts by cross correlating each individual component with an ideal sinusoid of the form in equation (4.1). The cross-correlation coefficient '*C*'

$$C = \sum D(x,y)I(x,y) \tag{4.5}$$

is maximum when the phases ϕ matches the phase ϕ_0 of the illumination pattern. Therefore by iteratively optimising the value of C, the corresponding phase shift can be estimated. But this approach also has the same problem that when the experimental data is corrupted by noise at the frequency range of illumination, the coefficient '*C*' is optimized for incorrect phases.

K.Wicker *et al.* [82] have proposed another way to tackle phase shift estimation problem in noisy acquisitions (with a noise variance of σ^2). The proposed technique works

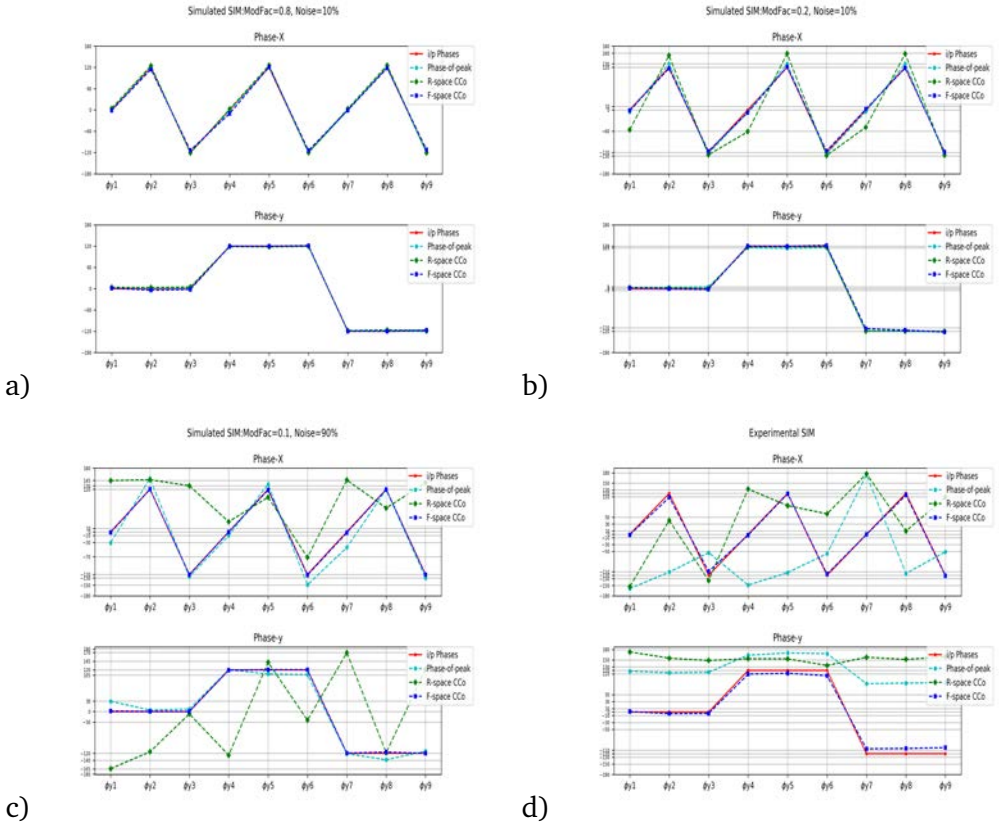

Figure 4.8: Phase estimations of Simulated and Experimental data. Simulations are compared for different values of Modulation contrast(ModFac) and ambient noise(assumed to be Gaussian). The higher errors in the experimental case reflect the fact that there is unaccounted noise coming from the background speckles that oscillate at frequencies around the frequency of illumination. In the Experimental case, it is clearly seen that only Fourier space weighted cross-correlation technique is able to estimate the phases correctly.

due to the fact that a perfect separation of Fourier components $\widetilde{S}_m(k_x, k_y)$ in equation 4.4 means that different components are not correlated. That is, once the components are well separated, there is no overlapping information among the different components. This only happens when the phase shifts in the mixing matrix M_{nm} have correct values. Therefore by way of minimizing a **weighted-cross-correlation (WCCo)** between different Fourier components, their corresponding phase shift matrix M_{nm} can be estimated. This method only determines the relative phase shift difference between the components and not their absolute values. However that is enough to successfully separate the different Fourier components. The procedure is as follows, first a cross-

correlation matrix is constructed by

$$\begin{aligned} C_{ij} &= \left[\widetilde{S}_i(k_x,k_y) \circledast_w \widetilde{S}_j(k_x,k_y)\right] \\ &= \frac{\sum_{k_x,k_y}\left\{w(k_x,k_y)\widetilde{S}_i(k_x,k_y)\widetilde{S}_j^*((k_x,k_y)-k_0)\right\}}{\sum_{k_x,k_y} w(k_x,k_y)} \end{aligned} \tag{4.6}$$

The coefficients of mixing matrix M_{nm} are then optimized as the values for which this correlation-matrix is the minimum. The indices here i, j are each over the components 1 to 9. This way of weighted CCo helps to tackle the noise by way of empirically choosing the values of $w(k_x, k_y)$ from the equation below. This allows for optimising on the signal correlation more than the noise correlation.

$$w(k_x,k_y) = \frac{\text{otf}_i(k_x,k_y)\quad \text{otf}_j^*((k_x,k_y)-k_0)}{\sigma^2[|\text{otf}_i(k_x,k_y)|^2 + |\text{otf}_i((k_x,k_y)-k_0)|^2]} \tag{4.7}$$

The performance of these *a posteriori* phase determination techniques is shown for the case of simulated and experimental images in Figure 4.8. In the simulations, we were able to alter the parameters such as modulation contrast and noise level, whereas it was not possible in the experiments. The determined phase shift values are compared to the intended phase shift values for each of the technique. The intended phase shift values (ϕ_x, ϕ_y) are always maintained to be $(\pm 2\pi/3, \pm 2\pi/3)$radians or $(\pm 120, \pm 120)$degrees, as this results in isotropic coverage of spatial frequencies around the origin and thereby uniform illumination in sample-space. As can be clearly seen in this figure, the real-space CCo and Phase-of-peak method work well when the modulation contrast is high and the noise level is low. However, they fail to determine the phase shift values in the presence of noise and when patterns with low contrast are used. The Fourier space WCCo method works very well in all the cases, including the experimental one.

The Figure 4.8 shows that the experimental images are more similar to the simulated case with ModFac=0.2 and Noise=90%. However in reality the ModFac determined for experimental illumination varied between $0.2 - 0.4$. Noise although present was not as high 90%, as it was possible to suppress the noise by allowing long exposure times. We also employed multiple SIM acquisitions and averaging of the multiple images which also greatly improved the signal. When determining the SIM phase shifts from these acquisitions, we made use of Fourier-space WCCo method, as we found it to be most reliable for our experimental conditions.

4.3.2 Wiener Filtering

By determining the illumination frequency and phases using the methods described in the Section 4.3.1, the various Fourier components of sample information can now be reliably separated out by inverting the mixing matrix M_{nm},

$$\text{Noisy}\big[\widetilde{S}_n(k_x, k_y)\big] = M_{nm}^{-1}\big[\widetilde{D}_n(k_x, k_y)\big] \tag{4.8}$$

Although well separated, these components $\widetilde{S}_m(k_x, k_y)$ are still corrupted by noise $\widetilde{N}_m(k_x, k_y)$. It is important to filter out the noise before shifting the components back to origin, as this ensures proper placement of the components in the Fourier space. Moreover, the enhancement in the resolution is better percieved in the absence of noise. Noise filtering is much favoured in the frequency domain rather than in the spatial domain, as the sample spectrum separates out neatly with frequencies. The noise is especially more dominant at higher sample frequencies, due to the lower magnitude of the optical support (OTF) at higher frequencies. In order to reliably retrieve high frequency information from the separated components, a noise filtering process is inevitable. If the OTF of an imaging system is well known, one can easily retrieve the sample S from the image D from $\widetilde{S} = \frac{\widetilde{D}}{\text{otf}}$. But due to the limited extent of the OTF, it's inversion is ill defined at places where it is zero (for example at frequencies greater than k_{cutoff} and such). A modification of this inversion is possible instead using a Wiener Filter[47]. It is given by,

$$[\widetilde{S}_n(k_x, k_y)]_{\text{filtered}} = \left[\frac{\text{otf}^*(k_x, k_y)}{|\text{otf}(k_x, k_y)|^2 + \frac{\phi_n(k_x,k_y)}{\phi_s(k_x,k_y)}}\right]\widetilde{S}_n(k_x, k_y)\widetilde{A}(k_x, k_y) \tag{4.9}$$

where the factor $[\frac{\phi_n(k_x,k_y)}{\phi_s(k_x,k_y)}]$ in the denominator is the ratio of Noise power spectrum to the Object power spectrum i.e the inverse of SNR. This factor in the equation (4.9) helps to enhance the sample information at only those frequencies at which SNR is high. The object power spectrum is determined as $\phi_s(k_x, k_y) = \beta^2 k_0^{-2\alpha}$ where the constants β & α define how the sample spectrum drops at the edge of the OTF. Finally, the Apodisation function $\widetilde{A}(k_x, k_y)$, is used to eliminate the ringing artefacts that may appear in the Wiener Filtered reconstructions.

The precise parameters of the Wiener Filter, i.e the signal and noise power spectra are determined empirically from the acquired SIM images. From a precise knowledge of the system OTF, it is possible to know the shape of the spectral distribution. Hence the object power spectrum is determined by iteratively optimizing the values α & β above,

that match the system OTF. The magnitude of the signal within this power spectrum gives $\phi_s(k_x, k_y)$. The amplitude of rest of the spectrum of acquired image constitutes as the noise power spectrum. The wiener filtering step consists of determining these parameters for each acquired SIM images. Once the spectral powers are determined, the application of Wiener filter removes the noise, thereby allowing the reconstruction of noise-free Fourier components of the sample $[\widetilde{S}_n(k_x, k_y)]_{\text{filtered}}$.

4.3.3 Shifting the components and recombination

The final steps towards achieving the SIM reconstruction consist of shifting the noise-free estimates $[\widetilde{S}_n(k_x, k_y)]_{\text{filtered}}$ of the Fourier components to their actual locations in the frequency domain and summing up of all the components. After filtering the components, their centers are actually located at the origin of the spectrum, whereas they in fact belong at the positions k_0 away from the origin. Shifting of the components to these original locations is made possible by Fourier Shift theorem [47]. A lateral shift of k_0 in the spatial domain is equivalent to multiplication by a phase factor $\mathrm{e}^{-\mathrm{i}2\pi k_0(m_x x + m_y y)}$ (with $m_x = m_y = \{-1, 0, 1\}$ as before). Hence, multiplication of the respective Fourier components by this phase factor will shift the corresponding real-space information by k_0. Once all the 9 components are shifted to their original locations they are summed up. This then extends the spectrum of the image which was conventionally limited at k_{cutoff} is now extended to $k_{\text{cutoff}} \pm k_0$ in all the directions. At this stage, the reconstructed image spectrum can be Inverse Fourier Transformed to reveal the super-resolved image of the sample in real-space.

4.4 Results and Discussion

Using the procedure outlined so far SIM images were acquired and processed to reconstruct high resolution information. The various parameters pertaining to the quality of these illumination patterns were scrutinised before subjecting them to SIM reconstruction. We observe that a proper alignment of the experimental setup influences the wavefront shaping mechanism. Although interferometric focus can be obtained with even a misaligned optical system, the quality of obtained focus i.e the intensity profile and the subsequent array of multiple foci were the best for a stable optical setup. Hence for the duration of measurements, we made sure that nothing in the laser beam path is disturbed. The multiple focal spots that are used as illumination pattern for SIM are

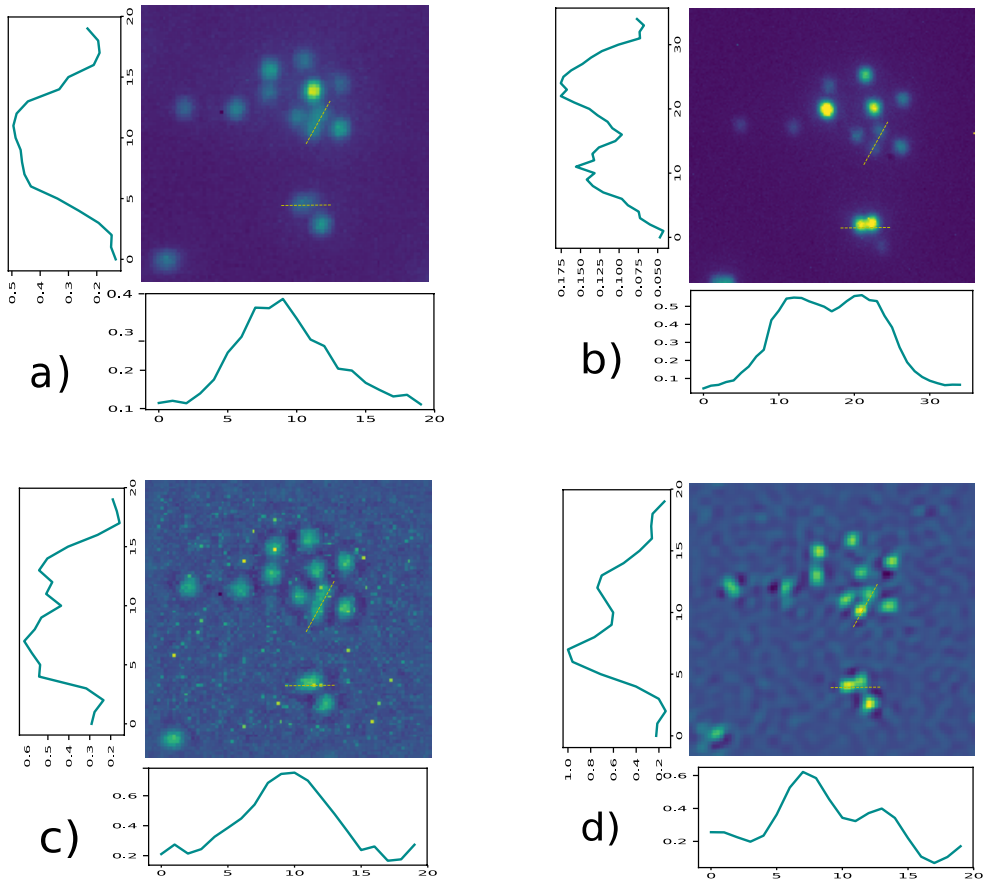

Figure 4.9: SIM reconstruction: a)speckle illuminated fluorescent sample scene captured using 40X objective. b) same scene as seen with a 100X objective. c) widefield reconstructed component taken from SIM algorithm performed with 40X objective. It contains only the diffraction limited information and hence looks similar to a). d) super resolved added to the widefield component in c). This shows a clear enhancement in resolution over c). The intensity cross sections along the dashed yellow line are plotted for corresponding images. The vertical plots are along the slanted lines and the horizontal plots are along the horizontal lines. d) clearly shows that the neighbouring beads are now resolvable due to SIM reconstruction. The resolution enhancement in d) is comparable to widefield image in b).

judged based on their intensity uniformity, spot spacing and modulation contrast. We were able to generate multiple foci with intensity uniformity close to 1, i.e almost all foci had similar intensities. The spot spacing among the foci corresponds to the spatial period of the SIM illumination. In our experiments, the spatial period was found to be

$= 1.8\mu m$. Also, the modulation contrast at this spatial period was found to vary from experiment to experiment in the range $0.2 - 0.4$.

The illumination patterns generated were translated to different locations to acquire SIM images as outlined in Section 4.2. The images of both illumination patterns and the illuminated fluorescent structures were captured, resulting in the data set $D_n(x, y)$. We first obtained the SIM images of the transmitted light without fluorescent samples in the field-of-view. After running these images through phase determination step, we were able to determine the experimental phase shifts. Even though intended phase shifts were $(\pm 120, \pm 120)$ degrees, the experimentally obtained multiple foci pattern drifted from this phase shift values by about $\pm 8 - 10$ degrees. We arrived at this conclusion after a substantial recordings of SIM images of the illumination pattern. This drift in the experimental phase shift values from the intended values means that, the fluorescent SIM images will also drift from the intended values by the same amount. This was indeed the case and hence we conclude that we can assume the experimentally obtained phase shifts to be the intended ones when evaluating phase shifts of fluorescent SIM images. That means, we are now comparing phase shifts of fluorescent SIM images with the phase shifts determined from SIM images of transmitted focal spots. When we did this comparison, we saw that the phase shifts of fluorescent images deviated from that of the focal spots only by about $\pm 2 - 4$degrees. This is indeed a remarkable result of *a posteriori* phase shift determination of SIM images using WCCo method.

a) 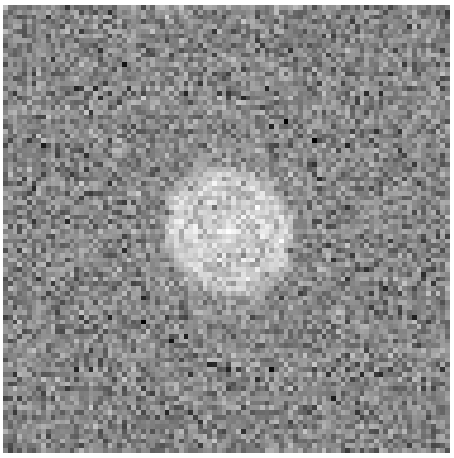 b) 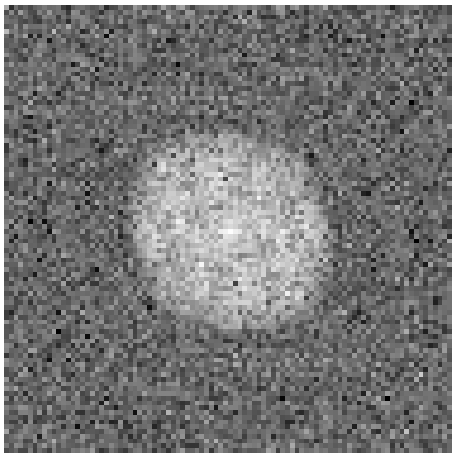

Figure 4.10: Widefield and SIM reconstruction spectra

Once the phase shifts of the illumination are determined, the Fourier components of the acquired images Noisy$\left[\widetilde{S}_n(k_x, k_y)\right]$ were obtained using equation (4.8). The next

step in the SIM reconstruction is to apply Weiner filtering as in equation (4.9). By doing this the noise from the Fourier components $\left[\widetilde{S}_n(k_x, k_y)\right]$ will be eliminated. The noise free Fourier components are all at this point centred at the origin of the frequency space, whereas in reality they belong respectively shifted off by $\pm k_0$ away from the origin. Hence the filtered components $[\widetilde{S}_n(k_x, k_y)]_{\text{filtered}}$ are shifted to their respective locations in the Fourier space by the procedure detailed above. After all the components are shifted to their original locations, they are added together to obtain the reconstructed spectrum of the sample image. This summed up spectrum is Inverse Fourier Transformed to get the reconstruction in sample-space. With this the reconstruction procedure is completed and a high resolution reconstruction of the image is obtained.

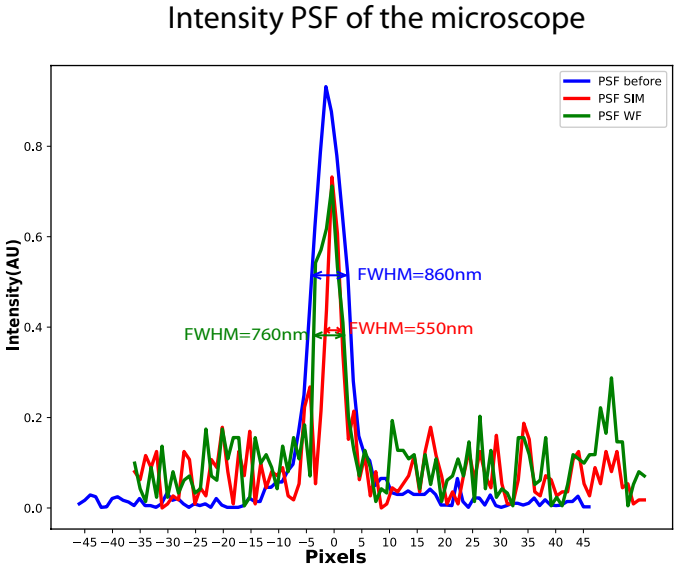

Figure 4.11: A plot of intensity PSF of the microscope after SIM reconstruction shows a narrowing compared to that before. For comparison the conventional widefield PSF obtained using wiener filtering of the central unshifted component is also plotted. From these plots it is clear that the PSF is narrower due to SIM reconstruction and not de to wiener filtering. The result corresponds to a ≈ 1.6 fold resolution enhancement.

The results of our SIM reconstruction of $0.5\mu m$ sized fluorescent beads is as shown in Figure 4.9. As can be seen from the subfigure d), the SIM reconstruction leads to enhancement in the resolution of our microscope. The intensity cross section over the beads clearly shows that using SIM, the fluorescent beads that were otherwise not resolvable are now resolved. The resolution enhancement can be compared with a widefield image obtained with another objective of superior magnification as shown

in subfigure b). As the corresponding intensity cross sections show, the resolution enhancement obtained with SIM reconstruction with 40X objective are comparable to those obtained conventionally with 100X objective. Whereas, the widefield component in subfigure c) can not resolve the same features, so is the case with subfigure a). The unresolved feature in the subfigure b) also proves that enhanced resolution is not a result of deconvolution but rather the addition of super resolution information from the extract high frequency components. Apart from the fact that the bead clusters are resolvable with SIM reconstruction, the figure also shows that the individual beads are much narrower in subfigure d) compared to those in a) and c). This means that the effective PSF of the microscope is narrower, which is also a sign of resolution enhancement. In the frequency space, the resolution enhancement is given by the broadening of the OTF support. This is clearly seen in the Figure 4.10.

As described before, due to the spatial frequency of illumination being $\sim 48\%$ of cutoff frequency, we expect a resolution enhancement by the same amount. Such a resolution improvement corresponds to a narrower PSF of width $= 549nm$. In order to quantify the improvement in resolution in real space, the PSF before and after SIM reconstruction are plotted in Figure 4.11. As shown in Figure 4.11, the PSF after reconstruction also has a FWHM $= 550nm$. This means we have obtained a ≈ 1.6 folds resolution improvement compared to the conventional widefield microscope. The PSF of wiener filtered widefield component is also plotted for comparison to show that the narrowing of PSF is due to SIM reconstruction and not simply due to deconvolution using wiener filtering. Although a full theoretical resolution enhancement of a factor two has not been achieved. This is due to the fact that we are limited by spatial frequency of SIM illumination. As the illumination frequency is not at the edge of the OTF but rather at $\sim 48\%$ of the cutoff frequency, we are also only able to extract $\sim 48\%$ of the super-resolution information. Nevertheless a narrower PSF due to SIM clearly shows that we are able to now access information beyond the diffraction limit of the optical system used.

The field-of-view of our scattering microscope used for SIM is currently limited by the number of foci that can be simultaneously generated. In our experiments, the area of the fluorescent samples simultaneously illuminated with a 9X9 array of foci corresponds to about $\approx 14\mu m * 14\mu m$. This can in principle be expanded by increasing the number of foci along each direction. However, it is important to note that with the increased number of foci, their respective intensities will be effectively lower. This means

that longer exposure times of the camera may have to be incorporated, which will in turn delay the total acquisition time of the SIM images. Alternatively increasing the number of foci can also achieved by simply tiling the 9foci next to each other in each direction so as to obtain say 18X18 foci thereby doubling the illuminated area. Another important factor for increasing the field of view is that, it greatly depends on the range of memory effect of the scattering lens used (refer Chapter-2). If the scattering lens is made up of ground glass diffuser, many more foci can be obtained in each direction, thereby increasing the field-of-view. Nevertheless depending on the intensity of the illuminating foci and the fluorescence response from the samples, there exists a trade-off. In our experiments we could not get reasonable images with increasing number of foci, but we did perform measurements with 5X5 foci in addition to the already stated 9X9 foci. This obviously smaller field-of-view nevertheless did not affect the achievable resolution. But it indeed affected the total exposure time. Due to the lesser number of foci in 5X5 case, their respective intensities were much higher than in the case of 9X9 foci. So each image could be recorded much faster. The Figure 4.12 shows the results of SIM reconstruction of a scene illuminated with 5X5 foci, and hence a smaller section in each image. As the figure shows, there is no impact on the resolution enhancement. Despite smaller area of illumination, SIM reconstruction nevertheless improves the resolution of the microscope.

4.5 Conclusion

We have developed a technique for super-resolution imaging behind scattering medium. We make use of Structured Illumination Microscopy to obtain high resolution information beyond the diffraction limit of the optical system. Using wavefront shaping and interferometric light focusing through scattering media we are able to obtain diffraction limited focus behind the medium. The focus is further split into an array of a number of foci. This way, we generate high frequency 2D sinusoidal focal spot array behind a diffuser. A focal spot array of this sort can be used as a source of periodic illumination required to perform SIM imaging. In order for a proper reconstruction of acquired images, the characteristics of the illumination pattern needs to be known precisely. By analysing the images of the illumination pattern and its corresponding movement in space, we are able to quantify the quality of the pattern produced. The intensity plots of the illumination patterns obtained from the images recorded on the camera, show

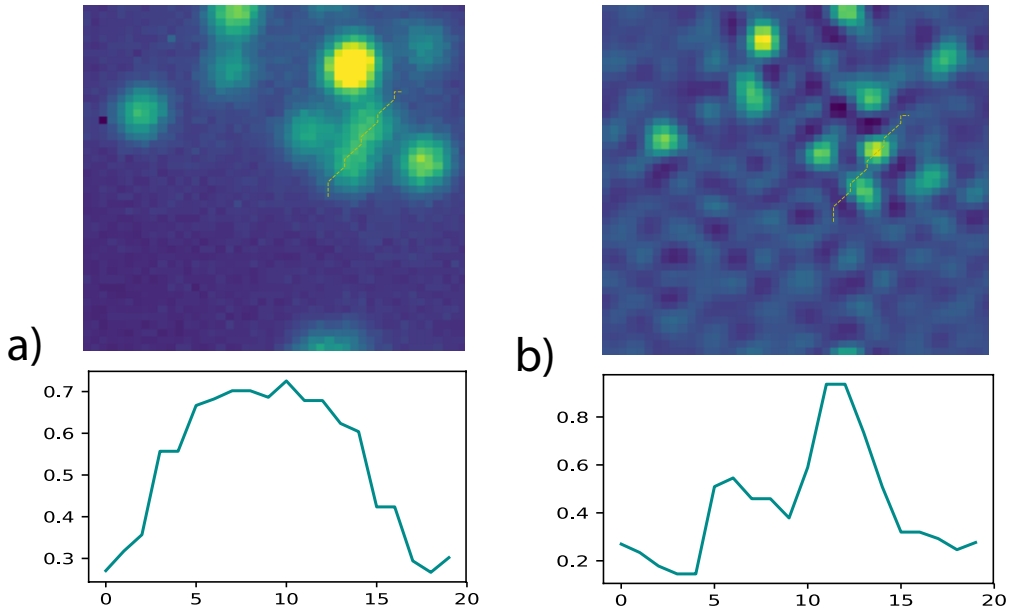

Figure 4.12: a)Widefield image of the scene b)SIM reconstructed image a). Their corresponding plots show that b) has superior resolution than a). SIM with reduced number of foci only implies a smaller field-of-view and does not affect resolution enhancement.

that the foci in the generated array have uniform intensities and reasonable modulation contrast.

Furthermore, we obtained an estimate of PSF of the optical system by recording the fluorescence from point sources. With sufficient knowledge of the imaging system and the illumination pattern, it is possible to perform SIM experiments. We imaged fluorescent beads using multiple foci and processed them using SIM algorithm. By shifting the illumination pattern in space multiple images of the beads were acquired. The illumination phase shifts are determined from the fluorescence images using *a posteriori* estimation technique. By applying various transformations and filtering using reconstruction algorithm, we are able to extract high resolution information from the diffraction limited images. The reported results in this chapter show that we are indeed able to enhance the resolution of our scattering microscope. The broadening of the system OTF after SIM reconstruction shows that we now have access to the high resolution information which was otherwise not accessible. The SIM reconstructed images of fluorescent beads are superior in resolution compared to their widefield counterparts. A closer examination reveals about ≈ 1.6 fold improvement in resolution over conven-

tional widefield imaging. This is as expected from the illumination frequency used in our recorded images.

Chapter 5

Summary and Outlook

In this thesis I have described a new approach to obtaining sub-diffraction images behind opaque scattering media. This approach involves the application of the high resolution reconstruction methods used in Structured Illumination Microscopy (SIM). In order to apply SIM behind scattering medium, firstly one needs to be able to generate a periodically varying illumination pattern behind the medium. Using wavefront shaping first an interferometric focus is formed from the light scattered through a scattering medium. As I have shown in this thesis, this focus can be subsequently split up into multiple foci arranged on a regular grid. This then serves as the required patterned illumination that enables to perform SIM imaging. By doing this we have obtained images of samples hidden behind scattering media. The subsequent processing of these images using SIM principles has indeed shown an improvement in resolution of the microscope.

In the recent years, wavefront shaping technique has been widely applied to control the transmitted light from a scattering medium. Wavefront shaping refers to controlling the shape of the incoming light using a wavefront modulator such that the scattered field behaves a certain way. Typically the idea is to make the scattered light focus to a point by adjusting the phase and/or amplitude of the incoming light. Due to interference between multiple scattered light paths, adjusting the phase in the input affects the intensity at the focus. An optimised input wavefront makes all the multiply scattered light paths to converge to a focus behind the scattering medium. This requires a feedback mechanism to get a measure of how the intensity of the focus is changing. By updating the incoming wavefront to increase the intensity at the focus, the optimum wavefront is determined iteratively. Once found, the intensity at the focus will be its maximum value. As the focus is obtained due to constructive interfernce of multiple scattered light paths, the technique is called interferometric focusing. Hence wavefront shaping transforms a scattering medium into a lens, a *scattering lens*.

The ability to focus light through a scattering medium calls for an application of the technique in microscopy. In biological samples that are typically multiple scatterers of light, imaging is difficult as the light used to image is strongly scattered. Hence by way of controlling light using wavefront shaping, the scattering from the biological samples can be utilised to focus the light. That way scattering doesn't pose a threat to imaging the samples any more, and imaging in the presence of scattering is made possible. The interferometric focus obtained via wavefront shaping can be scanned across in space due to memory effect and obtain 2D and 3D image stacks of samples.

One can call it a *scattering microscope* as the technique turns a scattering medium into a lens. However the obtained images have a resolution that is limited by diffraction, since the interferometric focus itself is diffraction limited. This poses a challenge for imaging when superior resolution is desirable.

The goal of our research is to find a way to enhance the resolution of the scattering microscope. In order to do so, we have explored SIM. It is a super-resolution microscopy technique that allows a resolution enhancement upto a factor two beyond diffraction limit. The principle of extracting high resolution information from the diffraction limited images of the sample using SIM relies on the fact that the sample information can be coupled to the structure of the illumination pattern. When a sample is illuminated with a periodically varying intensity pattern rather than illuminating uniformly, the otherwise inaccessible high resolution information is down-modulated by the illumination. This information can be later extracted by acquiring multiple images by translating the illumination.

In order to apply SIM behind scattering media, we first need to generate periodically varying intensity distribution behind scattering medium. As I have shown in this thesis, it is indeed possible to transform an interferometric focus behind scattering medium into an array of multiple focal spots. By exploiting the Fourier Transformation property of a *scattering lens*, it is possible to split up the focus into multiple foci. We have shown that, if an arrangement of foci on a lattice is known, the aperture that is required to generate such a lattice of foci can be determined. The thesis also describes techniques to determine such aperture designs offline, so that the experiments are not disturbed. The aperture design thus obtained is simply added to the scattering lens in the experiments, making it to split the focus in the same arrangement of multiple foci as desired. This means that we are able to turn a scattering medium into a lens of adaptable aperture. This can be a useful technique to apply in imaging, to parallelize image acquisition, or apply to optical trapping to simultaneously trap multiple objects that are hidden behind a scattering medium.

With these tools in hand, we have explored SIM behind scattering media. A uniform array of multiple foci is used to excite underlying fluorescent structures and record their response. The recorded images are processed using SIM algorithm to extract high resolution information. Such a reconstructed image reveals finer details of the fluorescent structures. Our experiments show about 1.6 fold improvement in the resolution of our *scattering microscope* over conventional images produced by single focus scanning.

Thus we have demonstrated that not only can a scattering medium be transformed into a lens, but also it is possible to obtain high resolution images beyond the diffraction limit of such a lens. This means beyond diffraction limited imaging is made possible with just a simple scattering medium.

During the course of this work, we have also demonstrated a technique of iterative refocusing that can be a useful tool that facilitates super-resolution imaging behind scattering media. As discussed in this thesis, iterative refocusing, as the name suggests works by iteratively scanning an interferometric focus behind scattering medium and refocus and repeat. Since the scanning of the focus is possible only within a range of memory effect, this can be a limiting factor for imaging larger regions of a specimen. By way of iterative refocusing, the focus can be refocused as soon as it falls outside of the memory effect range. This also means that the scannable region for SIM can also be increased by employing iterative refocusing. Hence by way of combining SIM with iterative refocusing, a larger region of the sample can be imaged with higher resolution than previously possible.

Bibliography

[1] R. K. Tyson, Principles of Adaptive Optics, Fourth Edition. Apple Academic Press Inc., 2015.

[2] J. Pawley, ed., Handbook of Biological Confocal Microscopy. Springer US, 2010.

[3] M. C. W. van Rossum and T. M. Nieuwenhuizen, "Multiple scattering of classical waves: microscopy, mesoscopy, and diffusion," Reviews of Modern Physics, vol. 71, pp. 313–371, jan 1999.

[4] E. Abbe, "Beiträge zur theorie des mikroskops und der mikroskopischen wahrnehmung," Archiv fr Mikroskopische Anatomie, vol. 9, pp. 413–418, dec 1873.

[5] C. B. Müller and J. Enderlein, "Image scanning microscopy," Physical Review Letters, vol. 104, may 2010.

[6] P. J. Shaw and D. J. Rawlins, "The point-spread function of a confocal microscope: its measurement and use in deconvolution of 3-d data," Journal of Microscopy, vol. 163, pp. 151–165, aug 1991.

[7] K. I. Willig, S. O. Rizzoli, V. Westphal, R. Jahn, and S. W. Hell, "STED microscopy reveals that synaptotagmin remains clustered after synaptic vesicle exocytosis," Nature, vol. 440, pp. 935–939, apr 2006.

[8] R. Heintzmann, T. M. Jovin, and C. Cremer, "Saturated patterned excitation microscopy—a concept for optical resolution improvement," Journal of the Optical Society of America A, vol. 19, p. 1599, aug 2002.

[9] S. W. Hell, "Fluorescence nanoscopy: Breaking the diffraction barrier by the RESOLFT concept," GBM Annual Fall meeting Berlin/Potsdam 2005, vol. 2005, sep 2005.

[10] M. J. Rust, M. Bates, and X. Zhuang, "Sub-diffraction-limit imaging by stochastic optical reconstruction microscopy (STORM)," Nature Methods, vol. 3, pp. 793–796, aug 2006.

[11] E. Betzig, G. H. Patterson, R. Sougrat, O. W. Lindwasser, S. Olenych, J. S. Bonifacino, M. W. Davidson, J. Lippincott-Schwartz, and H. F. Hess, "Imaging intracellular fluorescent proteins at nanometer resolution," Science, vol. 313, pp. 1642–1645, sep 2006.

[12] M. G. L. Gustafsson, "Surpassing the lateral resolution limit by a factor of two using structured illumination microscopy. SHORT COMMUNICATION," Journal of Microscopy, vol. 198, pp. 82–87, may 2000.

[13] A. Corlu, R. Choe, T. Durduran, M. A. Rosen, M. Schweiger, S. R. Arridge, M. D. Schnall, and A. G. Yodh, "Three-dimensional in vivo fluorescence diffuse optical tomography of breast cancer in humans," Optics Express, vol. 15, no. 11, p. 6696, 2007.

[14] W. Denk, J. Strickler, and W. Webb, "Two-photon laser scanning fluorescence microscopy," Science, vol. 248, pp. 73–76, apr 1990.

[15] A. F. Fercher, W. Drexler, C. K. Hitzenberger, and T. Lasser, "Optical coherence tomography - principles and applications," Reports on Progress in Physics, vol. 66, pp. 239–303, jan 2003.

[16] R. Corey, M. Kissner, and P. Saulnier, "Coherent backscattering of light," American Journal of Physics, vol. 63, pp. 560–564, jun 1995.

[17] P. Gross, M. Störzer, S. Fiebig, M. Clausen, G. Maret, and C. M. Aegerter, "A precise method to determine the angular distribution of backscattered light to high angles," Review of Scientific Instruments, vol. 78, p. 033105, mar 2007.

[18] J. C. Dainty, Progress in Optics XIV. North Holland, 1976.

[19] I. M. Vellekoop and A. P. Mosk, "Universal optimal transmission of light through disordered materials," Physical Review Letters, vol. 101, sep 2008.

[20] I. M. Vellekoop, Controlling the propagation of light in disordered scattering media. PhD thesis, University of Twente, 2008.

[21] M. Segev, Y. Silberberg, and D. N. Christodoulides, "Anderson localization of light," Nature Photonics, vol. 7, pp. 197–204, mar 2013.

[22] F. Scheffold and G. Maret, "Universal conductance fluctuations of light," Physical Review Letters, vol. 81, pp. 5800–5803, dec 1998.

[23] I. M. Vellekoop, A. Lagendijk, and A. P. Mosk, "Exploiting disorder for perfect focusing," Nature Photonics, vol. 4, pp. 320–322, feb 2010.

[24] I. M. Vellekoop, "Feedback-based wavefront shaping," Optics Express, vol. 23, p. 12189, apr 2015.

[25] Z. Zhang, Z. You, and D. Chu, "Fundamentals of phase-only liquid crystal on silicon (LCOS) devices," Light: Science & Applications, vol. 3, pp. e213–e213, oct 2014.

[26] L. G. Neto, D. Roberge, and Y. Sheng, "Full-range, continuous, complex modulation by the use of two coupled-mode liquid-crystal televisions," Applied Optics, vol. 35, p. 4567, aug 1996.

[27] S. Chavali, P. M. Birch, R. Young, and C. Chatwin, "Synthesis and reconstruction of computer generated holograms by a double pass technique on a twisted nematic-based liquid crystal spatial light modulator," Optics and Lasers in Engineering, vol. 45, pp. 413–418, mar 2007.

[28] E. G. van Putten, I. M. Vellekoop, and A. P. Mosk, "Spatial amplitude and phase modulation using commercial twisted nematic LCDs," Applied Optics, vol. 47, p. 2076, apr 2008.

[29] F. Kong, R. H. Silverman, L. Liu, P. Chitnis, K. K. Lee, and Y.-C. Chen, "Photoacoustic-guided convergence of light through optically diffusive media," in Imaging and Applied Optics, OSA, 2011.

[30] T. Chaigne, O. Katz, A. C. Boccara, M. Fink, E. Bossy, and S. Gigan, "Controlling light in scattering media non-invasively using the photoacoustic transmission matrix," Nature Photonics, vol. 8, pp. 58–64, nov 2013.

[31] O. Katz, E. Small, Y. Bromberg, and Y. Silberberg, "Focusing and compression of ultrashort pulses through scattering media," Nature Photonics, vol. 5, pp. 372–377, may 2011.

[32] I. Vellekoop and A. Mosk, "Phase control algorithms for focusing light through turbid media," Optics Communications, vol. 281, pp. 3071–3080, jun 2008.

[33] S. M. Popoff, G. Lerosey, R. Carminati, M. Fink, A. C. Boccara, and S. Gigan, "Measuring the transmission matrix in optics: An approach to the study and control of light propagation in disordered media," Physical Review Letters, vol. 104, mar 2010.

[34] D. B. Conkey, A. N. Brown, A. M. Caravaca-Aguirre, and R. Piestun, "Genetic algorithm optimization for focusing through turbid media in noisy environments," Optics Express, vol. 20, p. 4840, feb 2012.

[35] B. Blochet, L. Bourdieu, and S. Gigan, "Focusing light through dynamical samples using fast continuous wavefront optimization," Optics Letters, vol. 42, p. 4994, nov 2017.

[36] I. M. Vellekoop, E. G. van Putten, A. Lagendijk, and A. P. Mosk, "Demixing light paths inside disordered metamaterials," Optics Express, vol. 16, no. 1, p. 67, 2008.

[37] I. M. Vellekoop and A. P. Mosk, "Focusing coherent light through opaque strongly scattering media," Optics Letters, vol. 32, p. 2309, aug 2007.

[38] S. Feng, C. Kane, P. A. Lee, and A. D. Stone, "Correlations and fluctuations of coherent wave transmission through disordered media," Physical Review Letters, vol. 61, pp. 834–837, aug 1988.

[39] I. Freund, M. Rosenbluh, and S. Feng, "Memory effects in propagation of optical waves through disordered media," Physical Review Letters, vol. 61, pp. 2328–2331, nov 1988.

[40] E. G. van Putten, D. Akbulut, J. Bertolotti, W. L. Vos, A. Lagendijk, and A. P. Mosk, "Scattering lens resolves sub-100 nm structures with visible light," Physical Review Letters, vol. 106, may 2011.

[41] G. Ghielmetti and C. Aegerter, "Scattered light fluorescence microscopy in three dimensions," in Biomedical Optics and 3-D Imaging, OSA, 2012.

[42] S. Scheibler, "Focusing and scanning light through turbid media," Master's thesis, University of Zurich, 2018.

[43] G. Ghielmetti and C. M. Aegerter, "Direct imaging of fluorescent structures behind turbid layers," Optics Express, vol. 22, p. 1981, jan 2014.

[44] C. Maurer, A. Jesacher, S. Frhapter, S. Bernet, and M. Ritsch-Marte, "Tailoring of arbitrary optical vector beams," New Journal of Physics, vol. 9, pp. 78–78, mar 2007.

[45] M. Persson, D. Engström, A. Frank, J. Backsten, J. Bengtsson, and M. Goksör, "Minimizing intensity fluctuations in dynamic holographic optical tweezers by restricted phase change," Optics Express, vol. 18, p. 11250, may 2010.

[46] T. Čižmár and K. Dholakia, "Shaping the light transmission through a multimode optical fibre: complex transformation analysis and applications in biophotonics," Optics Express, vol. 19, p. 18871, sep 2011.

[47] J. W. Goodman, Introduction to Fourier Optics. W.H.Freeman & Co Ltd, 2005.

[48] H. Dammann and E. Klotz, "Coherent optical generation and inspection of two-dimensional periodic structures," Optica Acta: International Journal of Optics, vol. 24, pp. 505–515, apr 1977.

[49] F. Dickey, Laser beam shaping. CRC Press, jul 2014.

[50] L. A. Romero and F. M. Dickey, "Theory of optimal beam splitting by phase gratings i one-dimensional gratings," Journal of the Optical Society of America A, vol. 24, p. 2280, jul 2007.

[51] L. A. Romero and F. M. Dickey, "The Mathematical Theory of Laser Beam-Splitting Gratings," Progress in Optics, pp. 319–386, 2010.

[52] R. W. Gerchberg and W. O. Saxton, "A practical algorithm for the determination of phase from image and diffraction plane pictures," Optik, 1971.

[53] J. R. Fienup, "Phase retrieval algorithms: a comparison," Applied Optics, vol. 21, p. 2758, aug 1982.

[54] M. W. Farn, "New iterative algorithm for the design of phase-only gratings," in Computer and Optically Generated Holographic Optics; 4th in a Series (I. Cindrich and S. H. Lee, eds.), SPIE, dec 1991.

[55] J. R. Fienup, "Iterative method applied to image reconstruction and to computer-generated holograms," Optical Engineering, vol. 19, jun 1980.

[56] D. Engström, A. Frank, J. Backsten, M. Goksör, and J. Bengtsson, "Grid-free 3D multiple spot generation with an efficient single-plane FFT-based algorithm," Optics Express, vol. 17, p. 9989, may 2009.

[57] Y. Ogura, M. Aino, and J. Tanida, "Design and demonstration of fan-out elements generating an array of subdiffraction spots," Optics Express, vol. 22, p. 25196, oct 2014.

[58] C. Wu, H. Gu, Z. Zhou, and Q. Tan, "Design of diffractive optical elements for sub-diffraction spot arrays with high light efficiency," Applied Optics, vol. 56, p. 8816, nov 2017.

[59] A. Malavalli, M. Ackermann, and C. M. Aegerter, "Structured illumination behind turbid media," Optics Express, vol. 24, p. 23018, sep 2016.

[60] R. C. Dunn, "Near-field scanning optical microscopy," Chemical Reviews, vol. 99, pp. 2891–2928, oct 1999.

[61] M. G. L. Gustafsson, D. A. Agard, and J. W. Sedat, "Doubling the lateral resolution of wide-field fluorescence microscopy using structured illumination," in Three-Dimensional and Multidimensional Microscopy: Image Acquisition Processing VII (J.-A. Conchello, C. J. Cogswell, A. G. Tescher, and T. Wilson, eds.), SPIE, may 2000.

[62] A. G. York, S. H. Parekh, D. D. Nogare, R. S. Fischer, K. Temprine, M. Mione, A. B. Chitnis, C. A. Combs, and H. Shroff, "Resolution doubling in live, multicellular organisms via multifocal structured illumination microscopy," Nature Methods, vol. 9, pp. 749–754, may 2012.

[63] N. Chakrova, B. Rieger, and S. Stallinga, "Deconvolution methods for structured illumination microscopy," Journal of the Optical Society of America A, vol. 33, p. B12, may 2016.

[64] I. M. Vellekoop and C. M. Aegerter, "Scattered light fluorescence microscopy: imaging through turbid layers," Optics Letters, vol. 35, p. 1245, apr 2010.

[65] O. Katz, E. Small, and Y. Silberberg, "Looking around corners and through thin turbid layers in real time with scattered incoherent light," Nature Photonics, vol. 6, pp. 549–553, jul 2012.

[66] S. Popoff, G. Lerosey, M. Fink, A. C. Boccara, and S. Gigan, "Image transmission through an opaque material," Nature Communications, vol. 1, pp. 1–5, sep 2010.

[67] A. P. Mosk, A. Lagendijk, G. Lerosey, and M. Fink, "Controlling waves in space and time for imaging and focusing in complex media," Nature Photonics, vol. 6, pp. 283–292, may 2012.

[68] J. Bertolotti, E. G. van Putten, C. Blum, A. Lagendijk, W. L. Vos, and A. P. Mosk, "Non-invasive imaging through opaque scattering layers," Nature, vol. 491, pp. 232–234, nov 2012.

[69] O. Katz, P. Heidmann, M. Fink, and S. Gigan, "Non-invasive single-shot imaging through scattering layers and around corners via speckle correlations," Nature Photonics, vol. 8, pp. 784–790, aug 2014.

[70] J. Schneider and C. M. Aegerter, "Guide star based deconvolution for imaging behind turbid media," Journal of the European Optical Society-Rapid Publications, vol. 14, oct 2018.

[71] H. Yilmaz, E. G. van Putten, J. Bertolotti, A. Lagendijk, W. L. Vos, and A. P. Mosk, "Speckle correlation resolution enhancement of wide-field fluorescence imaging," Optica, vol. 2, p. 424, apr 2015.

[72] R. Heintzmann and C. G. Cremer, "Laterally modulated excitation microscopy: improvement of resolution by using a diffraction grating," in Optical Biopsies and Microscopic Techniques III (I. J. Bigio, H. Schneckenburger, J. Slavik, K. Svanberg, and P. M. Viallet, eds.), SPIE, jan 1999.

[73] M. A. A. Neil, R. Juškaitis, and T. Wilson, "Method of obtaining optical sectioning by using structured light in a conventional microscope," Optics Letters, vol. 22, p. 1905, dec 1997.

[74] S. W. Hell, S. Lindek, C. Cremer, and E. H. K. Stelzer, "Confocal microscopy with an increased detection aperture: type-b 4pi confocal microscopy," Optics Letters, vol. 19, p. 222, feb 1994.

[75] M. G. L. Gustafsson, D. A. Agard, and J. W. Sedat, "Sevenfold improvement of axial resolution in 3D wide-field microscopy using two objective lenses," in Three-Dimensional Microscopy: Image Acquisition and Processing II (T. Wilson and C. J. Cogswell, eds.), SPIE, mar 1995.

[76] "ZEISS Microscopy Online Campus."

[77] M. G. L. Gustafsson, L. Shao, P. M. Carlton, C. J. R. Wang, I. N. Golubovskaya, W. Z. Cande, D. A. Agard, and J. W. Sedat, "Three-dimensional resolution doubling in wide-field fluorescence microscopy by structured illumination," Biophysical Journal, vol. 94, pp. 4957–4970, jun 2008.

[78] R. Heintzmann, "Saturated patterned excitation microscopy with two-dimensional excitation patterns," Micron, vol. 34, pp. 283–291, oct 2003.

[79] N. Chakrova, R. Heintzmann, B. Rieger, and S. Stallinga, "Studying different illumination patterns for resolution improvement in fluorescence microscopy," Optics Express, vol. 23, p. 31367, nov 2015.

[80] A. Lal, C. Shan, and P. Xi, "Structured illumination microscopy image reconstruction algorithm," IEEE Journal of Selected Topics in Quantum Electronics, vol. 22, pp. 50–63, jul 2016.

[81] S. A. Shroff, J. R. Fienup, and D. R. Williams, "Phase-shift estimation in sinusoidally illuminated images for lateral superresolution," Journal of the Optical Society of America A, vol. 26, p. 413, jan 2009.

[82] K. Wicker, O. Mandula, G. Best, R. Fiolka, and R. Heintzmann, "Phase optimisation for structured illumination microscopy," Optics Express, vol. 21, p. 2032, jan 2013.

Acknowledgements

I would like to thank my supervisor Christof Aegerter for giving me this wonderful opportunity to work in the ”Disordered and Biological Soft Matter” group. I would also like to thank him for his kind support and encouragement through these years. His ”always open office doors” has made it very easy to approach him. He has also been very understanding and considerate during crisis situations and I thank him for that. His teaching and outreach activities have been particularly inspiring. It has been my great pleasure working for him on this project. In addition to research I have also enjoyed teaching undergraduate students and giving student lab-tours.

I would like to thank Mirco Ackermann with whom I have collaborated during my PhD. He has been my go-to person for programming tips & tricks. He has also been a great company for discussing various scientific concepts, coming up with new ideas etc. I have learnt a lot from Mirco, in a way he has been a mentor to me. I also thank him for proof-reading this thesis.

I would like to thank my colleagues, the present and (recent)past members of Aegerter group for a lively atmosphere at work. I would like to particularly thank my office mates Sahil, Paulé and Mirco who have also become my close friends. I thank them for making the office a healthy and ”nourishing” place to work at. I will cherish all the crazy and intense discussions on a variety of topics that we have shared. I have also derived comfort and support from them during the down times of my PhD and I thank them for being there for me. I would like to thank Jale Schneider for the various interesting discussions we have had with respect to our experiments. I have also enjoyed learning German (and Swiss German phrases) from them.

I would like to thank my family, most importantly my husband Bhargava Ram without whom this whole endeavour would have been impossible. I’m grateful for his support and the independence that he has given me to pursue this dream of mine. I would like to also thank my sister who has been a source of energy for me, that has kept me

going through my PhD. The past four and half years have been truly the best time of my life. It has been the peak of my intellectual and personal experience. Leaving my country behind and integrating into a new culture here in Switzerland has taught me a lot. For this reason I thank each and everyone who have made this possible for me.

I consider myself fortunate to have acquainted with all these wonderful people and I sincerely thank them for making this journey a huge success.

Research Article | Vol. 24, No. 20 | 3 Oct 2016 | OPTICS EXPRESS 23018
Optics EXPRESS

Structured illumination behind turbid media

A. MALAVALLI, M. ACKERMANN AND C. M. AEGERTER*

Physics Institute, University of Zurich, Winterthurerstrasse 190, 8057 Zurich, Switzerland
*aegerter@physik.uzh.ch

Abstract: In turbid media, light gets multiply scattered to an extent that all the information of its propagation is scrambled over a characteristic distance called the transport mean free path. Controlling light propagation through such media is therefore challenging. By using a feedback signal, the input wavefront of light can be shaped such that light gets focused through or even inside a scattering medium [Vellekoop et al., Opt. Express *36*, 67 (2008)]. In this article, we show that such an interferometric focus can be transformed into an array of multiple focal spots with a desired structure. These focal spots can serve as a structured illumination source to image the interior of thick scattering tissues as in deconvolution imaging or in the optical micromanipulation of microscopic targets.

OCIS codes: (110.0113) Imaging through turbid media; (110.2945) Illumination design; (120.5060) Phase modulation

References and links

1. I. M. Vellekoop and A. P. Mosk,"Focusing coherent light through opaque strongly scattering media," Opt. Lett. **32**(16), 2309–2311 (2007).
2. I. M. Vellekoop, E. G. van Putten, A. Lagendijk, and A. P. Mosk,"Demixing light paths inside disordered metamaterials", Opt. Express **16**(1), 67–80 (2008).
3. C. Maurer, A. Jesacher, S. Fürhapter, S. Bernet and M. Ritsch-Marte, "Tailoring of arbitrary optical vector beams", New J. Phys. **9**(78), 1367–2630 (2007).
4. B. Chang, L.Chou, Y. Chang and S. Chiang,"Isotropic image in structured illumination microscopy patterned with a spatial light modulator," Opt. Express **17**(17), 14710–14721 (2009).
5. M.G.L. Gustafsson. "Surpassing the lateral resolution limit by a factor of two using structured illumination microscopy," J. Microsc. **198**, 82–87 (2000).
6. M. A. A. Neil, R. Juskaitis, and T. Wilson, "Method of obtaining optical sectioning by using structured light in a conventional microscope," Opt. Lett. **22**(24), 1905–1907 (1997).
7. S. W. Hell, & J. Wichmann, "Breaking the diffraction resolution limit by stimulated emission: stimulated-emission-depletion fluorescence microscopy," Opt. Lett. **19**, 780–782 (1994).
8. C. Kuang, S. Li, W. Liu, X. Hao, Z. Gu, Y. Wang, J. Ge, H. Li & X. Liu,"Breaking the Diffraction Barrier Using Fluorescence Emission Difference Microscopy," Sci. Rep. **3**, 1441 (2013).
9. T. Čižmár & K. Dholakia,"Shaping the light transmission through a multimode optical fibre: complex transformation analysis and applications in biophotonics," Opt. Expres, **19**(20), 18871–18884 (2011).
10. T. Čižmár, M. Mazilu and K. Dholakia,"In situ wavefront correction and its application to micromanipulation," Nat. Photon. **4**, 388–394 (2010).
11. S. Bianchia and R.Di Leonardo, "A multi-mode fiber probe for holographic micromanipulation and microscopy," Lab Chip **12**, 635–639 (2012).
12. S. Popoff, G. Lerosey, M. Fink, A. C. Boccara & S. Gigan,"Image transmission through an opaque material," Nat. Commun. **1** 81 (2010).
13. I.M.Vellekoop, "Feedback-based wavefront shaping," Opt. Express **23**(9), 12189–12206 (2015).
14. G. Ghielmetti and C.M. Aegerter,"Scattered light fluorescence microscopy in three dimensions," Opt. Express **20**(4), 3744–3752 (2012).
15. I. M. Vellekoop, A. Lagendijk, and A. P. Mosk,"Exploiting disorder for perfect focusing," Nat. Photon. **4**, 320–322 (2010).
16. T. Chaigne, J. Gateau, O. Katz, E. Bossy, and S. Gigan, "Light focusing and two-dimensional imaging through scattering media using the photoacoustic transmission matrix with an ultrasound array," Opt. Lett. **39**(9), 2664–2667 (2014).
17. I.M. Vellekoop & A.P. Mosk, "Phase control algorithms for focusing light through turbid media," Opt. Commun. **281**, 3071–3080 (2008).
18. G. Ghielmetti and C. M. Aegerter,"Direct imaging of fluorescent structures behind turbid layers," Opt. Express **22**(2), 1981–1989 (2014).
19. I.M.Vellekoop, Doctoral dissertation "Controlling the propagation of Light in Disordered Scattering Media".
20. D. Engström, A. Frank, J. Backsten, M. Goksör, and J. Bengtsson, "Grid-free 3D multiple spot generation with an efficient single-plane FFT-based algorithm," Opt. Express **17**(12), 9989–10000 (2009).

#272460 http://dx.doi.org/10.1364/OE.24.023018
Journal © 2016 Received 3 Aug 2016; revised 16 Sep 2016; accepted 18 Sep 2016; published 26 Sep 2016
Corrected: 27 September 2016

21. J. W. Goodman, *Statistical Optics* (Wiley, 2000).
22. I. Freund, M. Rosenbluh, and S. Feng, "Memory Effects in Propagation of Optical Waves through Disordered Media," Phys. Rev. Lett. **61**, 2328–2331 (1988).

1. Introduction

Wavefront shaping is gaining much attention in the field of light microscopy to control the propagation of light in multiply scattering materials [1,2]. It is one of the ways to counter the effects of scattering when imaging through materials of biological interest. Wavefront shaping has also been used to structure the illumination pattern in light microscopy. Interference between multiple orders of diffraction from a grating forms a sinusoidally varying light field. First order Bessel modes or other higher order vector modes can be generated using Spatial Light Modulators (SLM) [3,4]. Such synthetic illumination patterns are known to enhance resolution in imaging beyond the diffraction limit [4–6] and Bessel or donut beams have been used for excitation-deexcitation beam configurations in STED microscopy [7,8]. However, when transmitting these illumination patterns through turbid media, light gets multiply scattered and the pattern is quickly lost. Hence, structured illumination approach is able to work with optically thin or transparent sections, which is often limited to superficial layers of samples.

Using SLMs, the wavefront of incoming light can be modulated in phase and amplitude in order to control the scattered light field. In adaptive optics, feedback based algorithms are used to correct for abberations from optical setups and to map the transmission matrix of abberated systems such as optical fibers [9]. This approach has been widely used for trapping and micromanipulation of particles [10,11]. But mapping such a transmission matrix can be time consuming when many configurations of output fields are to be realised [12]. It is however now possible to focus light through a multiply scattering medium using feedback based algorithms [13] and scan this focus in 3D [14]. In the present article we extend this technique to obtain multiple focal spots behind a multiply scattering medium.

The working principle of our technique as demonstrated by Fig. 1 is that a diffraction limited focus can be generated using a feedback based technique using an iterative algorithm [15–17] and such a focus can then be transformed into a user defined configuration of multiple focal spots. After the optimization process, the scattering medium acts as a turbid lens that focuses the spatially modulated optimum wavefront. By adding a desired phase mask to this wavefront, multiple focal spots can be generated by virtue of convolution theorem. As this technique does not depend on the type of feedback mechanism used to create the initial focus it can be beneficial especially when a direct access to the focal plane is not available [18]. The theory concerning this technique is decribed in section 2. The computation of such phase masks, also called Computer Generated Holograms (CGHs) is described in section 3 followed by the experimental results in section 4. Multiple foci can also be generated without the use of these CGHs- by directly

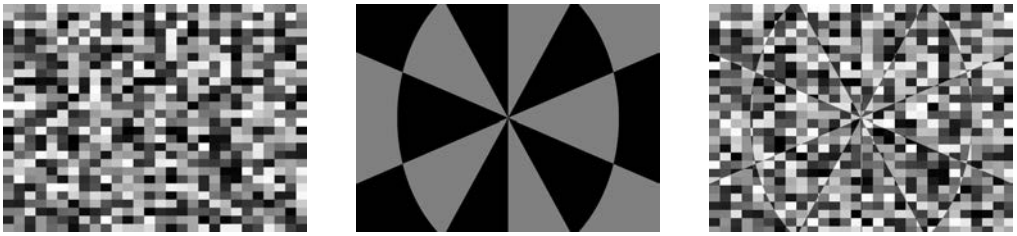

a) Optimum Wavefront b) Computed CGH c)Final SLM phase

Fig. 1. To the optimum wavefront a) leading to a focus behind the turbid medium, when a CGH such as b) is added, the resulting phase would look like c).

optimizing on multiple targets as previously described in [19]. In section 5 of this article we further describe and compare these methods.

2. Theoretical background

As shown in the experimental setup Fig. 2, the SLM plane and sample form conjugate planes such that an image of the SLM screen is formed on the sample. When a phase modulation scheme is used [17], the computer algorithm iteratively alters the phase of the pixels on the SLM to form an interferometric focus at the focal plane.

After focusing, the combination of SLM and the scattering medium acts as a lens. If the beam coming into the SLM is tilted, the focal spot moves. This tilting effect can also be implemented by just adding a suitable phase to the modulated wavefront at the SLM. The same works if we add a phase pattern that, like a grating, results in multiple beams. To this combination resulting in a lens, by adding the phase pattern of a grating, we bring the far field of the grating onto the focal plane, resulting in multiple spots.

If $\mathcal{E}_i = \mathcal{E}_0 \exp^{i\,\phi}$ is the electric field of the wavefront with phase ϕ modulated by the SLM to obtain a focus, the field at the focal plane on the CCD is given by [14],

$$\mathcal{E}_f = \iint_S \mathcal{E}_i\, t_{i\,s}\, g(r_f - r_s)\, d^2 r_s \tag{1}$$

integrated over the scattering plane of the sample. Here, $t_{i\,s}$ is the coefficient of the optical setup for transmitting light from each segment of the SLM to the output plane of the sample and the light propagaion from this plane to the CCD is described by the free space Green function $g(r_f - r_s)$ [15]. It has been shown experimentally [15] that the shape of this interferometric focus is same as the speckle correlation function [21].

Transformation of this focus into multiple foci can be understood using the convolution theorem. It states that,

if $\mathcal{F}\{\mathcal{E}_f(y,z)\} = E(k_y,k_z)$ and $\mathcal{F}\{f(y,z)\} = F(k_y,k_z)$, then

$$\begin{aligned}\mathcal{F}\{\mathcal{E}_f * f\} &= \mathcal{F}\{\iint_{-\infty}^{+\infty} \mathcal{E}_f(y,z)\, f(Y-y, Z-z)\, dy\, dz\} \\ &= \mathcal{F}\{\mathcal{E}_f(y,z)\}\ \mathcal{F}\{f(y,z)\} \\ &= E(k_y,k_z)\ F(k_y,k_z)\end{aligned} \tag{2}$$

i.e if $\mathcal{E}_f(y,z)$ represents the field distribution of the interferometric focus and $f(y,z)$ represents Dirac delta functions with their peaks located where the focal spots are desired,

$$f(y,z) = \sum_i \exp^{i\,\phi_i}\, \delta(y - y_i)\delta(z - z_i) \tag{3}$$

the convolution between the two leads to a multiple focal pattern in the image plane. Furthermore, the phase that needs to be added on the SLM plane in order to obtain this multiple focal pattern can be extracted by noticing that,

$$E(k_y,k_z) = \mathcal{E}_i\, t_{i\,s}\, g(r_f - r_s) \tag{4}$$

and as $t_{i\,s}$ and $g(r_f - r_s)$ are unaffected, $\mathcal{F}\{\mathcal{E}_f * f\} = \mathcal{E}_i\, F(k_y,k_z)$

Since we make use of phase only modulation scheme, the intensity contribution to the focal plane from different regions of sample is not the same, leading to fluctuations in intensity when focal spots move. However this could be rectified if both phase and amplitude modulation scheme were used in the optimization process.

Optics EXPRESS

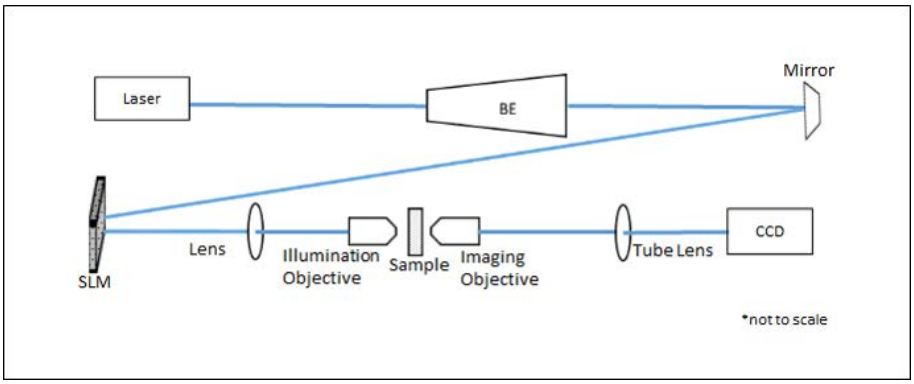

Fig. 2. Experimental Setup.

3. Experimental setup

The experimental setup is as shown in Fig. 2. Light from a Cyan laser (Newport Spectra-Physics) at 488nm is expanded with a beam expander setup (BE) to fill the screen of the SLM (HOLOEYE HEO 1080P). The SLM plane is imaged onto the sample using a lens and a 40x illumination objective, such that the SLM and the sample make a pair of conjugate planes. The back surface of the sample is imaged with a 50X objective and a CCD. We made use of opaque samples of microscope slide coated with TiO_2 with thicknesses ranging from 3-15μm. Light transmitted through such a sample is multiply scattered and forms a speckle pattern on the CCD. Using stepwise sequential algorithm [17], the SLM modulates the phase of the input wavefront while monitoring the intensity enhancement at a small target region (typically about the size of a single speckle) on the CCD. The input intensity before optimisation is kept low enough to avoid saturation on the CCD. After iterating over the whole SLM, an interferometric focus is formed at the target. Once this initial focus is formed, the CGHs can be loaded onto the optimized wavefront on the SLM plane and the resulting multiple foci can be visualised on the CCD. Using linear or parabolic phase gradients at the SLM, the focal spots can be translated on the CCD. For the experiments involving movement of the foci, a grit polished diffuser glass was used as a sample.

4. Phase mask generation

The generation of CGHs is a crucial step of these experiments. Depending on the complexity of the desired configuration of focal spots, one can choose from different methods to generate the CGH [3, 20]. As the Fourier transformation operation is reversible [22], the phase modulation by $F(k_y, k_z)$, as described in Eq. (2-3), in the scattering plane of the sample should lead to a 2D grid of Dirac delta functions in the image plane, as described in the previous section. To get a planar grid of equally spaced focal spots, we generated grayscale images such as shown in Fig. 3(a). The phase modulation is achieved using 8-bit bitmap images, whose grayscale values between 0-255 correspond to a phase modulation between 0-2π. These images constitute a combination of binary gratings of multiple periods extending in 2 dimensions. Furthermore, we computed the Fourier transform of the phase values of these images to verify that the intensity peaks in the image plane appear at the spatial frequencies defined by the periodicity of the gratings. These peaks in the Fourier transform correspond to the positions of the focal spots that would be formed on the image plane Fig. 3(b). The grayscale values and/or the period of the gratings in the images were altered to change the configuration and position of the spots in the Fourier plane. The smaller the period is, the farther away the spots move in Fourier space Fig. 4. In this manner

Optics EXPRESS

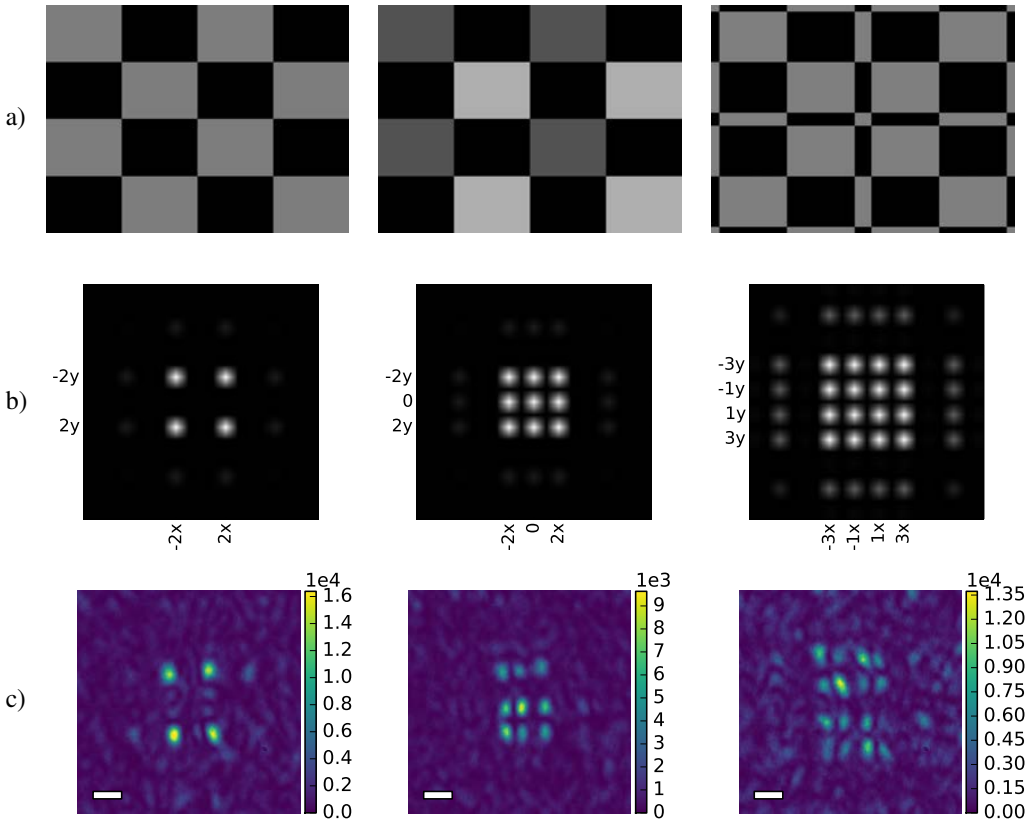

Fig. 3. a) Phase masks loaded onto the SLM for obtaining multiple focal spots through a layer of TiO_2 b) computed Fourier Transforms of (a). c) resulting pattern on the CCD for respective images in (a). Scalebar corresponds to 5μm.

we are able to generate different configurations of focal spots with rectangular as well as radial symmetry Fig. 5.

We have also used two algorithms that try to generate optimal phase masks. These algorithms simulate an SLM plane where the field is modulated such that when Fourier Transformed, the intensity is enhanced at certain predefined locations. The first approach is a genetic algorithm that optimizes the phase of the rectangular regions of the SLM. It works with a population of phasemasks, where each phasemask has phase values for each rectangular region. Through mutations and inheritance, the population evolves towards an optimal solution. For the second approach, we set the phase mask to $\phi(\mathrm{y}, \mathrm{z})$ = arg(ifft(F)) where F is zero everywhere except at the target spots and ifft corresponds to inverse Fourier transform operation. If we calculate F from $\phi(y, z)$ as described in section 2, then the central spots will have a much lower intensity than those at the edges Fig. 6. This is caused by taking the argument of the ifft which drops all intensity information of our spectrum. We can regain uniformity by optimizing the phase of the spots in F using stochastic optimization. Both algorithms result in multiple focal spots being formed on the image plane as shown in Fig. 6.

Optics EXPRESS

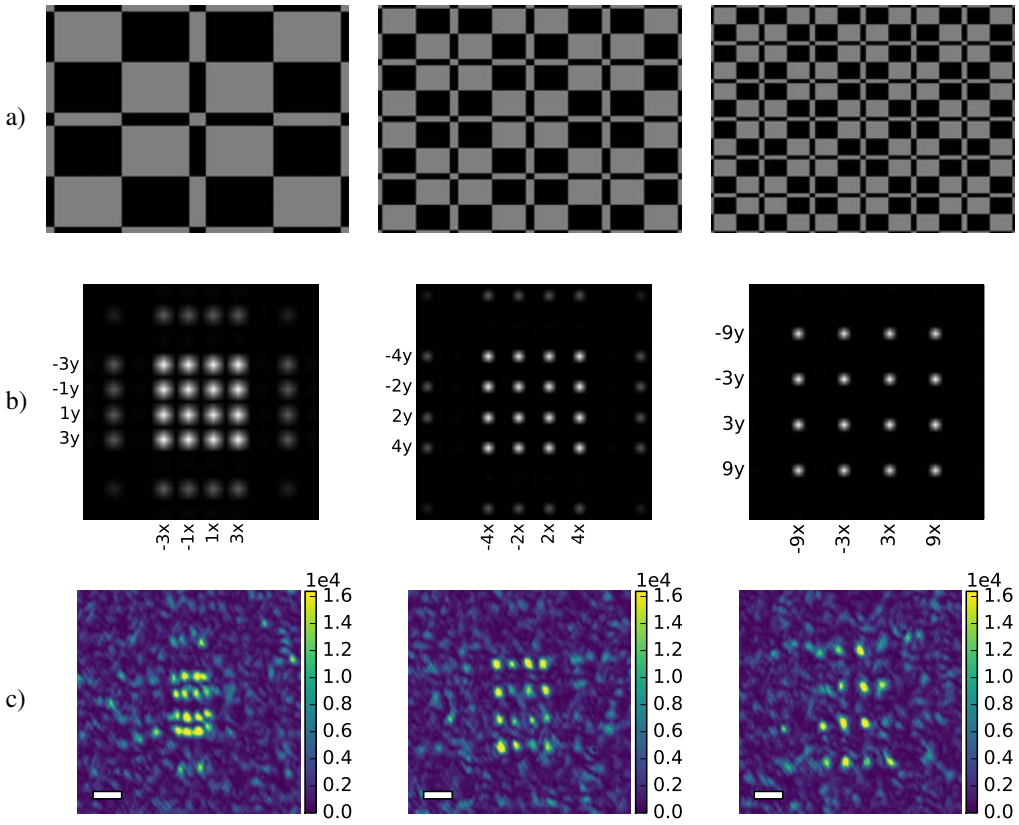

Fig. 4. Moving the focal spots in k-space: a) the SLM masks. b) computed Fourier Transforms c) resulting CCD images for diffuser glass used as sample. Scalebar corresponds to 5μm.

5. Results and discussion

The CGHs such as those described in the previous section can be generated independently of the real time experiments beforehand. In the real time experiments, once the interferometric focus is obtained, these CGHs can be added to the SLM and the resulting multiple foci can be visualised on the CCD. We demonstrate some sample configuration of focal spots which are formed by the respective CGHs as shown in Fig. 3 through 7.

Thus created multiple focal spots can be in turn used to illuminate–for example–flourescent targets in biological samples and image them. The ability to realise any configuration of focal spots can make it easier to acquire sample information from multiple locations parallely. It could also be possible to optically trap and micro manipulate targets hidden within turbid media, which would otherwise be inaccessible. The simplicity of the approach of Fourier transformation makes it easier to translate and rotate the focal spots. By adding a linear phase shift to the phase masks in the SLM plane, we are able to translate the spots. Similarly, a parabolic phase shift would move the spots in the forward direction out of the plane [4]. Also, when the coordinate axes of the images are rotated, the focal spots follow the drift and rotate in the image plane. (see Visualization 1). This freedom of moving the focal spots can accelerate image acquision process compared to raster scanning a single focal spot.

Translating the foci however depends on the range of memory effect [22], defined as the extent to which the transmitted light preserves the information about the input phase and amplitude

Optics EXPRESS

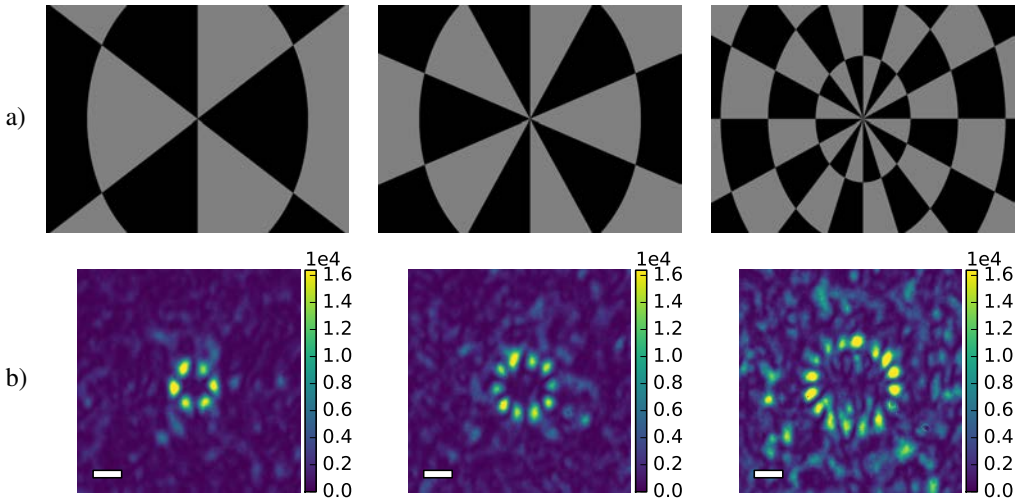

Fig. 5. a) Phase masks loaded onto the SLM to obtain focal spots with radial symmetry. b) Resulting patterns on the CCD respectively. Scalebar corresponds to 5μm.

variation. The memory effect range falls as the inverse of the thickness of the medium. For a thick 15μm layer of TiO_2, it is about 3μm and the pattern of multiple foci is lost when translated further than this range. This is also the case when the distance between the focal spots is more than the range of memory effect. Hence such experiments can only be perfomed on optically thin samples. Figure 4 shows the possibility of movement of focal spots through a diffuser for which memory effect range is theoretically unlimited [22]].

Although, the size and shape of the initial focus is retained in the multiple foci, their intensities are lower than the initial focus. Due to this, the input intensity was increased to make the focal spots visible, and thus rescaling the range of transmitted intensity on the CCD. This reduction is attributed to the intensity enhancement of initial focus with respect to the background- that gets redistributed among the multiple foci. Hence there exists a tradeoff between the contrast and the number of foci, which in turn are limited by the achievable intensity enhancement. Multiply scattering TiO_2 samples also cause this contrast to be lost quickly compared to less scattering diffuser glass. Fig. 7 demonstrates the limiting case for our signal to background ratio; where 36 focal spots are created through a diffuser, which was not possible with TiO_2 samples. Beyond this, the focal spots were indistinguishable from the background speckles in any sample.

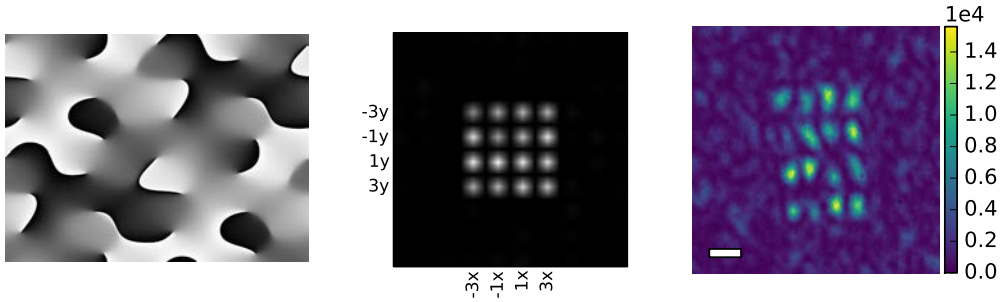

Fig. 6. CGH generated using Stochastic algorithm, computed Fourier Transform and resulting focal spots on CCD plane. Scalebar corresponds to 5μm.

Optics EXPRESS

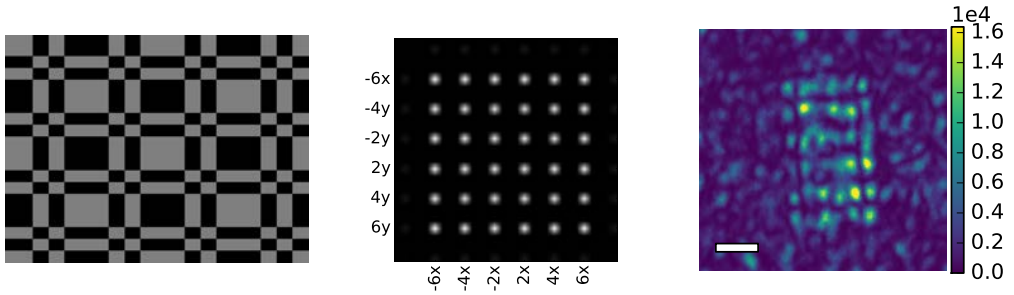

Fig. 7. Limiting case of number of foci demonstrated for diffuser glass: SLM mask,computed Fourier Transform and resulting CCD image. Scalebar corresponds to 10μm.

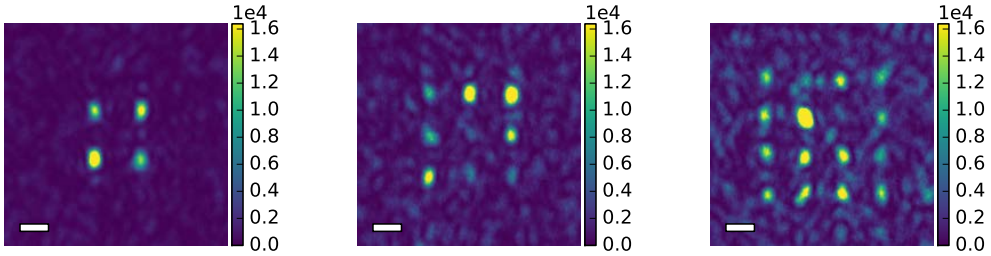

Fig. 8. Direct optimization on multiple configurations of a target. Scalebar corresponds to 5μm.

As a comparitive study to that noted previously in [19] we also perfomed the experiments by directly optimizing on multiple targets in the focal plane. We defined multiple configurations of a target Fig. 8 at the back of the sample and saw that the algorithm manages to optimize on all the targets well as long as the number of targets is small. For a large number of targets, the intensity distribution grows to be more non-uniform. This may not be desirable for applications where intensity destributions play a role. In addition, this technique by construction requires optical access to multiple locations of the focal plane and would not work well when such an access is not available.

6. Conclusion

In this article we have described a technique to obtain multiple focal spots behind a turbid medium. Computer generated phase masks can be used to transform an interferometric focus obtained behind a turbid medium into a desired configuration of multiple focal spots. With the ability of further manipulating these phase masks, the focal spots can be freely translated and rotated. This technique can find potential applications in the field of bioimaging such as structured illumination microscopy behind turbid media or optical control and micromanipulation of particles hidden in turbid environments.

Funding

Swiss National Science Foundation (Award Number 501100001711).

Optics EXPRESS

Acknowledgments

We would like to thank Dr. Jale Schneider for her contributions to the phase mask generation techniques using Genetic Algorithm.